TECHNISCHE UNIVERSITÄT WIEN

DISSERTATION

Electrochemical Detection of Fitness-relevant biomolecules in Human Saliva

ausgeführt zum Zwecke der Erlangung des akademischen Grades eines Doktors der technischen Wissenschaften unter der Leitung von

Dipl.-Ing. Dr. Rainer Hainberger
Center for Health & Bioresources
AIT Austrian Institute of Technology GmbH
und
Ao. Univ. Prof. Dipl.-Ing. Dr. techn. Günter Fafilek
Institut für Chemische Technologie und Analytik (E164)
Technische Universität Wien

eingereicht an der Technischen Universität Wien
Fakulät für Technische Chemie

von

Dipl.-Ing. **Julian D. Schrattenecker**, BSc
Mat.-Nr. 01026082

Wien, April 2020 Julian D. Schrattenecker

AUSTRIAN INSTITUTE OF TECHNOLOGY

Abstract

For sportsman and fitness enthusiasts the optimization of the training program is a major concern. To improve their daily training routine their fitness, health and stress level has to be tested at least daily and the information has to accessible as fast as possible. This can be achieved with POC devices which measure the level of relevant biomarkers. A saliva based electrochemical sensor was chosen to provide the necessary sensitivity and accessibility for the user. A two-electrode EIS based cortisol-immunosensor is able to detect cortisol from buffered solutions in the necessary sensitivity range, but because of the corrosive properties of the redox-couple ferro-/ferricyanide did not provide the necessary stability of the measurements. Different alternative redox-systems were tested and a three-electrode setup in combination with a DC-bias during the EIS measurement to produce the reduced form of hexaammineruthenium(III) in the solution was chosen. Thin-film produced electrodes on PET and glass, and screen-printed electrodes on ceramic substrates were tested in a three-electrode setup. Fully functionalised IgG-sensors on PET exhibited a reduced response in comparison to the glass and ceramic based immunosensors. An IgG and cortisol specific sensor was achieved on the ceramic substrate and was sufficiently sensitive for the detection of the biomarkers from saliva, but the IgG sensor on the ceramic substrate exhibited a high intra-batch variation. The intra-batch variation was the lowest with the glass based IgG-sensor. Saliva samples were analysed with the help of the IgG immunosensor on the glass substrate. The results were compared to a commercially available ELISA kit. A two-sample t-test with a confidence level of 0.05 revealed no difference between the results of the electrochemical IgG sensor and the ELISA kit.

Contents

1 Outline of Work

The main goal of this work is the development of a point-of-care (POC) device for the simultaneous measurement of several fitness-, health- and stress relevant biomolecules in human saliva. The overall setup is depicted in figure 1.1. Functional electrodes which specifically detect lactate, immunoglobulin G (IgG), fatty acid binding proteins (FABP), myoglobin, and cortisol are connected to a microchip which handles the electrochemical measurement. The signal is transmitted via near field connection to a hand-held device and gives the user information about their fitness, health and stress status. For the detection of these analytes suitable electrochemical detection procedures have to be developed. The receptor molecules and the functionalisation procedure have to be chosen and optimised to fabricate sensors which can bind each of the markers selectively. The fully functionalised sensors have to be tested thoroughly and the statistical parameters such as the limit of detection and the linear range have to be determined. A suitable method for the preparation of the human saliva samples has to be established and optimised. Additionally, the influence of the saliva sample preparation on the electrochemical assay has to be tested. The electrodes with the functionalisation have to be connected to the microchip and their functionality have to be tested.

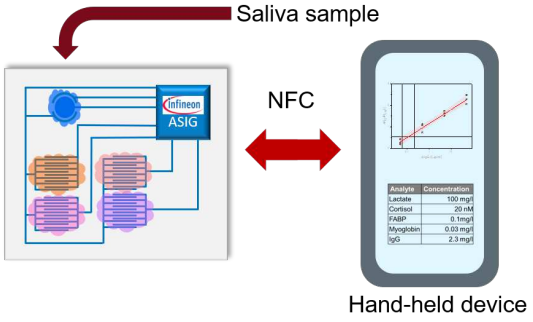

Figure 1.1: Concept of the sensor setup

2 Introduction

The awareness in the population for their personal health and fitness moves into focus. In Austria alone about 12 % of all Austrians are members in a fitness studio and the numbers are increasing from year to year [1]. People want to live healthy and determine their own fitness- and health-status with a scientific point-of-care method to check their own development over time. This is to choose optimal training times, avoid over training and check the increase of their own health. The number of fitness-studios also increases by about 5 % every year in Austria, so the studios are under a very severe competition pressure and have to stand out in comparison to their competitors and want to satisfy the needs of their customers. Further, statistics show that a nearly one in four Austrians with a job are in the critical area for burnout [2]. Usually, the analysis of stress biomarkers are performed in laboratories with the help of enzyme-linked immunosorbent assays (ELISA). These are time consuming and the results are available only after the whole assay procedure. A POC method to monitor the stress level is of high importance for companies, their employees and the health care, to prevent burnout. The medical cost of burnout cases can be drastically reduced if it can be determined in the early stages. A suitable method for POC testing is electrochemical biosensing. Sensors based on this detection method are already well established in the health sector for the determination of the glucose level in patients suffering from diabetes [3]. These sensors can be produced quite cheap and give a very fast measurement result. Applying this concept to different biomarkers can give the sportsman a profound knowledge about his personal health and fitness level in a short period of time and he can adjust his training plan accordingly. The market for electrochemical biosensors is growing every year by up to 9.7 % and according to market researches the market for POC sensors should reach up to $ 43 billion worldwide by 2029 [4]. Typically the concentrations of biomarkers are determined from human blood samples. Taking blood samples is an invasive technique. For most POC testing

devices only small sample volumes are needed, so already a single drop of blood from a cut is sufficient as with the blood glucose tests. Still, for many people the necessity to take blood for a test is the biggest obstacle and, therefore, would not use this invasive method. Further, drawing blood samples for tests can also lead to false positive results in cortisol tests for stress due to its invasive nature of the sampling procedure [5]. As a non-invasive alternative saliva would be viable for the detection of specific biomarkers [6]. Saliva is easily accessible without the need for any invasive sampling method and possible end users would be more inclined to use POC devices which analyses saliva instead of blood. All biomarkers found in blood are also available in saliva, but only in smaller quantities. This requires saliva based POC tests to have a high accuracy and good sensitivity, which can be achieved with electrochemical based biosensors.

2.1 Biomarkers

The most basic definition of a biomarker is as follows [7]:

> A defined characteristic that is measured as an indicator of normal biological processes, pathogenic processes or responses to an exposure or intervention.

This is a very broad definition and encompasses a multitude of different applications. In this work the focus will be on biomarkers which can be used to asses the fitness, health and stress status of a patient. From the multitude of possible biomarkers a few have been chosen, which can facilitate to determine these statuses. The chosen biomarkers are lactate, cortisol, heart fatty acid binding protein (H-FABP), myoglobin, and IgG.

Lactate is a small molecule with a molecular weight of $89.07\,\mathrm{g\,mol^{-1}}$ and its chemical structure is depicted in figure 2.1. It is an important biomarker for the fitness status. Determining the lactate concentration can be used to make conclusions on the anaerobic threshold. With high training intensities the aerobic production of adenosine triphosphate is insufficient and the metabolism switches to an anaerobic production. This produces lactate as a side product, which increases the lactate concentration in the blood and saliva. The better trained a sportsman is, the higher the training intensity can be without an increase in the lactate concentration. Depending on the goal of the individual

training plan, such as high intensity training or cardio training, the sportsman should stay either above or below the threshold. Also, the lactate level gives information about the length of the needed recovery time between each training period to avoid over training and to reach peak performance in each training. [8, 9]

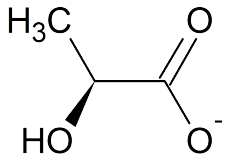

Figure 2.1: Chemical structure of L-lactate

Cortisol, also known as hydrocortisone, is a steroid hormone with a molecular mass of 362.46 g mol^{-1}. The chemical structure is depicted in figure 2.2. Cortisol is an important hormone in the human body and influences several biological processes. It controls the carbohydrate degradation by stimulating the gluconeogenesis. Additionally, it can activate anti-inflammatory pathways and it can lessen the activity of the immune system. Cortisol levels can be increased by several different health related issues, such as Cushing's syndrom, diabetes mellitus, or chronic and acute stressors, such as trauma, intensive aerobic exercise. Singular stressful events can already cause an increase in the cortisol levels, but should decrease over time. If the hydrocortisone concentration does not decrease, or stays on the same level over the whole day, the risk for burnout increases dramatically. [9, 10, 11]

There are about 9 known subtypes of FABP. For fitness and health monitoring the most promising biomarkers is the H-FABP. It is a quite small protein with a molecular weight of 15 kDa. In the case of muscular damage, caused by training, H-FABP can be found in significant quantities in saliva. With the information about the extent of the muscle damage, the training plan can be evaluated and adjusted accordingly. Further, H-FABP can be a released into saliva in the case of different cardiovascular diseases, such as acute myocardial infarction. [12, 13, 14]

Myoglobin is a small protein composed of 153 aminoacids with a size of 18 kDa.

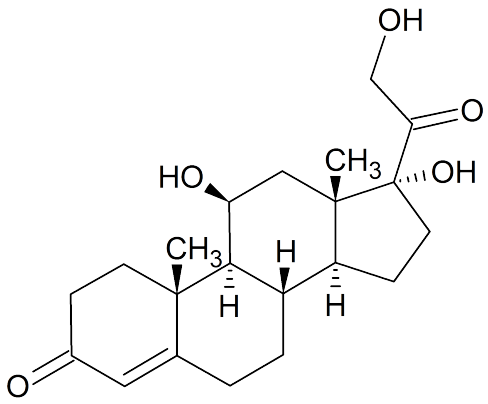

Figure 2.2: Chemical structure of Cortisol

Its main function is the transport of oxygen to the muscle cells. Increased values of myoglobin in saliva indicates similar situations as does the H-FABP. When muscles are damaged due to training, the concentration of myoglobin can increase significantly. Also, in the case of cardiovascular diseases, the concentration can increase. [15, 13, 14]

IgG is a protein with a size of 150 kDa. The overall structure of the protein is depicted in figure 2.3. It consists of two long chains, called heavy chain (H), and two short aminoacid chains, called light chain (L). These chains are linked together with disulfide bridges an form a dimer. The upper half of the IgG is responsible for the binding of an antigen. The upper dimer is called $F(ab)_2$ region and the immuno-active monomer is called Fab. The lower part of the antibody, which consists only of the end parts of the two heavy chains, is called constant region or F_C. This half of the IgG is not active and can not bind any antigen. The main function of IgG is to bind to antigens of pathogens in the immune response of the hosts body. Decreased concentrations of IgG indicate a possible risk for infections and with this information the sportsman or trainer should adjust the training schedule accordingly. In the case of psychological stress, the IgG levels in saliva and blood can increase significantly and give in combination with other markers detailed information on the stress level of the person in question. [16, 17, 18]

For an evaluation of the state of the art analysis methods and surface functionalisation protocols, the concentration of the analyte molecules in human saliva is of utmost importance. The typical concentrations of lactate, cortisol,

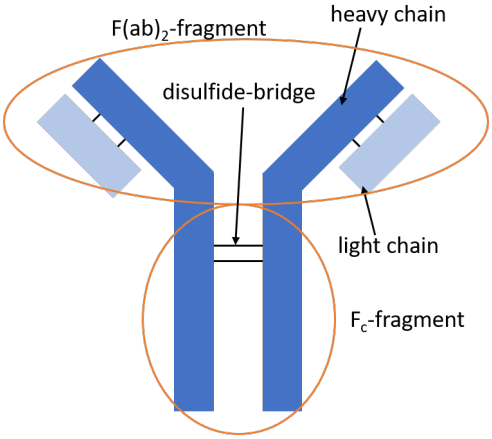

Figure 2.3: Schematics of the IgG structure

	Concentration
Lactate	$45\,\mathrm{mg\,L^{-1}}$ (Rest) to $315\,\mathrm{mg\,L^{-1}}$ (Workout) [19]
Cortisol	$4.3\,\mathrm{ng\,mL^{-1}}$ to $9.4\,\mathrm{ng\,mL^{-1}}$ [20]
Myoglobin	$20\,\mathrm{ng\,L^{-1}}$ to $110\,\mathrm{ng\,L^{-1}}$ [21]
H-FABP	$12.3\,\mathrm{\mu g\,L^{-1}}$ [22]
IgG	$124\,\mathrm{mg\,L^{-1}}$ [23]

Table 2.1: Biomarker concentration of healthy individuals in human saliva samples

myoglobin, H-FABP and IgG in human saliva are summarised in table 2.1. IgG and lactate have the highest concentrations in saliva. Other analytes such as cortisol and myoglobin are only present in the $\mathrm{ng\,L^{-1}}$ range.

A comparison of the analyte concentrations in saliva (table 2.1), with the limit-of-detection (LOD) values and linear range of the state of the art electrochemical techniques (table 2.2) reveals that the currently published methods are sufficient for the analysis of nearly all molecules of interest. The only exception is myoglobin which is much lower concentrated in human saliva than the best LOD value reported in literature [24]. The surface functionalisation for this molecule has to be improved to lower the LOD and enlarge the linear range. An improvement in the other cases would also be advantageous because if the limit of detection can be lowered further the saliva samples could be diluted during the preparation.

Analyte	LOD	Linear Range
Lactate	$0.36\,\mathrm{mg\,L^{-1}}$	$0.36\,\mathrm{mg\,L^{-1}}$ to $10.8\,\mathrm{mg\,L^{-1}}$ [25]
Cortisol	$0.36\,\mathrm{ng\,L^{-1}}$	$0.36\,\mathrm{ng\,L^{-1}}$ to $36\,\mathrm{\mu g\,L^{-1}}$ [26]
Myoglobin	$5.2\,\mathrm{\mu g\,L^{-1}}$	$10\,\mathrm{\mu g\,L^{-1}}$ to $650\,\mathrm{\mu g\,L^{-1}}$ [24]
H-FABP	$0.236\,\mathrm{ng\,L^{-1}}$	$98\,\mathrm{ng\,L^{-1}}$ to $25\,\mathrm{\mu g\,L^{-1}}$ [27]
IgG	$0.02\,\mathrm{\mu g\,L^{-1}}$	$0.5\,\mathrm{\mu g\,L^{-1}}$ to $125\,\mathrm{\mu g\,L^{-1}}$ [28]

Table 2.2: LOD and lineare range of current sensors

2.2 Electrochemical Methods

2.2.1 Electrochemical Impedance Spectroscopy

When an alternating potential is applied to an electrical circuit, several different elements can impede the flow of the alternating current, such as an electrical resistance or a capacitor. All these elements, which oppose the alternating current, are called electrical impedances. In the case of a direct potential (U_{DC}), the resistance (R) to the flowing direct current (I_{DC}), can be expressed by Ohm's Law (Equation 1).

$$R = \frac{U_{DC}}{I_{DC}} \tag{1}$$

The impedance is defined similarly, but a major difference is that the potential and the current are alternating sinusoidal. The applied potential and current over time is depicted in figure 2.4a. The alternating potential is defined by an amplitude ($\hat{U}$) and a frequency (f) as shown in equation 2. When the alternating potential is applied the current response is shifted by a phase angle φ, as shown in equation 3.

$$U_{AC} = \hat{U} \cdot sin(2\pi \cdot f \cdot t) \tag{2}$$

$$I_{AC} = \hat{I} \cdot sin(2\pi \cdot f \cdot t + \varphi) \tag{3}$$

Expressed as complex numbers, using Euler equations, the equations change as shown in equation 4 and 5.

$$U_{AC} = \hat{U} \cdot e^{i \cdot 2\pi \cdot f \cdot t} \tag{4}$$

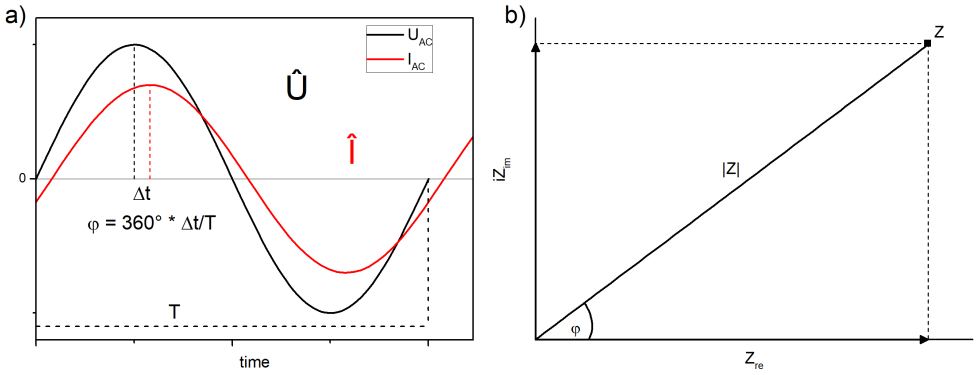

Figure 2.4: a) applied alternating potential and recorded alternating current over time for an EIS measurement; b) impedance Z and corresponding imaginary and real part of the impedance

$$I_{AC} = \hat{I} \cdot e^{i \cdot 2\pi \cdot f \cdot t + \varphi} \tag{5}$$

The impedance Z is defined analogous to Ohm's Law. When both the alternating current and potential from equation 4 and 5 are inserted we yield the following equation:

$$Z = \frac{U_{AC}}{I_{AC}} = |Z| \cdot e^{i \cdot \varphi} \tag{6}$$

If the Euler equations are used again we gain the following results:

$$Z = |Z| \cdot (cos(\varphi) + i \cdot sin(\phi)) = Z' + i \cdot Z'' \tag{7}$$

As equation 7 shows, the impedance consists of a real part Z' and an imaginary part Z". When complex numbers are represented in the complex plane as a phasor, as shown in figure 2.4b, they are called Argand diagrams. In electrochemical impedance spectroscopy (EIS), when the impedance is depicted with the real number on the x-axis and the imaginary part on the y-axis, these diagrams are called Nyquist plots. When $\log(|Z|/[\Omega])$ and the phase angle are plotted against the log(f/[Hz]), the diagrams are called Bode plot.
In EIS an alternating potential is applied over a wide frequency range, from Mhz to mHz. The corresponding current is recorded and the impedance of the electrical circuit is determined. Depending on the type of elements, e.g. resistor

or capacitor, and their position in the electrical circuit, the form of the Nyquist and Bode plot can change significantly. The usual elements, which are used in a circuit to describe the general electrochemical properties of a measured system, are: electrical resistor, capacitor, inductor, Warburg impedance and constant phase element (CPE).
Investigating an electrical circuit which consists only of an electrical resistor (figure 2.5a) with EIS would yield a very simple Bode and Nyquist plot. The singular electrical resistor is frequency independent and gives the same impedance at each frequency, and is represented by only a singular dot in the Nyquist plot, as shown in figure 2.5b and a horizontal line in the Bode plot, as depicted in figure 2.5c.

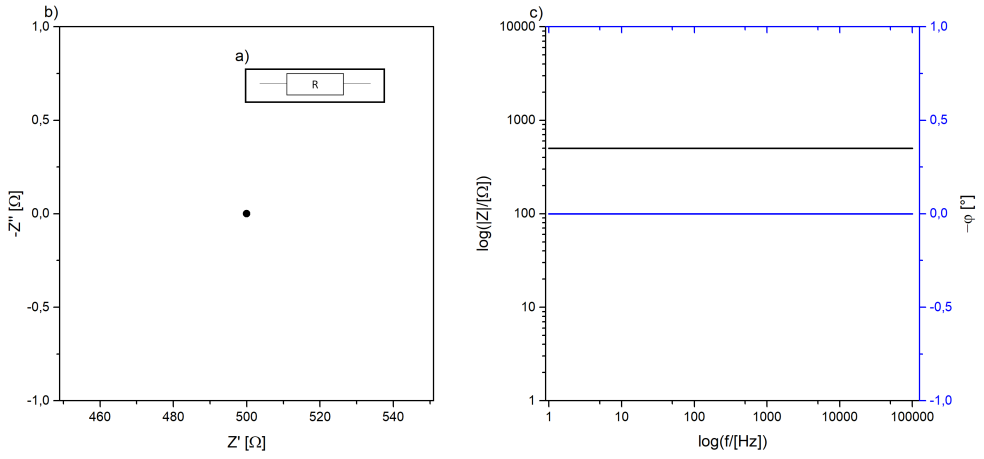

Figure 2.5: a) Circuit consisting of a singular electrical resistor; b) Nyquist plot of an electrical resistor; c) Bode Plot of an electrical resistor

In the case, that only a capacitor is present in the electrical circuit (figure 2.6a), the result would be quite different. When an alternating current is applied to a capacitor, it is continuously charged and discharged. At very high frequencies, charging and discharging happens in very short times and therefore the current must increase accordingly. This leads to low impedances as depicted in the Bode plot in figure 2.6c. When the frequency is very low, the charge of the capacitor is transferred much slower and this leads to very low current. This yields a very high impedance, as depicted in in figure 2.6c. A capacitor does only have an imaginary part in the complex plane. Therefore, the Nyquist plot

is only a vertical straight line, as shown in figure 2.6b. At high frequencies the impedance is nearly zero and increases with lower frequencies.

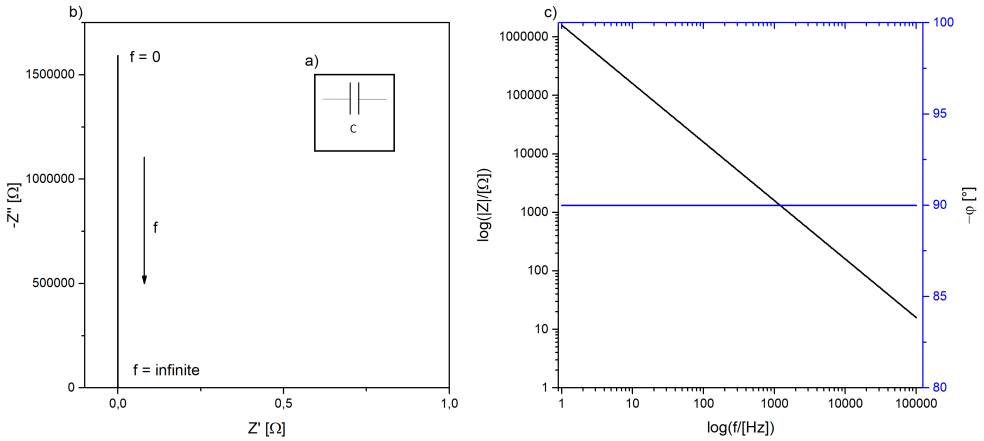

Figure 2.6: a) Circuit consisting of a single capacitor; b) Nyquist plot of capacitor; c) Bode Plot of a capacitor

In several practical cases, a perfect capacitor does not form on a solid electrode. This kind of "leaky" capacitor is best described with a CPE. The impedance of a CPE can be described with the following equation:

$$Z_{CPE} = \frac{1}{T \cdot (2\pi \cdot f)^n} \tag{8}$$

T is a constant, which is related to the capacity of the electrode. The constant phase exponent n have values between zero and one. If the value of the exponent is close to one, the more similar the behaviour of the CPE is to that of a perfect capacitor. At a value of zero it would be similar to a ohmic resistor. At a value of 0.5, the behaviour would be that of a Warburg impedance, as depicted in figure 2.7.
When an electrical circuit consisting of only a CPE (figure 2.8a) is measured with EIS a Nyquist and Bode plot similar to the Warburg impedance is the result. As mentioned previously a CPE exhibits a behaviour in between a capacitor and a Ohmic resistor. At high frequencies the impedance of the imaginary and the real part are very low and increase at lower frequencies. The constant phase exponent correlates with the angle of the curve in the Nyquist plot. At

a value of one the incline of the curve would be perpendicular to the x-axis, as shown in figure 2.6b. When the value of the exponent is decreased, the angle between the curve and the x-axis also decreases, as shown in figure 2.8b.

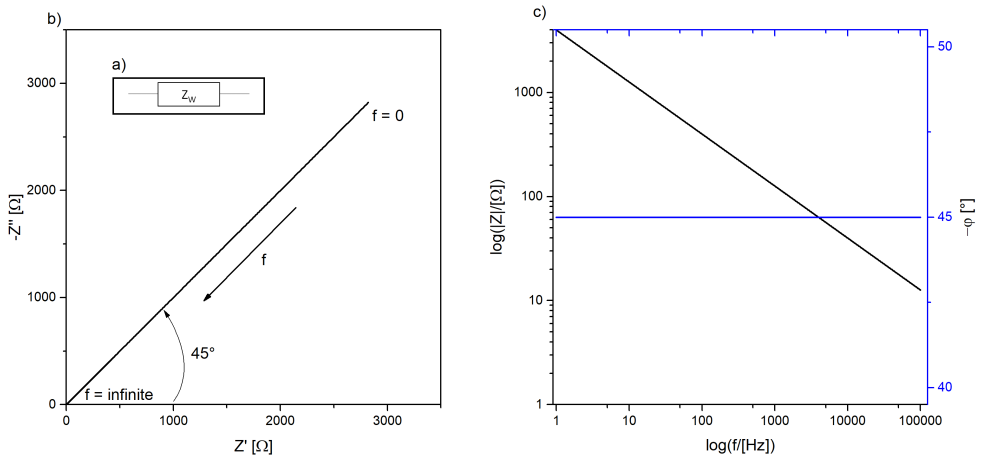

Figure 2.7: a) Circuit consisting of a single Warburg impedance; b) Nyquist plot of a Warburg impedance; c) Bode Plot of a Warburg impedance

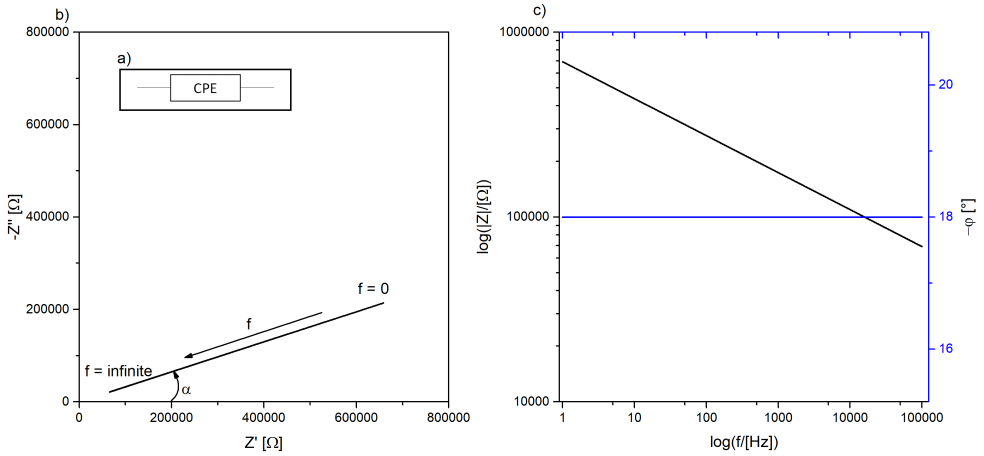

Figure 2.8: a) Circuit consisting of a single CPE; b) Nyquist plot of a CPE; c) Bode Plot of a CPE

A simple series connection of a electrical resistor and a capacitor, as depicted in figure 2.9a, yields a simple EIS spectrum. At high frequencies the capacitor does not inhibit the flow of the current and the inhibition increases with lower

frequencies, similarly to the single capacitor. The electrical resistor is, as mentioned previously, frequency independent and only moves the vertical line in the Nyquist plot on the x-axis, as shown in figure 2.9b. Figure 2.9c shows the Bode plot, which also exhibits a similar behaviour as in the case of the single capacitor. At low frequencies the impedances are very high and decrease at higher frequencies, until it reaches the impedance of the resistor in the electrical circuit.

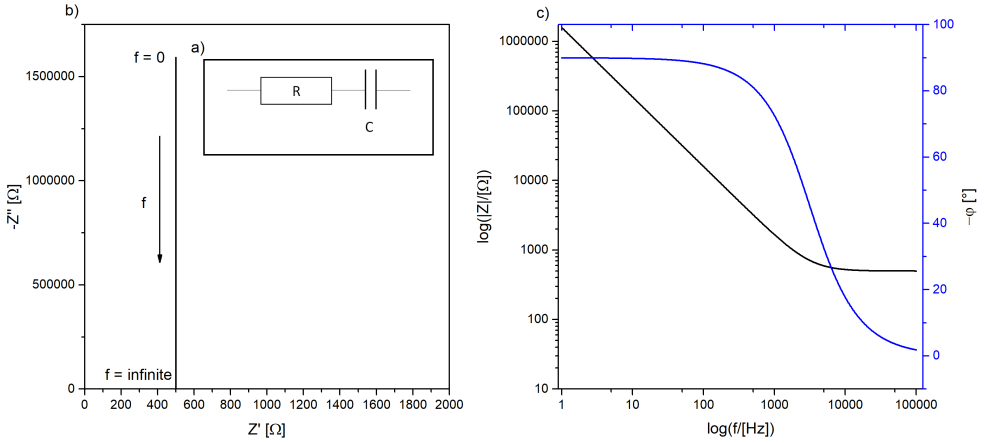

Figure 2.9: a) Circuit consisting of a resistor and capacitor in series; b) Nyquist plot of a resistor and capacitor in series ; c) Bode Plot of a a resistor and capacitor in series

The EIS spectra of the same elements in a parallel configuration, shown in figure 2.10a, look quite different. The Nyquist plot, figure 2.10b, forms a semicircle. At very low frequencies the capacitor completely inhibits the current flow. The only way the current flow is through the resistor. Therefore, the total impedance is equal to the resistor, as depicted in figure 2.10c. At very high frequency the capacitor does not inhibit the flow at all and the determined impedance drops to zero. As can be seen in figure 2.10b and c, there is a break-point in the Bode plot when the imaginary part reaches a maximum. The frequency is called the break-point frequency f_0 and can be calculated by the following equation:

$$f_0 = \frac{1}{2\pi \cdot R \cdot C} \tag{9}$$

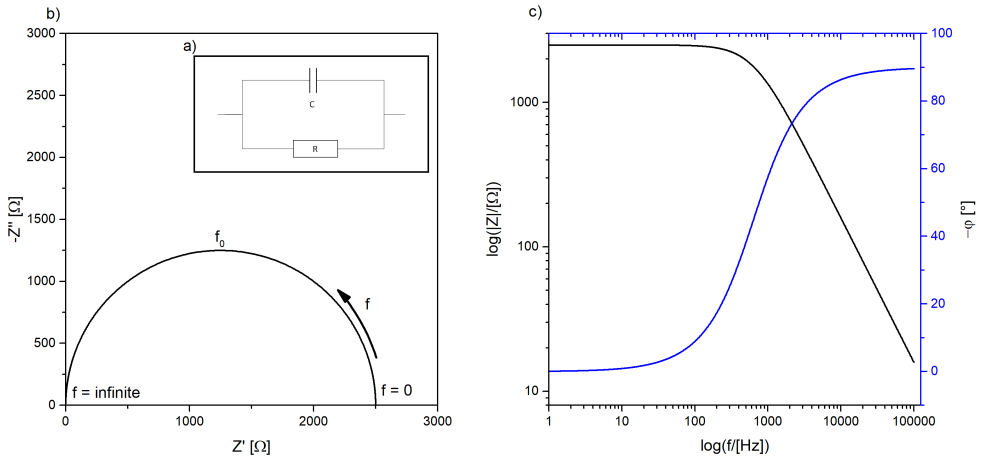

Figure 2.10: a) Circuit consisting of a resistor and capacitor in parallel; b) Nyquist plot of a resistor and capacitor in parallel; c) Bode Plot of a a resistor and capacitor in parallel

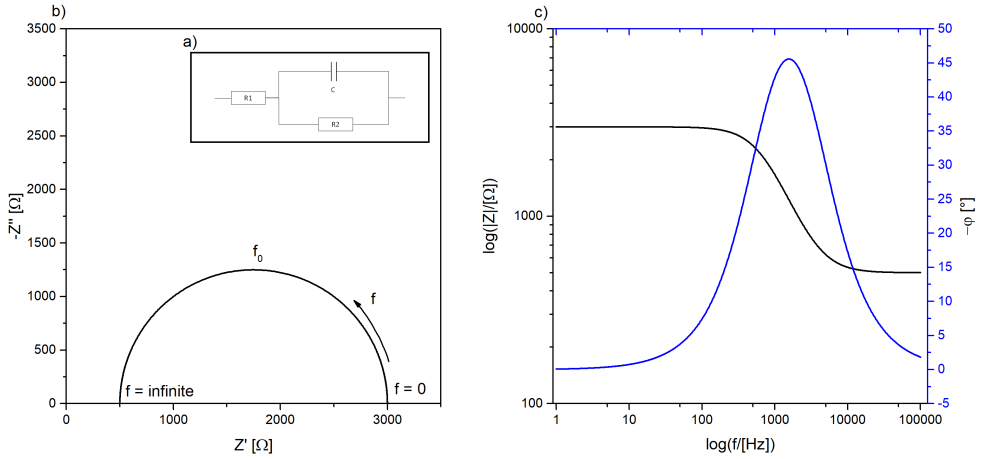

Figure 2.11: a) Randles circuit consisting of only an electrical resistor in series to a electrical resistor and capacitor, which are in parallel; b) Nyquist plot; c) Bode Plot

The electrical circuit from figure 2.10a is called Randles circuit. It is obtained when an additional ohmic resistor is added in series to the circuit shown in figure 2.11a. As can be clearly seen in figure 2.11b the semicircle in the Nyquist plot shifts along the real axis by R1. At low frequencies, the semicircle meets the x-axis at the sum of the first and second Ohmic resistor. At very high frequencies the lowest impedance in the Bode plot, as shown in figure 2.11c, is

equal to the additionally added resistor.

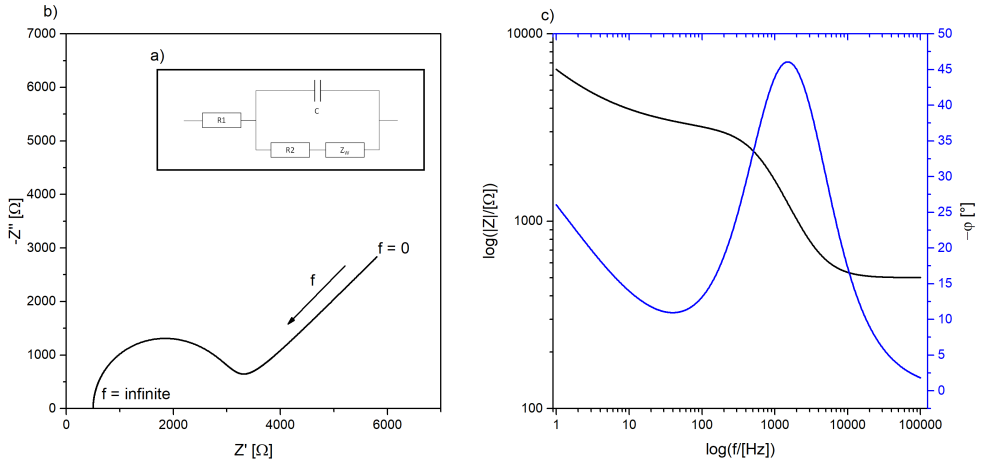

Figure 2.12: a) Randles circuit complemented with a Warburg element suitable to represent the frequency response of a typical biosensor; b) Nyquist plot of a typical biosensor; c) Bode Plot of a typical biosensor

Most of the biosensors based on EIS, as will be discussed in chapter 2.3.3, exhibit a response that can be described best with an electrical circuit depicted in figure 2.12a. [29, 30]

2.2.2 Chronoamperometry

In the chronoamperometry the potential is changed with a step and kept constant afterwards. The change of the current in response to the potential step is recorded over time, as depicted in figure 2.13. At the initial potential no oxidation or reduction takes place. The applied potential then promotes either of these electrochemical reactions. When the potential change is applied the change of the current is recorded over time and exhibits in the case of an unstirred solution a characteristic curve as depicted in figure 2.13. The measured current consists of two different currents: a Faradaic current and a capacitive current. The capacitive current is even present in the absence of an oxidation or reduction reaction. When the potential is changed the electric double layer at the metal-solution interface is charged. This behaves in the same way as a capacitor according to equation 10.

$$i_c = \frac{E_{applied} - E_{initial}}{R_S} \cdot e^{\frac{t}{R_S C}} \tag{10}$$

R_s is the solution resistance and C the capacitance of the double layer. The capacitive current i_c decreases over time t exponentially, as can be seen in figure 2.13.

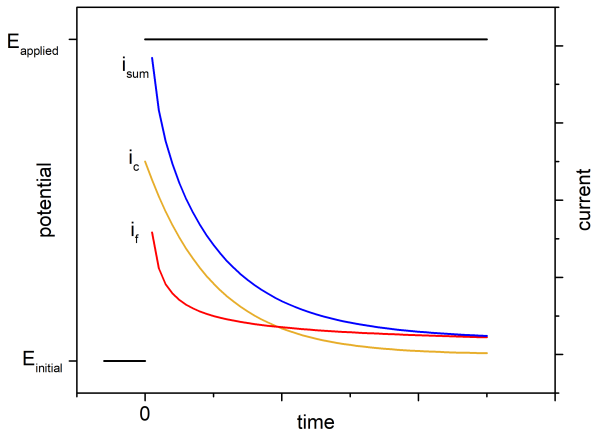

Figure 2.13: Measurement principle for chronoamperometry; potential step of the chronoamperometry (black), change of Faradaic current i_f (red), capacitive current i_c (orange) and the measured current i_{sum} (blue) over time when the potential step is applied

When the applied potential is high enough to induce the electrochemical reaction, the measured Faradaic current i_f decreases over time according to equation 11. The electrochemical substance is used up in the electrochemical process. It is only resupplied by the diffusion process and decreases continuously over time as shown in figure 2.13. The higher the diffusion constant D and the initial concentration c of the electrochemically active substance, the higher the initially recorded Faradaic current i_f.

$$i_f = nFA\sqrt{\frac{D}{\pi t}}c \tag{11}$$

The measured current i_{sum} is a combination of the capacitive and the Faradaic current. When the concentration of the electrochemically active substance is very low, the faradaic current is also very low and is completely hidden by the capacitive current. This impacts the limit of detection greatly. There are

several methods to overcome this problem. One solution is to wait for an extended period of time. According to equation 10 the capacitive current decreases exponentially and the Faradaic current decreases much slower, with a factor $t^{-1/2}$. When the waiting time is sufficiently long, the measured current i_{sum} is nearly equal to the Faradaic current. Another solution is to decrease the solution resistance and increase the initial capacitive current. With this solution either the Faradaic current is no longer overshadowed by the capacitive current or the waiting time for the decrease of the capacitive current is reduced significantly. [29]

2.2.3 Voltammetry

There are several different methods depending on voltammetry. In all of these methods different electrical potentials are applied and the corresponding currents are measured. The main difference is the shape of the applied potentials. The most simple voltammetric method is the linear-scan voltammetry (LSV). In this method the potential is changed constantly over time from a start value until a chosen end value of the potential is reached, as depicted in figure 2.14a. The starting potential is chosen in a way that no electrochemical reaction takes place and only the change of the capacitive current is recorded. When the potential is sufficient to induce the redox-process of the redox-active substance, the Faradaic current increases. This current reaches a maximum and then decreases, because the concentration of the redox-substance decreases according to the boundary condition determined by the applied potential on the electrode surface. The reactant is brought via diffusion to the electrode surface and reacts continuously. Because of this process, the thickness of the diffusion layer increases and the current decreases asymptotically, as depicted in figure 2.14b. The LSV method is used to study the electrochemical behaviour of redox-systems, but with the constant increase of the potential only the anodic or the cathodic reaction can be studied. To study both reactions, the cyclic voltammetry (CV) can be chosen. This method is in the beginning very similar to the LSV. In the CV the potential is also changed at a constant rate, with the starting potential apart from any faradaic reaction. When the potential reaches the redox potential of the corresponding reaction, the faradaic current is recorded, but after the asymptotic decrease of the current the potential scan direction is changed, as shown in figure 2.15. The absolute value of the new scan rate is usually the same as

previously, but it is multiplied with -1 and changes now with this new constant rate. In this way both the oxidation and the reduction of the redox-couple are recorded with the same measurement. [29]

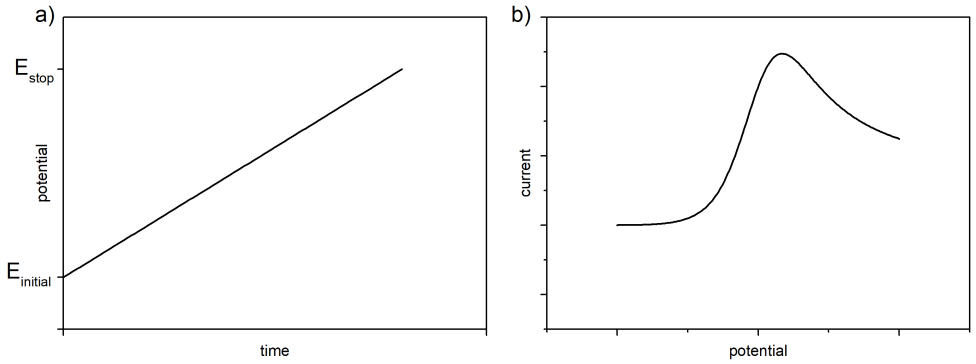

Figure 2.14: Principle of LSV; a) potential change over time; b) characteristic potential-current graph with diffusion controlled faradaic-process

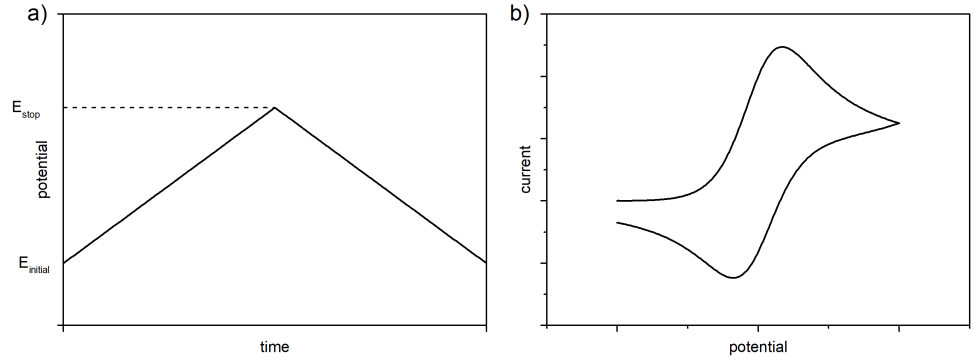

Figure 2.15: Principle of CV; a) potential change over time; b) characteristic potential-current graph with diffusion controlled faradaic-process

2.3 Electrochemical biosensors

Biosensors are used in a wide range of fields, such as the food industry to monitor the production quality. In fermentation industry they can be used to monitor the overall fermentation process, e.g. the production of acetic acid. Further, they are widely used in the medical field to monitor different biomarkers in the

human body. The most prominent medical biosensor is the glucose sensor to measure the blood-glucose concentration in diabetics which accounts for about 85 % of the world market [31]. All chemical or biochemical sensors consist of two key components: a recognition element and a transducer. An overview of the different elements in a biosensor is depicted in figure 2.16. The main difference between a chemical and a biochemical sensor is the recognition element. According to IUPAC a biosensor uses a biochemical reaction or mechanism as recognition element [32]. The recognition can be an enzyme, an antibody, a short piece of DNA or even whole cells. There are also artificial recognition elements which can bind the analyte similarly to an antibody. These recognition elements are for example cyclodextrans or molecular imprinted polymers (MIP). The most common transducers in biosensors are physical, optical, and electrochemical transducers. In physical transducers the change of a physical parameter is detected. This can be the change of temperature, as in a thermometric transducer, or a change in mass, as in a quartz-crystal-microbalance. For an optical transducer the signal can be absorption, as in an Mach-Zehnder interferometer. In the case of an electrochemical transducer the directly produced signal is an electrical one. The most common electrochemical transducers are based on impedance, amperometry or voltammetry.
The main focus of this work are the electrochemical transducers. In section 2.2.1 EIS, CV and chronoamperometry are discussed in detail. The combination of the right recognition element and electrochemical transducer is of great importance to ensure a working electrochemical biosensor. Also, the binding of the recognition elements on the electrodes of the electrochemical sensor have a great impact on the performance and sensitivity of the sensor. The receptor molecules can be bound to the surface via adsorption or covalently.

2.3.1 Recognition elements

The function of the recognition element is to capture the analyte of interest. This can be achieved either by affinity binding or by an enzymatic reaction. The affinity binding is based on a key and lock principle. Only the biomarker of interest binds specifically to the recognition element and all other biomolecules are not bound. This binding process changes the electrical properties and can be read by the transducer. In the case of an enzymatic reaction the analyte undergoes a chemical reaction which is promoted by the enzyme in the recognition

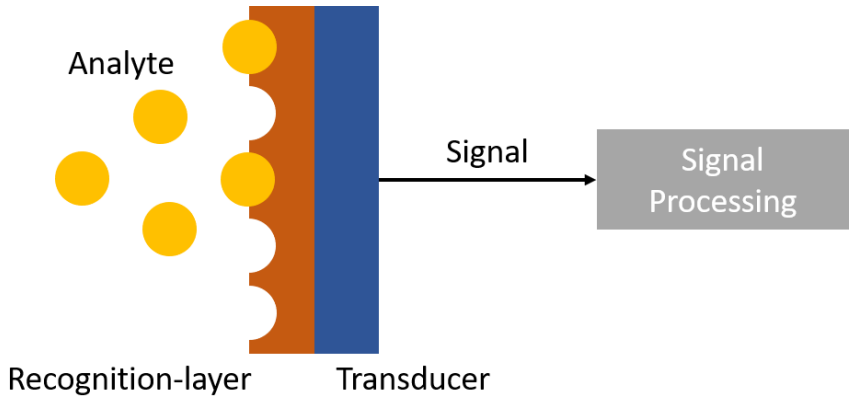

Figure 2.16: Schematic of the different parts of a biosensor

element. Electrochemical sensors utilize either the product of the enzymatic reaction or the electrons of the redox-reaction directly.
Two main strategies are used to bind the receptor molecules: non-covalent and covalent strategies. The most simple way to immobilise the receptor molecule on a surface is non-covalently. This is achieved via adsorption on the surface. The receptor molecule is bound by hydrophobic interactions, hydrogen-bonding, van der Waals interaction or electrostatic interaction. Qi et al have shown a biosensor in which the IgG binding Protein A can be immobilized by adsorption on a cleaned gold surface to produce a label-free electrochemical impedance sensor for IgG [33]. This kind of sensor is produced very easily and does not need any additional chemicals. A big disadvantage is the possibility of leaching processes because of low binding strength between receptor molecule and gold surface. When the sensor is washed multiple times during the preparation or the use of the sensor, the response can be very differently because of lost receptor molecules and can therefore decrease the precision of the sensor. Another problem is the lower storage stability of the sensors. A study of Pagán et al has shown that sensors based on adsorption of the receptor molecules exhibited a lower storage stability in comparison to covalently bound receptor molecules [25].

2.3.2 Covalent binding strategies on electrodes

To ensure optimal working conditions of an electrochemical biosensor a multitude of steps and materials have to be considered in the covalent binding

strategies. These are: the support substrate, the electrode preparation, the electrode functionalisation, the receptor molecules and the electrode materials of working, counter and reference electrode. From these the choice of the working electrode (WE) has the biggest impact on the covalent binding strategy. On graphite electrodes binding platforms can be attached via pi-stacking or activation via oxidation of the surface. Metal electrodes like gold or platinum can be functionalised by using thiols which self-assemble on these materials and attach covalently to the surface. These initial functionalisations on the electrodes have to be activated further to bind the receptor molecules. [29]

Substrates

Typical substrates for the electrodes of the biosensors are either non-flexible or flexible materials. Biosensors on different non flexible substrates have been reported, such as glass [34] and ceramics [35]. The biggest advantage of these materials is the stability of the substrate. Glass and ceramics have a high temperature stability and a high chemical stability. Biosensors on flexible substrates, such as paper [36] and polymers [37] have also been reported. The reduced weight and the reduced waste production are not the only advantages of these kind of substrates. Also, the mass-production capabilities of the flexible substrates, such as roll-to-roll processing, are of great interest for the industry and, therefore, a new focus of research in biosensors.

Electrode materials

As previously mentioned the choice of the electrode material has the biggest influence on all further steps in the functionalisation. A big number of biosensors use noble metals as electrode materials and in most of these cases gold is used. The main reason for the use of gold electrodes is the high stability and the self-assembly of thiols on the surface. Further, the use of gold for functionalisation and in biosensor application is studied in great detail in literature. Other noble metals, such as platinum, palladium, silver and copper, are also used in biosensors, but less than gold. [29]

Electrode deposition

The deposition and structuring of the electrode material is based on thick-film or thin-film processes. The main difference between these two types of processes is the thickness and the surface morphology of the resulting films. The thickness of electrodes produced by thin-film processes is below 5 µm and above 5 µm when they are produced by thick-film processes.
In thin-film processes the electrodes can be produced by photolithography or shadow masks. The procedure of the photolithography process is depicted in figure 2.17. First, a suitable substrate is chosen for the photolithography process. Next, a photosensitive resist is deposited onto the substrate via spin-coating. In the spin-coating process the substrate is rotated with a high speed and the photosensitive resin is dropped onto the middle of the substrate. The rotation speed and the viscosity of the resin control the thickness of the deposited film. Subsequently, a photomask with the electrode structures covers the substrate and the photo resist is illuminated with UV light. There are two types of photosensitive resins used in photolithography: positive and negative photosensitive resists. When positive photoresists are used, as depicted in figure 2.17, the illuminated areas can be removed with the developer solution. With negative photo resists the non illuminated areas are soluble in the developer solution. After the illumination the substrate is developed and the electrode material is deposited onto the substrate. The last step is the so called lift-off process in which the remaining photo resist covered with the electrode material is removed from the substrate with organic solvents. The procedure to structure the electrodes for the thin-film deposition is much easier with the shadow mask, as the schematic in figure 2.18 shows. A mask with the cut out electrode structures is positioned onto the substrate. Next, the electrode material is deposited through the shadow mask onto the substrate. For each additional material which is patterned onto the substrate a different shadow mask has to be used. The biggest advantage of the process with the shadow mask is the easy usage. For each structure only the shadow mask has to be prepared by milling or laser cutting and changed for each material. With the photolithography process a photomask for each structure has to be produced and for each batch the substrate has to be prepared with the photoresist. After the development and the deposition the remaining photo resist has to be removed by lift-off. Residues of the photo resin can remain on the deposited electrodes and have to be removed thoroughly to

ensure a completely clean surface for the following functionalisation of the electrodes. A major disadvantage of the shadow mask is the lower possible resolution of the produced patterns. Further, the deposited material can build up on the shadow mask and can cause a roughness around the edges of the structures. [29]

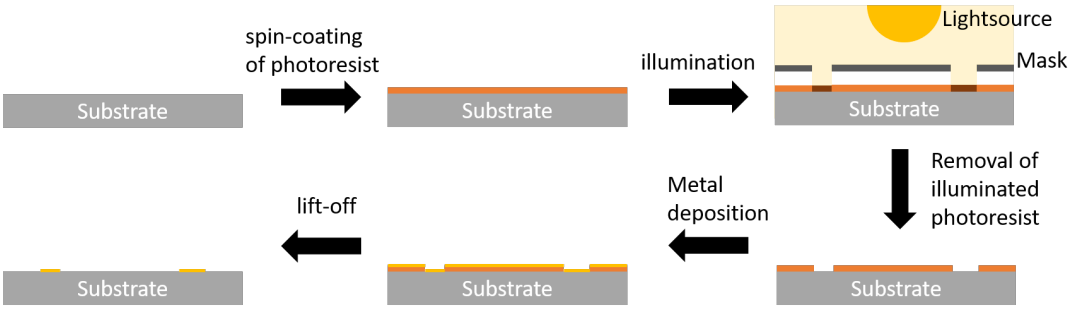

Figure 2.17: Photolithography thin-film process for metal deposition

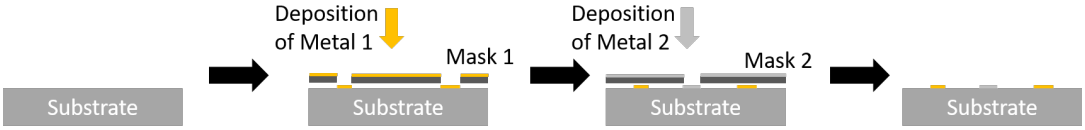

Figure 2.18: Thin-film process with shadow mask

The typical method for the deposition of thin-films of the electrode materials is the physical vapour deposition (PVD). The two most common methods are deposition by sputtering and thermal evaporation (TE). The schematic of TE is shown figure 2.19a. The substrate is put into a vacuum chamber above a holder with the electrode material used for the deposition. The pressure in the PVD chamber is lowered and the electrode material is evaporated by heating. Next, the metal gas condensates on the substrate and forms a thin and pure layer. The second method is sputter deposition, as shown in figure 2.19b. This method is very similar to the TE. The substrate is placed in a vacuum chamber under the electrode material which is called target. A vacuum is applied to lower the pressure in the chamber. When a sufficiently low pressure is reached, the deposition can be started by bombarding the target with an ionized gas. This sets off a collision cascade in the target material and atoms from the target material are ejected. These are then deposited onto the substrate. [29]

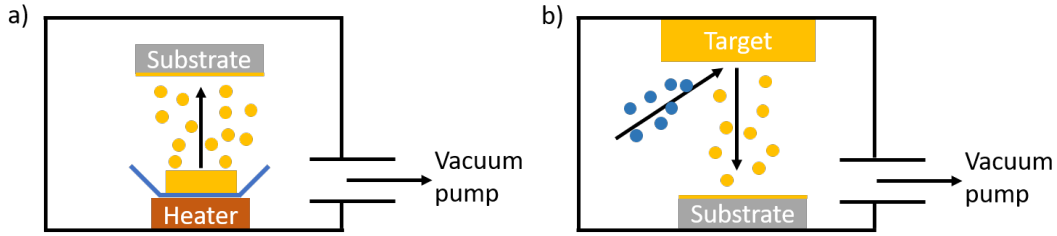

Figure 2.19: PVD methods, a) thermal evaporation; b) sputter deposition

The process for the production of thick-films with screen-printing is depicted in figure 2.20. The substrate is covered with the screen-printing mask and the screen-printing ink is added onto the mask. The ink is distributed evenly over the whole mask area. The used ink consists of metal particles which form the electrode, organic additives which influence the viscosity of the paste and a solvent. After the mask is removed the paste has to be dried and then has to be heat treated to form a electric conducting electrode. Depending on the temperature of the heat treatment some substrates can not be used. Ceramics or glass substrate are usable at high temperatures. Polymer and paper substrate can only be used at sufficiently low temperatures. A concern of this production method are possible residues of the additives in the electrode material which could inhibit the functionalisation of the electrodes, but the production of thick-film electrodes is quite simple and cost effective. The thin-film electrodes are more laborious, but ensure a clean and pure electrode surface. [29]

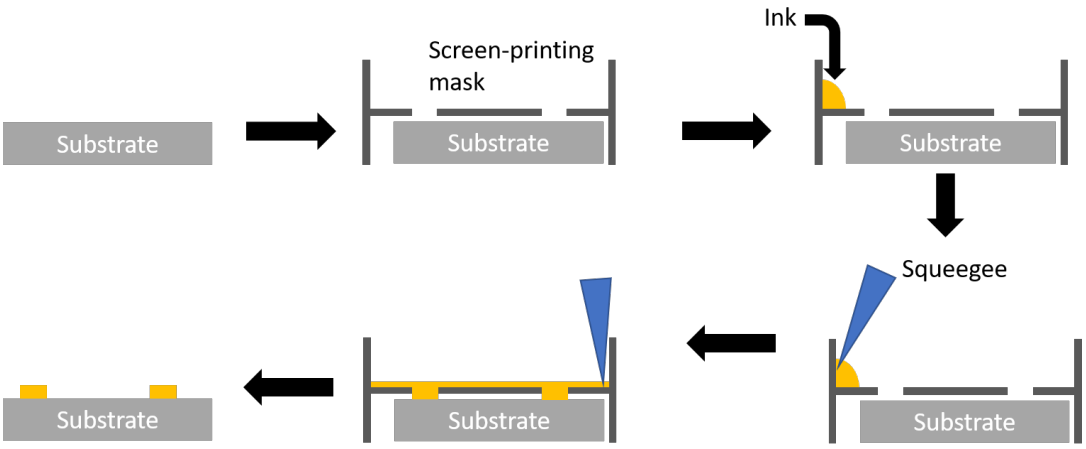

Figure 2.20: Screen-printing process

Electrode preparation

A completely clean surface is needed to guarantee the formation of a reproducible functionalisation. Adsorption of other organic materials to the surface can cause defects in the monolayer or reduce response signals to the analyte molecules and inhibit the measurement greatly. In literature several different methods are described to achieve a clean surface. The methods with the best results are electrochemical and chemical cleaning. In electrochemical cleaning a voltage sweep with potassium hydroxide, CV with sulfuric, and CV with a mixture of nitric acid and hydrogen peroxide are described as best choices [38, 39]. For chemical cleaning the best results were achieved by a treatment with a mixture of potassium hydroxide and hydrogen peroxide [38]. There is a concern with using sulfuric acid, because it can possibly cause corrosion of the gold surface and inhibit the cleaning [39]. Further methods which are commonly used to clean gold surfaces are piranha solution, a mixture of sulfuric acid and hydrogen peroxide, and oxygen plasma cleaning [40, 41].

Surface Functionalisation

The functionalisation of the electrodes depends on the used electrode material. Noble metals can easily be functionalised with thiols. The sulfur head can bind to the metal surface and form a monolayer. These are called self-assembled monolayers (SAM). Gold is the most used metal for the formation of these monolayers, because it is very stable, easy to pattern and has a high affinity to bind thiols. The formation of the thiols is also studied on other metals, such as copper, silver and platinum. Bondings to copper and silver are less stable than gold and are oxidised more easily. On platinum also dense monolayers form, but the formation is less studied and the material is not used that often because of its cost. [42]. When the alkane thiols bind to the surface they form a dense monolayer with the sulfur-group on the surface and the hydrophobic tail standing up. These layers can be formed with thiols of the same length as shown in figure 2.21a or heterogeneous, with differing tail length as depicted in figure 2.21b. The stability of the monolayer can be increased if monomers with multiple thiols is used and can bind via multiple sites onto the metal surface, as shown in figure 2.21c. [29, 43]

The functional group on the other end of the monomer is of great importance

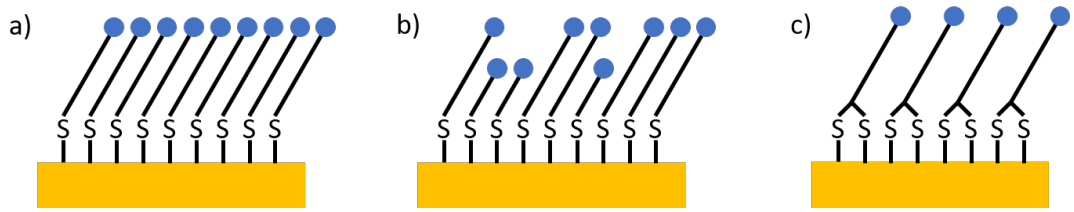

Figure 2.21: Formation of different thiols in self-assembled monolayers; a) Homogeneous monolayer with thiols of the same length; b) heterogeneous monolayer with thiols of different lengths; c) homogeneous monolayer with thiols with multiple binding sites

for the further functionalisation of the biosensor and binding of the receptor molecule. Figure 2.22 gives an overview of different end groups and the pathways of their activation. In many cases the carboxylic acid group is used and the reaction path is shown in figure 2.22a. This is activated with a carbodiimide. A highly reactive and unstable intermediate is formed. NHS or Sulfo-NHS is added to react with this intermediate and increase the stability. The molecule which should bind with this activated carboxylic acid group has to contain an amine group and is bound by forming an amide. When the end group of the alkane thiol is a hydroxy group, the activation is performed with a carbonyldiimidazole (CDI) as depicted in figure 2.22b. This forms a reactive intermediate, which can react with an amine to form a carbamate. CDI can also be used to activate carboxylic acid groups to form an amide as shown in figure 2.22c. [29, 43]

The functionalisation of graphite electrodes differs little from the strategies for noble metals. The carbon electrodes can be functionalised either non-covalently with pyrene, which can bind via pi-stacking, as shown in figure 2.23b. The functional groups of these pyrenes can then be activated with the same strategies as depicted in figure 2.22. For a covalent attachment of the receptor molecules the edges of the graphite are oxidised chemically or electrochemically. This introduces different functional groups, such as carboxylic acid or hydroxy groups, to the graphite electrode as depicted in figure 2.23a. These can then be further activated as shown in figure 2.22. [29, 43]

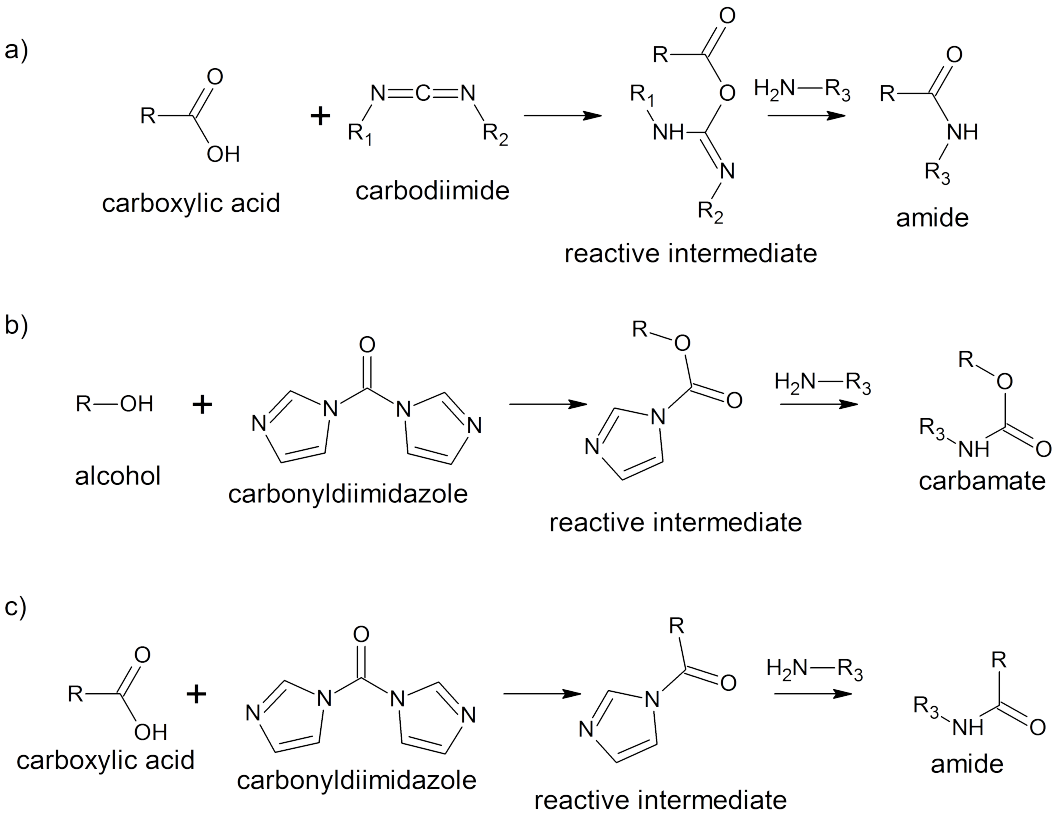

Figure 2.22: Crosslinking strategies for different end groups: a) crosslinking to carboxylic acid group with a carbodiimide; b) crosslinking to an alcohole group with carbonyldiimidazole; c) crosslinking to carboxylic acid group with a carbonyldiimidazole

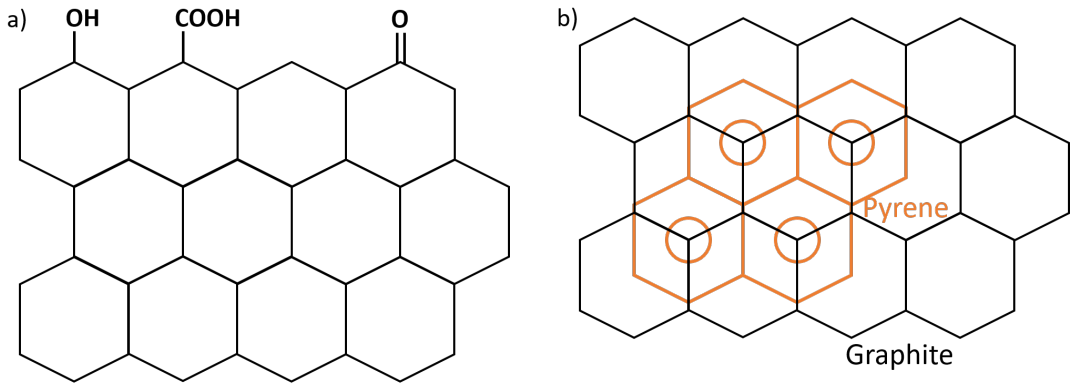

Figure 2.23: Binding methods on graphite electrodes; a) covalent binding with oxidation of graphite sheet edges; b) non-covalent binding with pyrene pi-stacking on the graphite sheet

Receptor Molecules

As mentioned previously a working recognition element of a biosensor needs a capture molecule, which binds the molecule of interest on the surface, or an enzyme, which catalyses a reaction with the biomarker molecule. For the affinity binding of the analyte many different receptor molecules have been reported, such as: antibodies, MIPs, and aptameres. Antibodies are proteins consisting of amino acids. The basic structure of an antibody is depicted in figure 2.3. Antibodies consist of a long chain of amino acids, called heavy chain, and a short amino acid chain, called light chain. The upper part of the antibody with the light chain is called $F(ab)_2$ region and is responsible for the binding of the antigen. The lower region is called Fc region. Antibodies are dimers of heavy and light chains linked with a disulfide bridge. The $F(ab)_2$ region bind the antigen because of the specific 3-dimensional structure and functional groups which can bind only very specific antigens or biomolecules very similar to the antigen. MIPs are similar to antibodies, but they are not made of amino acids. They are made artificially with polymers. The production method is depicted in figure 2.24. Monomers of the used polymers with functional groups are added to the antigen and bind specifically to the biomolecule. Next, the functional monomers are polymerised with other non-functional monomers. After the polymerisation the antigen is washed out of the formed cavities. These can now specifically bind the antigen and work in the same way as antibodies. MIPs for different biomolecules can be easily gained, but they exhibit a worse specificity than antibodies. Aptamers are small DNA sequences which form three dimensional structures which can bind specific molecules. The big advantage of aptamers is that they can be easily reproduced with the help of DNA replication in the laboratory, but the aptamers also have a worse specificity in comparison to antibodies. [29]

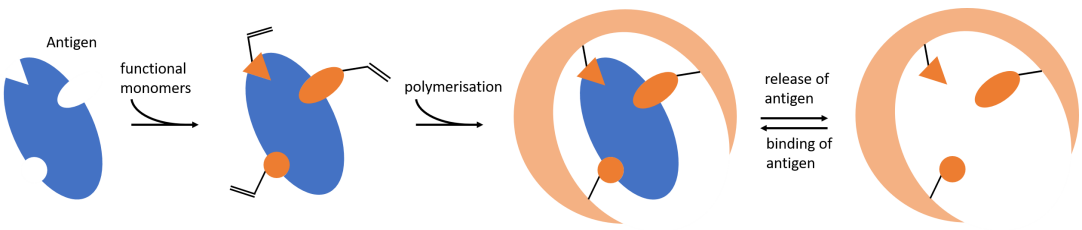

Figure 2.24: Process of MIP production

For several small biomolecules, such as lactate, antibodies are not available. In these cases enzymes are used which catalyse a chemical reaction. The most common enzymes which are used are oxidases, dehydrogenases, hydrolases and lyases. Oxidases are enzymes which oxidise a specific small molecule, use up oxygen and produce either hydrogenperoxide or water with the help of a cofactor. Which cofactor is needed, depends on the enzyme. Several common oxidases, such as glucose oxidases and galactose oxidases, require Flavine adenine dinucleotide as cofactor. Dehydrogenase enzymes also promote a redox-reaction. This enzyme promotes the transfer of a hydride ion between a secondary alcohol and a cofactor. Nicotinamide adenine dinucleotide is the required cofactor for several common dehydrogenases, such as alcohol dehydrogenase or glucose dehydrogenase. Oxidases and dehydrogenases catalyse redox-reactions and can be easily used in electrochemical sensors. Either the electrochemically active products are used for the detection or the electrons from the enzymatic reaction are detected directly, as in third generation amperometric sensors. Hydrolases are enzymes which promote the hydrolysis of chemical bonds. These can be for example ester bonds, then they are called esterases, or of peptide bonds, then they are called proteases. The enzymatic reaction is not a redox-reaction and cannot be detected directly with electrochemical methods. In this case the substrate of the enzymatic reaction is not electrochemically active and can be used in an electrochemical reaction after the hydrolysis. An example for this are amperometric sensors with alkaline phosphatase (ALP). The ALP catalyses the hydrolysis of p-nitrophenyl phosphate by taking up a water molecule. This produces a phosphate molecule and a p-nitrophenol. Under the alkaline conditions the p-nitrophenol is deprotonated to p-nitrophenolate and can be irreversibly oxidised at a potential of 0.95 V. [44]

2.3.3 Electrochemical Sensors

Sensors based on Amperometry

The analysis method of choice for very small molecules is an enzymatic biosensor employing amperometric readout. This type of sensors has been available for years and the method has been refined and improved over the years. The different stages of amperometric sensors have been categorized in generations by

the developers. [29]

The most simple design of a first generation of amperometric biosensors is shown in figure 2.25. The enzyme is immobilised on the electrode, either by a covalent or non covalent interaction. The enzyme takes up the lactate and oxidises it to pyruvate. During this reaction oxygen is reduced to hydrogenperoxide, which is transported to the electrode surface by diffusion. There, the peroxide is oxidised and an electron is transferred to the surface. This creates an electrical current, which can be measured and is proportional to the analyte concentration. The biggest advantage of this type of sensor is its easy production because it requires very few functionalisation steps. However, the production of hydrogenperoxide makes the sensor dependant on the oxygen concentration in the solution. Another drawback is the diffusion of the molecules to the electrode surface which can result in long response times.

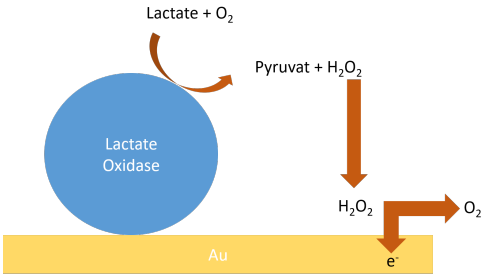

Figure 2.25: First generation amperometric biosensor

The structure of a second generation amperometric sensor is shown in figure 2.26 and is very similar to the first generation sensor. The only addition is the mediator. This substance, for example Prussian Blue, takes up the electron from hydrogenperoxide and transports the electron to the electrode surface. With this setup the sensor becomes less oxygen dependent because of the following reaction with the mediator, but still has a rather long response time because of the diffusion process. Another problem can arise if the mediator is not covalently bound to the electrode surface and, therefore, can dissolve during the measurements. With each washing step more and more mediator is lost and influences the amperometric measurement.

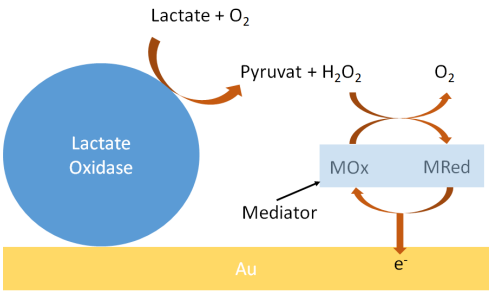

Figure 2.26: Second generation amperometric biosensor

The most important addition in the third generation of amperometric sensors is the direct electrical connection of the active site of the enzyme with the electrode (figure 2.27). When the analyte is oxidised by the enzyme, the electron is directly transported via carbon-nanotubes or other electrical conductive connectors from the active site to the surface. With this setup the response of the sensor is very fast and there is no dependence on the mediator or oxygen. The greatest disadvantage is the costly and complex functionalisation of the surface.

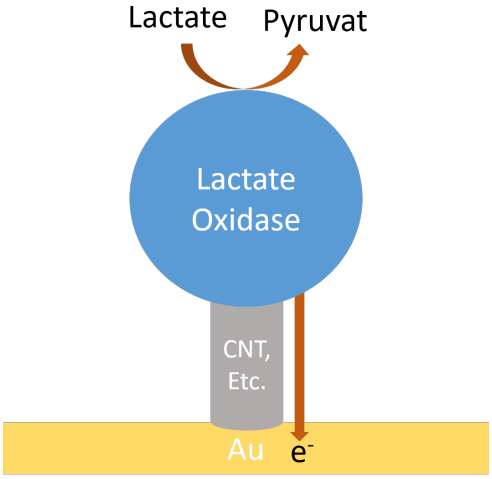

Figure 2.27: Third generation amperometric biosensor

Sensors based on Electrochemical impedance spectroscopy

With the help of EIS surface conditions and reactions on an electrode can be characterised. Biosensors based on EIS can utilise either faradaic or non-faradaic processes. In case of the non-faradaic biosensor no redox-active substance is available in the measurement solution. When the antigen is captured on the

electrode surface, only the change in the electrode capacitance is recorded. [30] When using a faradaic EIS-biosensor, a redox-couple is necessary in the measurement solution. This redox-active substance can be oxidised and reduced by an electron transfer to and from the electrode surface. When an antigen is bound on the electrode surface, this electron transfer is inhibited and the charge transfer resistance increases.

In the solution there has to be a redox-couple, for example a mixture ferro-/ferricyanide. The most simple way for EIS is to work at the standard potential. For this method the reduced and the oxidised states have to be present in the same concentration in the solution and the DC current has to be zero. Additionally, an alternating current with a very low amplitude (around 5 mV) is applied. The impedances are measured in a frequency range of 100 kHz to 10 mHz. When the AC voltage is applied, the reduced state is oxidised and oxidised state is reduced, depending on the polarization of the electrodes.

An overview of the electrical elements to model the electrochemical process on the electrode surface is depicted in figure 2.28a. The most important parameters are the solution resistance (R_S), the charge transfer resistance (R_{CT}), the double-layer capacitance (C_{DL}) and the Warburg impedance (Z_W). The equivalent circuit is depicted in figure 2.28b. In the case of additional features on the surface, for example pores or multiple layers, the model has to be expanded. [30]

The solution resistance represents the ohmic resistance of the solution. An electrical double layer is formed at the charged metal-solution interface. Ions in the solution keep a well defined distance from the electrode surface, which form a double-layer and give rise to the double-layer capacitance. The charge transfer resistance describes how much the rate of the electron transfer is suppressed. In the case of most biosensors capture molecules such as antibodies or aptamers are immobilised on the gold surface. The target molecule in the solution binds to the capture molecule and the charge transfer resistance increases proportional to the analyte concentration. The Warburg impedance describes the effect of diffusion of the redox-probe to the surface, which limits the current flow. Figure 2.29 depicts a curve as an example for an EIS measurement. The charge transfer resistance is the diameter of the semi-circle and can be calculated by fitting a curve through the measured points based on the equivalent Randles circuit (figure 2.28b). [29, 30]

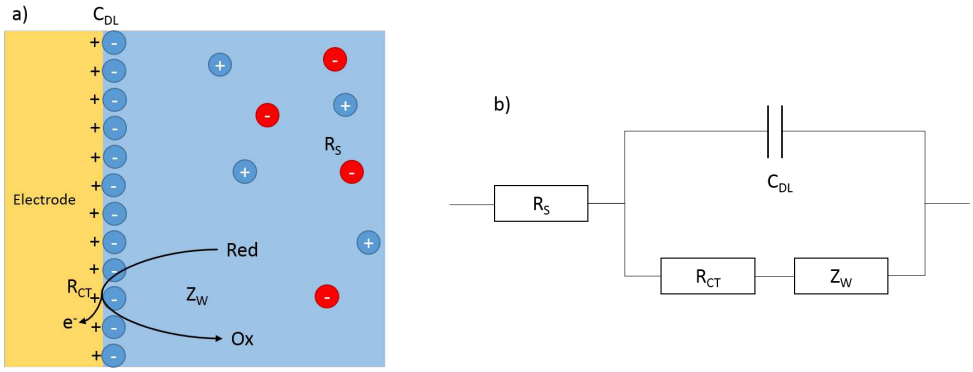

Figure 2.28: a) Overview of the electrical elements to model the redox-process on the surface, b) Equivalent Randles circuit

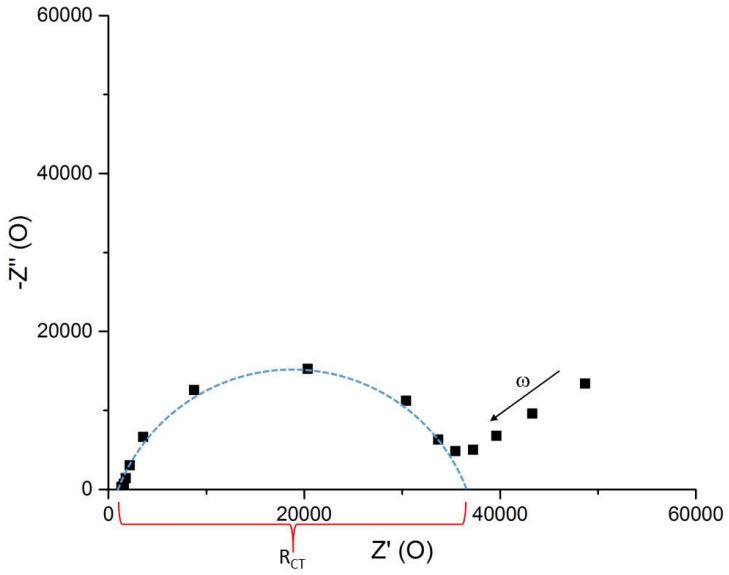

Figure 2.29: Schematic EIS-curve with inserted semi-circle and R_{CT}

2.4 Disposal, preparation and recycling of bioelectronics

After the use of biosensors for POC testing they are considered electronic waste. For the waste management of biosensors similar approaches as used for electronic circuit boards can be utilised. These are: disposal, preparation for re-use and recycling of the materials. [45] Disposal means that the materials cannot be recycled and used for manufacturing. The electronic waste would end up in a landfill. Preparation of re-use in the case of biosensors would mean, that

either the sensor itself is regenerated or the covalently bound biofunctionalisation is detached from the electrode structures. The regeneration of biosensors is described extensively in literature [46]. For this process the sensor is washed with either high acidic solutions, high basic solutions, aqueous solutions with high salt concentrations, aqueous solutions with low salt concentrations or with apolar solutions. These methods promote the breaking of the antigen-antibody binding. The binding sites are once again available to bind the analyte from new samples. Depending on the functionalisation methods the signal loss can go up to 50 %, which would render the sensor completely useless. The detachment of self-assembled monolayers and the cleaning of gold electrodes is also researched in great detail [47, 38]. The removal of the SAMs is achieved either chemically or electrochemically. For the chemical desorption strong acids, e.g. piranha, or oxidation agents, e.g. oxygen-plasma, are used to remove the biofunctionalisation and leave the gold electrodes intact. For electrochemical methods diluted acidic or basic solutions are used and additionally oxidising currents are used to desorb the covalently bound thiols from the gold electrodes. Lastly, the materials used in the biosensor can be recycled. The sensor consists of the functionalisation, the electrode materials and the substrate. The functionalisation can not be recycled because it is destroyed in the recycling process. Also, because of long time periods between the use of the biosensor and the recycling process, the receptor molecules on the sensor will most likely have lost their functionality in ambient conditions. The recycling of precious metals are very well researched and already applied in the recycling of printed circuit boards [45]. The whole recycling process consists of several steps. First, is a pretreatment, which consists of a dismantling of the boards and a shredding or pulverizing process to reduce the size of the materials. The particles are then separated by different physical methods. These methods are based on the different material properties, such as density and magnetic properties. Next, the metals are extracted by leaching processes. Improving the different extraction methods and developing new methods are highly researched topics [45]. The processes range from simple methods, such as melting of the metals, to more complex ones, such as leeching with microorganisms. After the extraction the metals are purified and can be reused for the production of electronic devices. The recycling of the substrate material depends on the material. Ceramic substrates are hardly recycled as literature indicates [48, 49]. When ceramics are recycled, they can only be used in

coarse ceramics. In most cases the waste ceramics are used as filling materials in road construction. The recycling of glass is very common and recycled glass can be smelted and reused nearly indefinitely. The removal of impurities is one of the major obstacles in the glass recycling process [49]. The recycling of polymer based substrates depends strongly on the kind of polymer. Often the different kinds of polymers are collected all together, which makes the recycling process more difficult. In some countries PET bottles are collected and the old bottles can be easily recycled. In the case of a mixture of polymers, either the polymers can be separated because of the their physical differences or they are separated in the course of a solvent base separation process. Both processes are time, cost and energy consuming [49]. Paper is one of the most recycled materials. It is considered that paper can be reused for the production of recycled paper five to eight times. The production of paper consumes less energy in comparison to glass or ceramic and it is a sustainable resource in comparison to PET [49].

2.5 Limitations of ferro-/ferricyanide in EIS sensors

Immunosensors based on EIS suffer from some shortcomings and some researchers even concluded that EIS will never become a reliable detection method for biomolecules. The biggest issue is the stability of the sensor surface and the measurement signal [50]. Bogomolova et al. have shown this instability issue with an EIS-sensor specific to Thrombin [51]. In their experiments, the R_{CT} increased either with the binding of the analyte or with multiple measurements. Other studies suspected that the ferro-/ferricyanide redox-couple itself is the cause of these instabilities [52, 53]. Lazar et al. have thoroughly investigated the effect of ferro-/ferricyanide on gold electrodes. At commonly used concentrations of 1 mmol L^{-1} ferro-/ferricyanide in PBS buffer, the R_{CT} increased over a time period of about 200 min and then started to decrease. The resistance dropped over the next 500 min without reaching a constant value. Lazar et al. assumed that the ferro-/ferricyanide exchanges one of its ligands with a water molecule and releases cyanide. In literature it is reported that cyanide solutions can dissolve gold [54]. Dijksma et al. reported that even surface modification, such a self-assembled monolayer does not protect the gold surface. Over long periods of time the ferro-/ferricyanide corroded the gold surface and as a result the monolayer desorbed, which led to a decrease of the R_{CT} [53].

2.6 ELISA

The most commonly used method for the quantification of biomarkers in biological samples is the ELISA. An immunoassay is a term for all assays which are used to identify and or quantify an analyte from a liquid sample with a binding of an antigen to an antibody. The analyte can be either the antigen or the antibody. As the name ELISA implies, an enzyme is linked to an antibody which is used in the assay. This enzyme is responsible for the signal generation when the antigen-antibody interaction takes place. Depending on the enzyme this signal can be a change in colour, a fluorescence or a chemiluminescence. The usual types of ELISA are: direct, indirect, sandwich, competitive and reverse ELISA. The differences between these types of ELISA are how the antibodies and antigens are bound to a solid surface. The basic process of the direct ELISA is shown in figure 2.30. The antigen of interest is bound to the solid surface. In a subsequent step, an antibody with a covalently attached enzyme is added, and binds via protein-protein interaction to the antigen molecules, which are attached to the surface. Next, a substrate is added which can be processed by the enzyme. The product of this reaction creates the signal which can be a colour change. This change can be quantified by spectrometry.

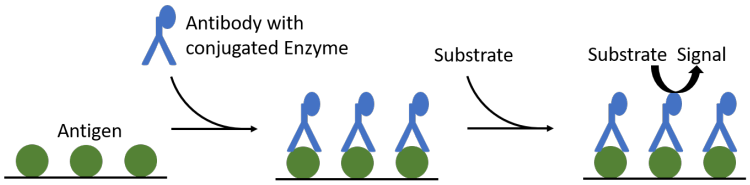

Figure 2.30: Schematics of a direct ELISA

The main difference between a direct and indirect ELISA is that the enzyme is linked to a secondary antibody. The schematics in figure 2.31 shows an overview of the process. The beginning is very close to the direct ELISA depicted in figure 2.30. The antigen is fixed on the surface. Subsequently, a primary antibody, which can bind to the antigen, is added. This time the antibody does not have a conjugated enzyme for the signal generation. A secondary antibody which can bind to the presented primary antibody is added. The enzyme for the signal generation is linked to this secondary antibody and can produce the

signal after the binding to the primary antibody. This method is used mostly because of flexibility and economical reasons. The primary antibody can be easily changed and does not have to be linked to the enzyme. Only the secondary antibody, which can bind to a multitude of different antibodies, needs the linking. In this way fewer antibodies need the enzyme labeling and the assay concept can be used for different applications. A disadvantage of this method is, that it needs more steps during the preparation.

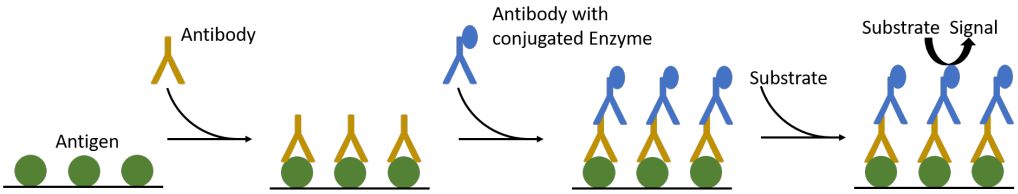

Figure 2.31: Schematics of an indirect ELISA

Sandwich ELISA is used to detect antigens from a liquid sample. As seen in figure 2.32, a capture antibody is presented on the solid surface. Next, the liquid sample is added, and the antigen of interest is bound by the prepared antibody. Next, the antibody with the conjugated enzyme is added and binds to the analyte via antigen-antibody interaction. After this binding process is finished, the substrate is added and the signal is generated.

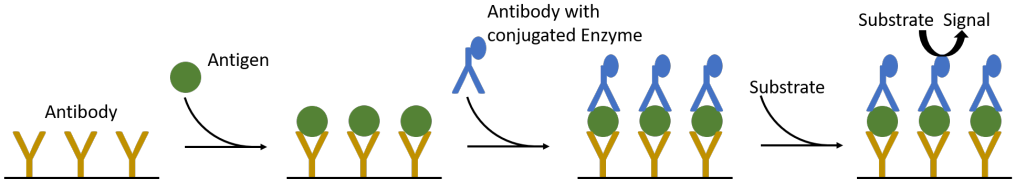

Figure 2.32: Schematics of a sandwich ELISA

The competitive ELISA is the most complex type of ELISA. This method is commonly used when only one antibody is available for the antigen or the antigen is too small to have multiple available binding sites, for example in the case of hormones. How the competitive ELISA works depends on which of the

components is of interest, either the antigen or the antibody. The case, when the antibody is of interest, is depicted in figure 2.33a. The antigen is presented on the surface. Next, the well is incubated with the sample solution. The antibody binds to the antigen on the surface and leaves some unoccupied antigens on the surface. After a washing step the surface is incubated with a solution containing an enzyme labelled antibody which binds to the remaining antigens with an unoccupied binding site. Subsequently, after an additional washing step, a substrate is added and the signal is produced. In comparison, when no sample is added to the well, all the antigen sites are occupied by antibodies with an enzyme label. When in this case the substrate is added, the produced signal is the highest. The higher the concentration of antibody, which can bind to the antigen, the lower the produced signal after addition of the substrate will be.
The second method of ELISA, when the antigen is of interest, is depicted in figure 2.33b. This time, the antibody is prepared on the surface and is incubated with a liquid sample, containing the antigen of interest, and some of the free binding sites are occupied by antigen. Next, after a washing step, a solution with a labelled antigen is added to the surface and bind to the remaining free antibodies. Subsequently, the substrate is added and the signal is produced. Similarly to the previously mentioned method, the more antigen is in the liquid sample, the lower the measured signal will be, because fewer antigen with the conjugated enzyme is bound to the surface.

The signal generation in all the ELISA methods is based on the enzymatic catalysis of a substrate. Depending on the chosen enzyme and substrate, the produced signal can be either a colour change, fluorescence or luminescence. The easiest case is the colour change. The enzyme catalyses the substrate in the solution. The optical density of the colour change is proportional to the amount of enzyme on the surface and, therefore, directly proportional to the analyte concentration. In most cases, three different enzymes are used in this assay: horse radish peroxidase, alkaline phosphatase and beta-D-Galactosidase. A fluorescence based ELISA, is very similar to a colourimetric assay. The enzyme catalyses the reaction of the substrate, but this time, the product of the enzymatic reaction does not change the colour and is fluorescent active. After excitation the produced fluorescence is directly proportional to the concentration of the analyte. Assays based on the chemiluminescence are also very similar to

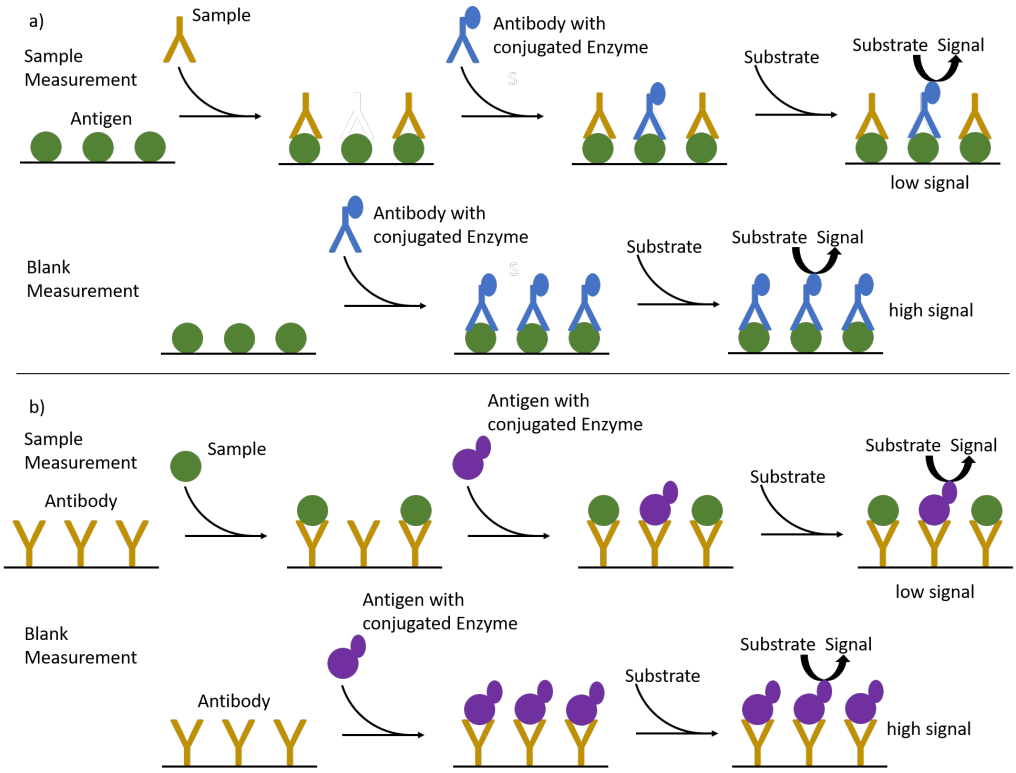

Figure 2.33: Schematics of a competitive ELISA; a) antibody is of interest, b) antigen is of interest

the previously mentioned methods. The only difference is, when the substrate is catalysed by the enzyme, photons are emitted and can be detected. The amount of produced photons is directly proportional to the analyte. [55]

3 Materials and methods

3.1 Chemicals and reagents

AffiniPure Goat Anti-Human IgG Fcy fragment specific antibodies (109-005-098; IgG-Ab) were obtained from Jackson ImmunoResearch Europe Ltd (Newmarket, UK). The human IgG total uncoated ELISA kit from invitrogen (88-50550-88) and cortisol Monoclonal Antibody (F4P1A3) were obtained from Thermo Fisher Scientific Inc. (Waltham, MA, USA). TI-prime was obtained from MicroChemicals GmbH (Ulm, Germany). The negative photoresist maN 1440 and the developer ma-D 533/S were obtained from micro resist technology GmbH (Berlin, Germany). The Ag/AgCl ink for reference electrodes (011464) was obtained from ALS Co., Ltd (Tokyo, Japan). The three-electrode sensors on the ceramic substrate (AC1.W1.R2) were obtained from BVT Technologies, a.s.(Strážek, Czech Republic). 11-mercapto undecanoic acid 95 % (MUA), 3-mercaptopropionic acid 99 % (MPA), 3-mercapto-1-propanol 95 % (MPOH), 16-mercaptohexadecanoic acid 99 % (MHDA), 1-butanethiol 99 % (BT), 1-decanethiol 99 % (DT), 1-undecanethiol 98 % (UT), N-(3-Dimethylaminopropyl)-N'-ethylcarbodiimide hydrochloride 99 % (EDC), ethanolamine hydrochloride 99 % (EA), N-hydroxysulfosuccinimide sodium salt 98 % (Sulfo-NHS), N-Hydroxysuccinimide 98 % (NHS), IgG from human serum with a concentration of 4.87 $\mathrm{mg\,mL^{-1}}$ in buffered aqueous solution, cortisol 98 %, 2-(N-morpholino)-ethanesulfonic acid 99 % (MES), potassium hexacyanoferrat(II) trihydrat 99 %, pentaamminechlororuthenium(III) chloride, L-ascorbic acid 99 %, potassium hexacyanoferrat(III) 99 %, europium(III) chloride 99 %, iron(III) chloride 99 %, iron(II) chloride 99 %, 1,4-benzoquinone 98 %, hydroquinone 99 %, methylene blue, and hexaammineruthenium(III) chloride 98 % were obtained from Sigma-Aldrich (St. Louis, MO, USA).
Other chemicals were of analytical quality and were used without further treatment.

The phosphate buffer saline (PBS) consisted of: 137 mmol L^{-1} NaCl, 2.7 mmol L^{-1} KCl, 10 mmol $L^{-1}$$Na_2HPO_4$, 1.8 mmol L^{-1} KH_2PO_4.

3.2 Preparation of sensors on glass substrate

3.2.1 Thin-film deposition of electrodes

The layout of the sensor for the measurements is shown in fig 3.1. The pads are connected in the following order, top to bottom 1 to 9. 1 is connected to the common reference electrode for five electrochemical cells, 2 connected to the counter electrodes in the cells, 3 and 4 unconnected and 5 to 9 individually connected to the five working electrodes.
The substrate for the electrodes are microscope slides. The slides were cleaned with 5 % soap in tap water in a 60° ultrasonic bath for 1 h. Next, the slides were cleaned with ultrapure water and isopropyl alcohol. In the last cleaning step the slides were dried under a nitrogen stream.
Prior to the spin coating, the slides were dried on 120 °C hot plates. Next, TI-Prime was spin coated onto the slides (t=20 s, 3000 rpm). The primer coated slides were heated to 120 °C for 1 min. After the heating the negative photoresist was spin coated onto the microscope slides (t=20 s, 3000 rpm) and then it was annealed at 100 °C for 1 min. The slides with the photoresist were exposed to light with an energy of about 300 mJ cm^{-2} in the mask aligner. The illuminated slides are incubated in the developer ma-D 533/S for 4 min. To remove the rest of the developer and the dissolved photoresist, the slides were rinsed two times with ultrapure water and dried in a nitrogen stream.
Prior to the deposition of the metals, the slides were treated with oxygen plasma (room temperature, 5 min, 1 mbar, 60 % of maximum power). After the plasma etching about 5 nm chromium and 200 nm gold were deposited in the UNIVEX 450 vacuum evaporator. The lift-off was done by incubation of the slides in DMSO at 70 °C for several hours. Next, the slides were cleaned by ultrasonic cleaning in isopropanol and water for 1 h each. Then the slides were rinsed two times with isopropyl alcohol and dried under nitrogen.

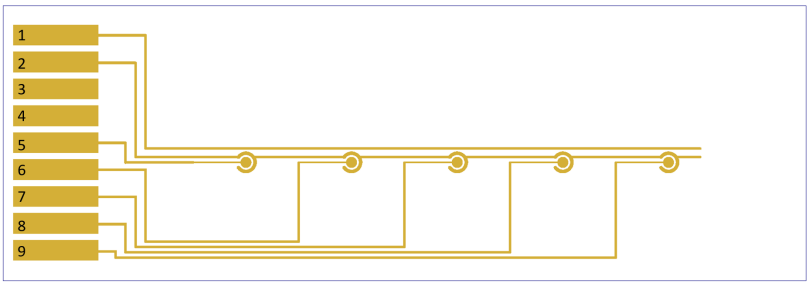

Figure 3.1: Sensor Layout

3.2.2 Cleaning of the electrodes on the glass substrate

The electrodes on the glass substrates are cleaned for 30 min by ultrasonication in water and then in ethanol. Next, the sensors are immersed in piranha solution (mixture of H_2SO_4:H_2O_2 = 3:1) in an ultrasonic bath at 70 °C for 30 min. After the cleaning, the sensors are washed thoroughly with ultrapure water and dried with nitrogen.

3.2.3 Addition of the silver/silverchloride reference electrode

In the case a three-electrode setup is used, the Ag/AgCl-reference electrode has to be applied with a syringe tip by hand on the gold reference electrode. The silver paste has to be annealed at 120 °C for 15 min.

3.3 Electrode preparation on PET substrates

The PET foil, Melinex from the company Dupont, is cut and taped onto the substrate holder. A shadow mask for the deposition of the silver reference electrode is put onto the PET foil. The substrate holder is placed into the UNIVEX evaporator. First, a 15 nm thick adhesion layer of chromium is deposited by thermal evaporation with an deposition speed of about 1 Å s^{-1}. Subsequently, a 200 nm thick silver layer is deposited with a speed of about 3 Å s^{-1}. After the deposition of the reference electrode, the vacuum of the evaporator is broken and the substrate holder is removed. The shadow mask for the silver electrode is removed from the holder without changing the position of the PET substrate and the shadow mask for the gold electrode is positioned over the PET substrate. A 15 nm thick chromium layer and a 200 nm thick gold layer is deposited with the

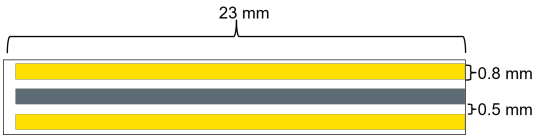

Figure 3.2: Layout of the PET sensor

same deposition speeds as mentioned previously. One production batch consists of 31 sensors with a electrode layout as shown in figure 3.2. All three electrodes have a width of 0.8 mm and a length of 23 mm. The distance from one electrode to the next is 0.5 mm. After the deposition of the electrode materials, the silver electrode has to be chlorinated to produce a Ag/AgCl reference electrode. The sensors are incubated for about in a 5 % sodium hypochlorite solution for about 5 seconds to produce a stable reference electrode. After the chlorination the sensor is washed 10 times with ultrapure water and dried under nitrogen.

3.4 Pretreatment of electrodes on ceramic substrates

First, the sensors AC1.W1.R2 from BVT are washed with deionised water and ethanol. Next, the sensors are dried under a stream of nitrogen. Then a 50 mmol L^{-1} sulfuric acid was applied to the sensors. The potential was cycled from −400 mV to 1400 mV with a scan rate of 100 mV s^{-1} for about 12 cycles. After this electrochemical cleaning process the sensor was washed with deionised water and ethanol. The remaining ethanol is removed by drying under a stream of nitrogen.

3.5 Surface functionalisation

The procedure for the surface functionalisation is shown in fig 3.3. The mentioned functionalisation procedure applies for all used sensors. If changes from this functionalisation procedure were made, they are noted in chapter 4. On the cleaned electrode surface a SAM is formed by immersion in a suitable precursor solution. The different solutions used for the monolayer formation are depicted in table 3.1.

Table 3.1: SAM solutions and parameters for the monolayer formation

Monolayer	concentration	solvent	time
MPA	$10\,\mathrm{mmol\,L^{-1}}$	water	16 h
MUA	$10\,\mathrm{mmol\,L^{-1}}$	95 % ethanol	16 h
MHDA	$10\,\mathrm{mmol\,L^{-1}}$	100 % ethanol	16 h
MUA-MPOH	$0.7\,\mathrm{mmol\,L^{-1}}$ & $0.3\,\mathrm{mmol\,L^{-1}}$	95 % ethanol	16 h
MUA-BT	$0.7\,\mathrm{mmol\,L^{-1}}$ & $0.3\,\mathrm{mmol\,L^{-1}}$	95 % ethanol	16 h
MUA-DT	$0.7\,\mathrm{mmol\,L^{-1}}$ & $0.3\,\mathrm{mmol\,L^{-1}}$	95 % ethanol	16 h
MUA-UT	$0.7\,\mathrm{mmol\,L^{-1}}$ & $0.3\,\mathrm{mmol\,L^{-1}}$	95 % ethanol	16 h

After formation of the SAM, the electrodes are removed from the SAM-solution and washed with their corresponding solvent and ultrapure water. The activation of the formed monolayer is performed with different EDC and NHS concentrations in $60\,\mathrm{mmol\,L^{-1}}$ MES buffer at pH 7.4. The used concentrations are $5\,\mathrm{mmol\,L^{-1}}$, $10\,\mathrm{mmol\,L^{-1}}$, $25\,\mathrm{mmol\,L^{-1}}$, $50\,\mathrm{mmol\,L^{-1}}$, $100\,\mathrm{mmol\,L^{-1}}$, and $250\,\mathrm{mmol\,L^{-1}}$. The sensor is incubated with the activation solution for 1 h. After the activation the sensor is washed with PBS pH 6.0. Then the cortisol specific antibody or Fc-IgG-Ab are bound to the surface. The antibodies are used in concentrations of $100\,\mathrm{\mu g\,mL^{-1}}$ in PBS pH 6.0 and the incubation time is 1 h. Next, the sensor is washed with PBS pH 7.4 and is incubated with a 10 % EA solution in PBS pH 7.4 for 30 min to block the remaining activated carboxylic acid groups. The sensors are then washed with PBS buffer pH 7.4, dried with nitrogen and stored at 4 °C.

3.6 Measurement setup

For the measurements the potentiostat PGSTAT30 (fig 3.4) from the company Metrohm Autolab BV is used. The potentiostat is connected to a sensor holder. The sensor holder of the glass slide sensor is depicted in figure 3.5. When the sensor is used with the sample holder, a sealing ring is pressed down by the cover to form a measurement chamber around each working electrode and the counter electrode with a volume of about 30 µL. The layout and position of the sealing rings are depicted in figure 3.6. The PET sensors used a similar sample holder in which a single PET sensor was fixed. The size of the sealing ring was the same. The sensor on the ceramic substrate only required a commercially available connector for the measurement and no further holder, because the

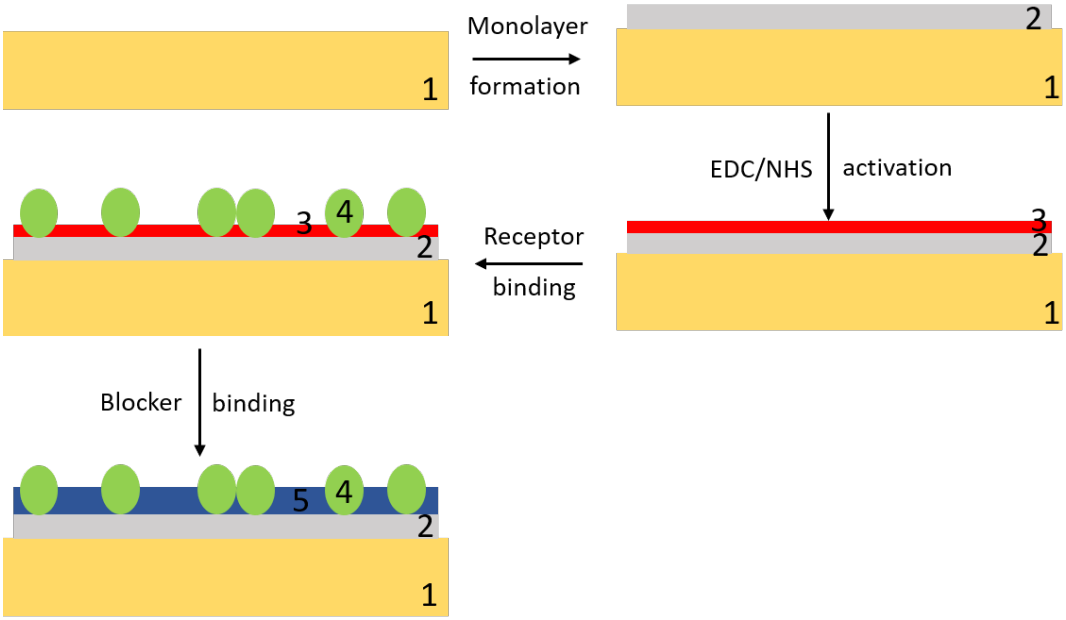

Figure 3.3: Process flow of surface functionalisation comprising of the following components: (1)Electrode surface, (2)Self-assembled monolayer, (3)Activated surface, (4)Receptor molecule, (5)Blocking agents

electrode surface was confined by a passivation layer.

Figure 3.4: Potentiostat Autolab PGSTAT30

3.7 EIS parameters of two-electrode sensors

The EIS spectra of the two-electrode sensors were recorded, unless mentioned otherwise, with a 5 mmol L^{-1} hexacyanoferrat(III) and (II) solution in PBS with

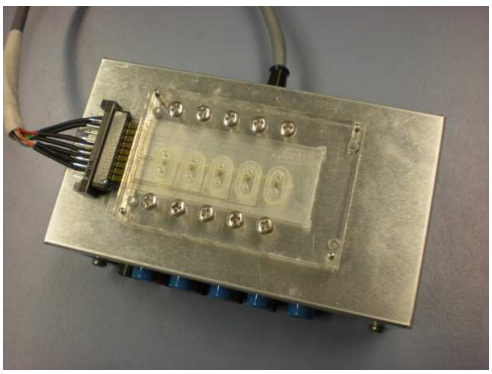

Figure 3.5: Sensor holder of glass slide sensors

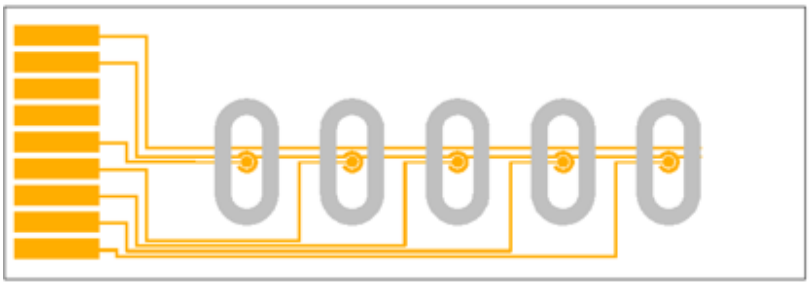

Figure 3.6: Sensor layout with measurement chambers for each working electrode

pH 7.4. An alternating potential with an amplitude of 7.1 mV was applied. The measured frequency range is listed in table 3.2.

3.8 EIS parameters of three-electrode sensors

The EIS spectra of the three-electrode sensors were measured, unless mentioned otherwise, with a 10 mmol L^{-1} hexaammineruthenium(III) chloride solution in PBS with pH 7.4 with an additional DC-bias of −160 mV. An alternating potential with an amplitude of 7.1 mV was applied. The measured frequency range is listed in table 3.3.

3.9 Analysis of EIS resuts

The NOVA autolab software was used to determine the R_{CT} by fitting the parameters of the Randles circuit given in figure 3.7 to the recorded EIS curves. The R_{CT} values of sensors after the incubation with the antigen solution were

Table 3.2: List of measured frequencies in EIS

Nr.	Frequency [Hz]	Nr.	Frequency [Hz]
1	10000	11	78.5
2	6159	12	48.3
3	3793	13	29.8
4	2336	14	18.3
5	1438	15	11.3
6	886	16	7.0
7	546	17	4.3
8	336	18	2.6
9	207	19	1.6
10	127	20	1.0

Table 3.3: List of measured frequencies in EIS

Nr.	Frequency [Hz]	Nr.	Frequency [Hz]
1	1000000	11	143.7
2	412796	12	59.3
3	170399	13	24.5
4	70339.2	14	10.1
5	29035.6	15	4.17
6	11985.6	16	1.72
7	4947.8	17	0.71
8	2042.4	18	0.29
9	843.1	19	0.12
10	348.0	20	0.05

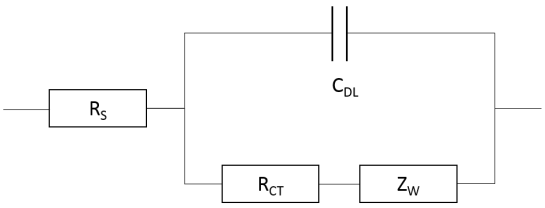

Figure 3.7: Randles circuit; solution resistance (R_S), double-layer capacity (C_{DL}), Warburg impedance (Z_W), charge transfer resistance (R_{CT})

normalised with the charge transfer resistance of the blank measurement R_{CT0} according to equation 12.

$$R_{CT,norm} = \frac{R_{CT} - R_{CT0}}{R_{CT0}} \tag{12}$$

3.10 ELISA Kit

For the analysis of saliva samples, the ELISA kit from the company Invitrogen, sold by Thermo Fisher Scientific, with the name IgG (Total) Human Uncoated ELISA Kit with Plates (catalog number 88-50550) was used. The analysis was performed identical to the experimental procedure mentioned in the product information sheet.

The stock solution of the coating buffer is diluted 1:10 with deionised water. Next, the coating buffer is used to dilute the capture antibody from the kit 1:250. Each used well from the 96 Well Plate which is used for the ELISA assay is filled with 100 µL of the diluted capture antibody solution. The well plate is sealed and incubated over night at 4 °C in the refrigerator. The stock solution of assay buffer A is diluted 1:10 to prepare the blocking buffer. After the over night incubation of the ELISA plate, the sealing and the capture antibody solution is removed from the wells. Each used well is washed twice with 400 µL of washing buffer (PBS solution with 0.05 % Tween 20) and soaked each time for about 1 min. After each solution is removed, the ELISA plate is blotted on absorbent paper to remove buffer solution residues. Next, 400 µL of blocking buffer are added to each well and incubated at room temperature for 2 h. When the incubation time is finished, the blocking buffer is removed and the wells are washed with 400 µL per well of washing buffer twice. The wells are soaked for about 1 min. The ELISA plate is blotted onto an adsorbent paper to remove

residual washing buffer. A human IgG standard vial from the ELISA kit is reconstituted with 400 µL deionised water for about 30 min. The reconstituted standard has a concentration of 200 ng mL^{-1}. The wells A1 and A2 to H1 and H2 are filled with 100 µL Assay Buffer A. To the wells A1 and A2 100 µL of the IgG stock solution are added to each well, to reach a concentration of 100 ng mL^{-1}. The wells are mixed by aspiration, without scratching the well surface. Next, 100 µL of well A1 and A2 are pipetted to B1 and B2 respectively, and mixed by aspiration to reach a concentration of 50 ng mL^{-1}. This procedure is continued five more times (wells C1 and C2 have a concentration of 25 ng mL^{-1}, wells D1 and D2 have a concentration of 12.5 ng mL^{-1}, wells E1 and E2 a concentration of 6.25 ng mL^{-1}, wells F1 and F2 a concentration of 3.125 ng mL^{-1} and wells G1 and G2 a concentration of 1.5625 ng mL^{-1}). The wells G1 and G2 are used as blank wells. To all sample wells, 100 µL of diluted sample solution is added. Next, the ELISA plate is sealed and incubated on a microplate shaker for 2 h. After the incubation, the used wells are washed four times each, as mentioned previously. The stock solution of the detection antibody is diluted 1:250 with assay buffer A and 100 µL are added to all used wells. The ELISA plate is sealed again and incubated on the microplate shaker for 1 h. Then the used wells are washed again four times, as mentioned previously. Next, 100 µL of the substrate solution are added to each well and incubated at room temperature for 15 min. The enzymatic reaction is topped by adding 100 µL of 4 mol L^{-1} H_2SO_4 to each well. The plate is analysed in an EnsPire Plate reader at 450 nm and 570 nm.

4 Results and Discussion

4.1 Functionalisation of two-electrode biosensors

4.1.1 Self-assembled monolayer

As foundation for the surface functionalisation three different monolayers were tested: MPA (fig 4.1a), MUA (fig 4.1b) and a mixed monolayer consisting of MUA and MPOH (fig 4.1c). The length of the monolayer has a major influence on the impedances and on the sensor fouling. The longer the chains of the molecules, the higher is the resistance and the lower the measured current gets. When the layer is too thick, the error in the current measurement increases. Further, when the thiolic acids are too long, it is possible, that no dense monolayer forms. The monomers do not stand upright any more and the end groups on the chain can interact unspecifically with the electrode surface. An advantage of the long chains is, that the unspecific interactions of the sample with the electrode surface is lowered and, therefore, the sensor fouling suppressed. So, the optimal length of the precursor has to be identified to still have an easily measurable R_{CT} and also little sensor fouling.

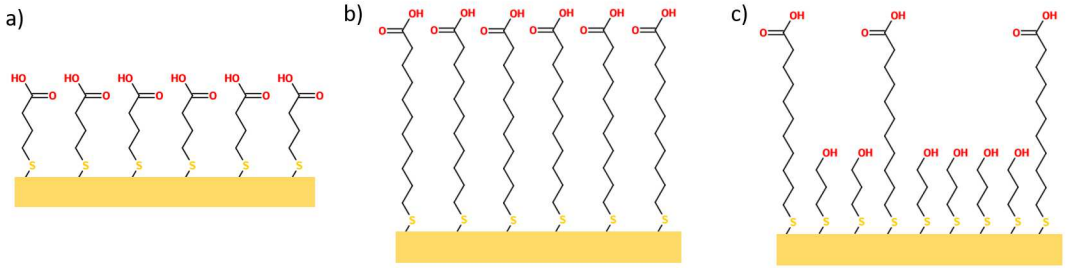

Figure 4.1: a) Homogeneous MPA-SAM on gold electrode; b) homogeneous MUA-SAM on gold electrode; c) heterogeneous MPOH-MUA-SAM on gold electrode

Prior to the functionalisation the EIS spectra of the cleaned gold electrodes were recorded. The Nyquist plots of five different working electrodes are shown in figure 4.2a. The semicircles and the determined impedances in the measured frequency range are quite small. After the cleaning procedure all adsorbed or bound molecules should be completely removed and the R_{CT} should possess reproducibly a very low value. The impedances of each working electrode were recorded in triplicates. The average R_{CT} of the sensors was quite small with about 400 Ω to 700 Ω, as shown in figure 4.2b.

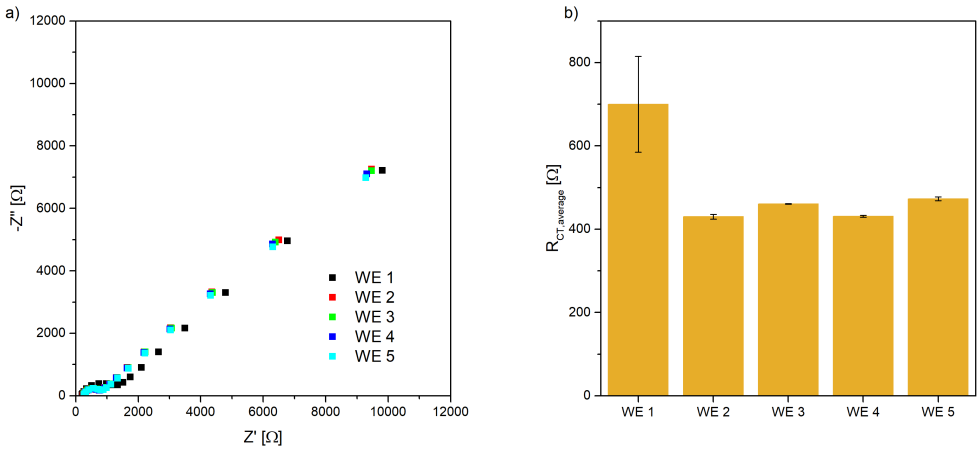

Figure 4.2: Sensor on glass substrate after cleaning, measured with 2.5 mmol L^{-1} ferro-ferricyanide solution in PBS: a) Nyquist plots of the EIS spectra; b) average R_{CT} values of the different WE

To optimise the binding of the monolayer from aqueous solution, different binding times and concentrations have been tested. First, the sensors were incubated in a 1 mmol L^{-1} MPA solution in PBS buffer for 16 h. The recorded EIS spectra of five different WE are depicted in figure 4.3a. The functionalisation of all five working electrodes seemed to be comparable and exhibited a very similar electrochemical behaviour. The R_{CT} of the five WE, depicted in figure 4.3b, were about 12.5 kΩ. In comparison to the gold sensor the R_{CT} value increased by about 20 times. The binding of the monolyer seems to have worked and is quite reproducible.

To check if the monolayer has formed completely, the incubation time of the MPA solution was increased to 22 h. The impedance spectra of the sensors are depicted in figure 4.4. Comparing the determined impedances of this monolayer

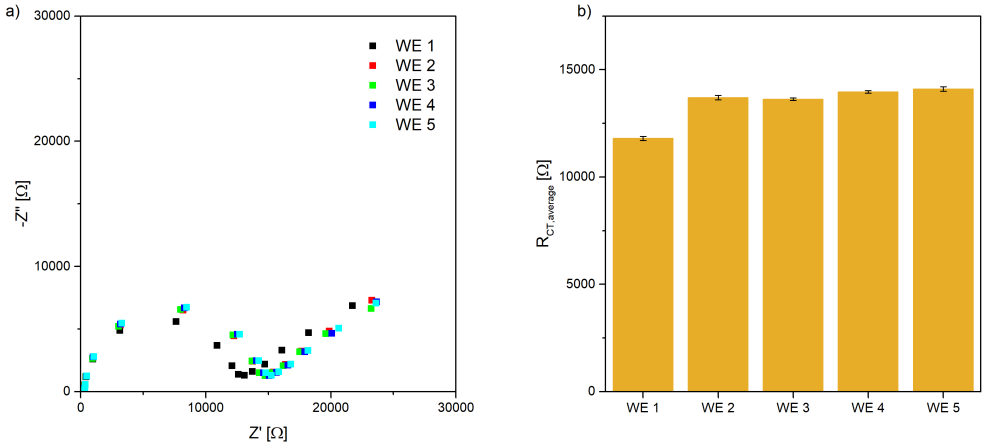

Figure 4.3: Sensor on glass substrate after 16 h of incubation in 1 mmol L^{-1} MPA in PBS, measured with 2.5 mmol L^{-1} ferro-ferricyanide solution in PBS: a) Nyquist plots of the EIS spectra; b) average R_{CT} values of the different WE

with the impedance spectra of the sensor with the 16 h MPA monolayer from figure 4.3a it is apparent that the longer incubation time did not improve the density of monolayer in any significant way. If the monolayer was not completely formed it would be expected that the impedances increase with the longer incubation time. In this case the impedance decreased slightly with the incubation time which can be attributed to differences of the electrodes of the glass slide sensors themselves and not to the incubation time.

A major concern for the assembly of SAM is the formation of multilayers. In literature the use of weak acidic solutions is recommended for the formation of monolayers [56, 57]. The pH of an aqueous solution of MPA was lowered with hydrochloric acid to pH 2 and the gold working electrodes were incubated with the solution for 16 h. The Nyquist plots of the modified working electrodes are depicted in figure 4.5a. A comparison of the EIS spectra of the MPA modified sensors from an acidic solution with the plots from MPA modified sensors from a PBS solution from figure 4.3 did not reveal any clear difference between both functionalisation methods. Also, the R_{CT} of the sensors functionalised by the acidic modification method, shown in figure 4.5b, were nearly the same as the modification from PBS solution. In the case of the MPA monolayer the acidification of the functionalisation solution did not improve the formation of the monolayer in any significant way.

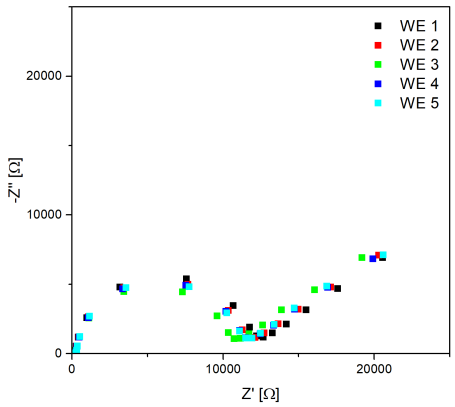

Figure 4.4: Nyquist plots glass slide sensors after 22 h of incubation in 1 mmol L^{-1} MPA in PBS measured with 2.5 mmol L^{-1} ferro-ferricyanide solution in PBS

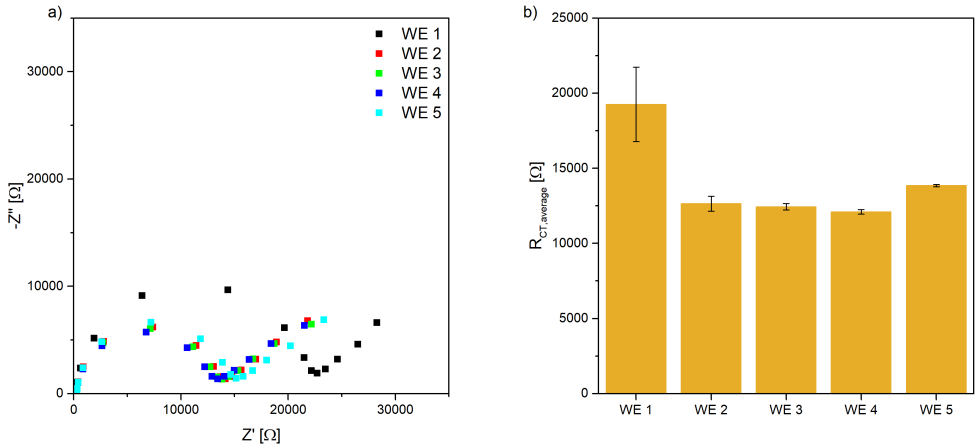

Figure 4.5: Sensor on glass substrate after 16 h of incubation in 1 mmol L^{-1} MPA in PBS with pH 2, measured with 2.5 mmol L^{-1} ferro-ferricyanide solution in PBS: a) Nyquist plots of the EIS spectra; b) average R_{CT} values of the different WE

MPA is dissolvable in water. With the increase of the chain length of the thiolic acids, their solubility in water is decreased. MUA for example can only be dissolved in small amounts in hot water. More apolar solvents such as ethanol have to be used. A homogeneous monolayer of MUA was formed from an ethanolic solution for 16 h and the impedance spectra were recorded, as depicted in figure 4.6. It is immediately apparent that the spectra changed significantly

from the spectra of the MPA monolayers. The recorded impedances are now much larger with an R_{CT} of about 80 MΩ. Also, the semicircle was not fully recorded in the measured frequency range. The lowest used frequency in the recording was 0.05 Hz. Further decrease of the lower frequency would increase the measurement time too much and would not be feasible in a POC test.

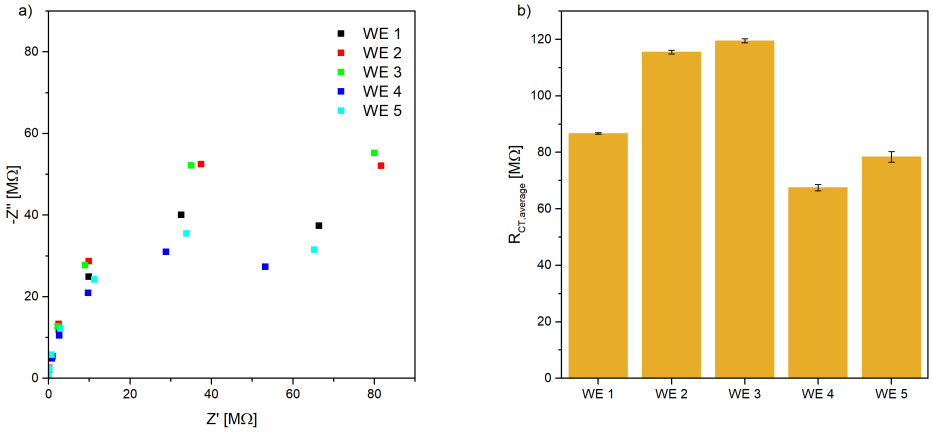

Figure 4.6: Sensor on glass substrate after 16 h of incubation in 1 mmol L^{-1} MUA in ethanol, measured with 2.5 mmol L^{-1} ferro-ferricyanide solution in PBS: a) Nyquist plots of the EIS spectra; b) average R_{CT} values of the different WE

In literature the use of mixed monolayers is recommended to improve the sensitivity and the signal of the biosensors [58]. A mixed monolayer of MUA and MPOH was tested. A glass slide sensor was incubated with a mixture of 0.7 mmol L^{-1} MUA and 0.3 mmol L^{-1} MPOH in ethanol for 16 h. The Nyquist plots of ten different WE, which were functionalised with the heterogeneous monolayer, are depicted in figure 4.7a. The differences between the sensors are immediately noticeable. The determined R_{CT} values range from 1 MΩ to about 20 MΩ. The functionalisation with a mixed monolayer produced quite scattered results and did not exhibit a good reproducibility. With these results the use of a mixed monolayer can not be recommendable for biosensor applications.

As mentioned previously in the discussion of the MPA functionalisation, low acidic solutions can inhibit the formation of multilayers. Adding inorganic acids to the ethanolic MUA solution can reduce the formation of possible multilayers, but there is the possibility, that the acid catalyses the reaction of the free carboxylic acid groups with the ethanol to form esters. The formation of these

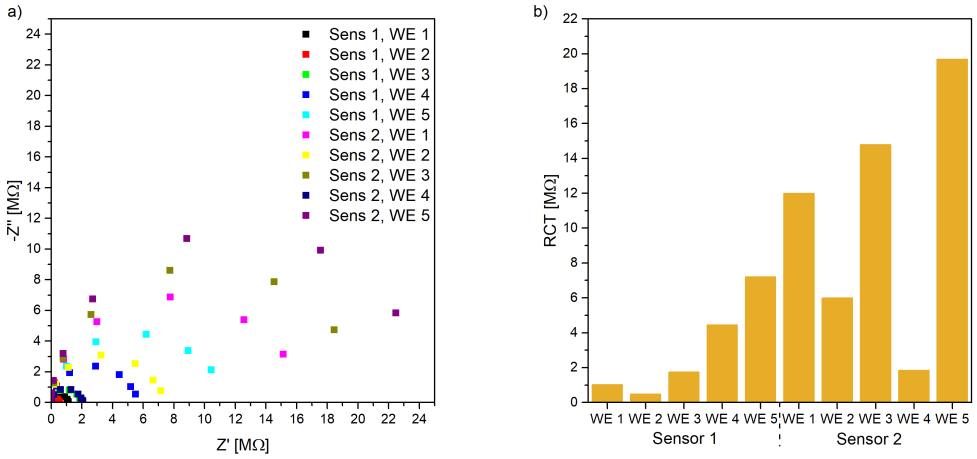

Figure 4.7: Sensor on glass substrate after 16 h of incubation in 0.7 mmol L^{-1} MUA and 0.3 mmol L^{-1} MPOH in ethanol, measured with 2.5 mmol L^{-1} ferro-ferricyanide solution in PBS: a) Nyquist plots of the EIS spectra; b) average R_{CT} values of the different WE

esters can prevent the activation of carboxylic acid groups on the surface with EDC and NHS in the next functionalisation steps. To test the influence of inorganic acids in the functionalisation solution glass slide sensors were functionalised with an MUA monolayer from an acidic 1 mmol L^{-1} MUA solution with ethanol as solvent. The EIS spectra are depicted in figure 4.8a. The form of the Nyquist plots are comparable to the plots of the monolayers formed from an ethanolic solution, as depicted in figure 4.6a. The semicircles do not completely show up in the measured frequency range which was already observed in the previous experiment. Comparing the determined R_{CT}, figure 4.8b, it is apparent that the resistances of WE 1 to 3 are much lower with about 20 kΩ than the other WE of the same sensor and the sensors with the MUA monolayer from the ethanolic solution, figure 4.6b, with about 100 kΩ. This result can have several influences. One possibility is, that there is a difference in the surface roughness of the different WE and, therefore, the formed monolayers differ between the electrodes. This can be disregarded, because the difference between the gold WE functionalised with MPA is much smaller and nearly non existent. Another possibility is that no dense monolayer is formed from the solution and some of the carboxylic acid groups attach themselves to the gold surface. Further, it is possible, that the acidic ethanolic solution did not inhibit

the formation of multilayers completely and the layers differ from WE to WE. All in all, the use of an acidic solution did not improve the reproducibility of the MUA monolayers in any way.

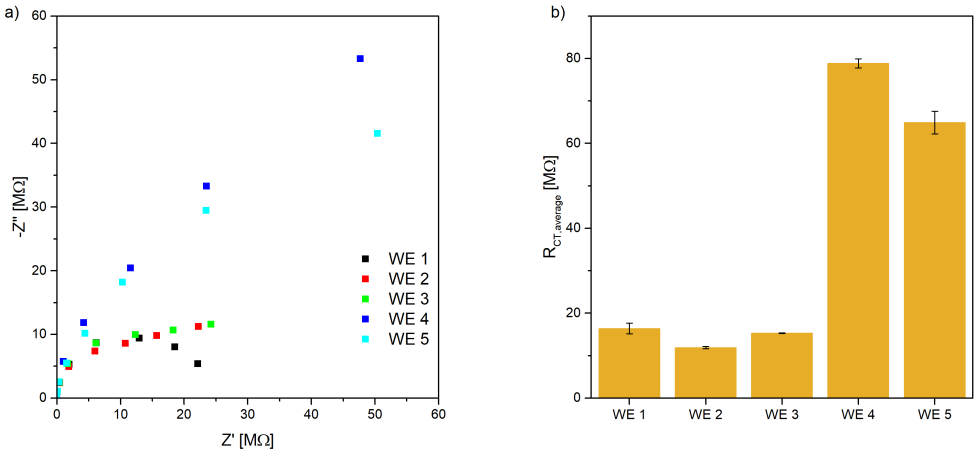

Figure 4.8: Sensor on glass substrate after 16 h of incubation in 0.7 mmol L^{-1} MUA and 0.3 mmol L^{-1} MPOH in acidic ethanol, measured with 2.5 mmol L^{-1} ferro-ferricyanide solution in PBS: a) Nyquist plots of the EIS spectra; b) average R_{CT} values of the different WE

4.1.2 Activation of carboxylic acid groups

After the formation of the monolayer the carboxylic acid groups have to be activated by EDC and NHS, as depicted in the schematics in figure 4.9.

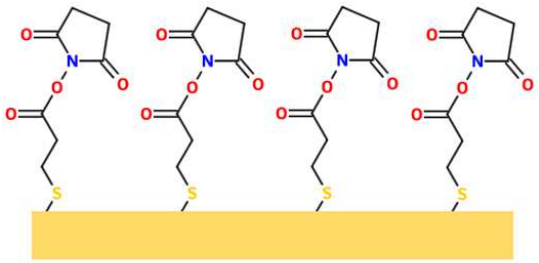

Figure 4.9: Activated MPA monolayer

Sensors with the MUA monolayer and the mixed MUA-MPOH monolayer were activated with a solution containing 10 mmol L^{-1} EDC and 10 mmol L^{-1} sulfo-NHS in an MES buffer solution at a pH of 4.2. The Nyquist plots for the

MUA sensor activated for 1 h are depicted in figure 4.10a. The variation in the impedance spectra of the activated MUA monolayer is still present. Also, the semicircle of the curves are still not completely recorded in the measured frequency range. Comparing the R_{CT} of the activated monolayers from figure 4.10b with the R_{CT} of the MUA monolayer, shown in figure 4.6, it is immediately apparent, that the R_{CT} increased only little with the activation with the carbodiimide. Further, the variation in the impedances of the different activated WE remains high. The R_{CT} of the activated monolayer ranged from 80 MΩ to 150 MΩ, which is slightly higher than the impedances of monolayer prior to the activation. This indicates that the surface changed and the activation of the carboxylic acid groups was successful.

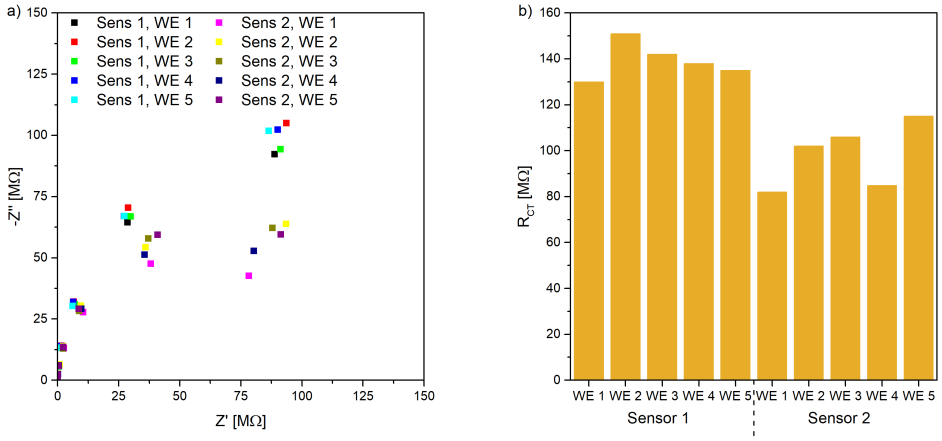

Figure 4.10: Sensor on glass substrate with MUA monolayer, activated for 60 min with 10 mmol L^{-1} EDC and 10 mmol L^{-1} NHS in MES buffer pH 4.7, measured with 2.5 mmol L^{-1} ferro-ferricyanide solution in PBS: a) Nyquist plots of the EIS spectra; b) average R_{CT} values of the different WE

The mixed monolayer of MUA-MPOH was also activated for 1 h with the above mentioned EDC and NHS concentration. The Nyquist plots of the activated sensors are depicted in fig 4.11a. The impedances vary drastically from WE to WE, which was already observed with the monolayer alone, as shown in figure 4.7a. The determined R_{CT} range from about 1 MΩ to about 12 MΩ, as shown in figure 4.11b. The range of the determined R_{CT} values is a little bit smaller than of the monolayer alone, which ranges from 1 MΩ to about 20 MΩ, but with this variation an application as biosensor would not be advisable.

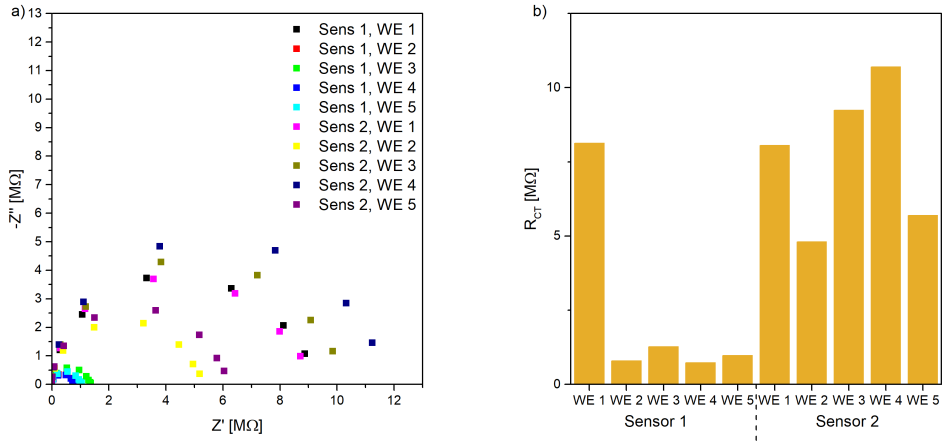

Figure 4.11: Sensor on glass substrate with mixed MUA-MPOH monolayer, activated for 60 min with 10 mmol L^{-1} EDC and 10 mmol L^{-1} NHS in MES buffer pH 4.7, measured with 2.5 mmol L^{-1} ferro-ferricyanide solution in PBS: a) Nyquist plots of the EIS spectra; b) average R_{CT} values of the different WE

Sensors with MPA monolayers have been activated with a 10 mmol L^{-1} EDC and 10 mmol L^{-1} NHS solution in MES buffer at a pH of 4.7. The advantage of using NHS instead of sulfo-NHS is that it bears no charge. The NHS and sulfo-NHS molecules are very small and the binding of these leads to almost no change of the R_{CT}, as was observed with the activated MUA and MUA-MPOH monolayers. The carboxylic end groups of the monlayer have a negative charge and repel the used redox-couple ferro-ferricyanide. The previously used sulfo-NHS also has a negative charge and the activated carboxylic acid groups would keep their negative charge. When NHS is used instead, the monolayer looses its negative charge and does not repel ferro-ferricyanide anymore. This can lead to a decrease of the R_{CT}. When all of the carboxylic end groups of the monolayer are activated, the negative charge is removed completely and, therefore, the measured R_{CT} is the lowest. For the optimisation of the activation process the MPA monolayers were incubated for 30 min, 60 min, 90 min, and 120 min each with the previously mentioned activation solution. The Nyquist plots of these activated monolayers are depicted in fig 4.12a. The EIS spectra of the different activation times are very similar and only exhibit small differences. Comparing the R_{CT} values of the sensors activated with the different time periods in

figure 4.12a, it is obvious, that the lowest R_{CT} are present with an activation time of 60 min, about 5.1 kΩ, or 90 min, about 4.8 kΩ. The highest R_{CT}, about 5.9 kΩ, were recorded when the sensors were activated for 30 min. With this short activation period it seems, that the carboxylic acid groups of the sensor are not fully activated. With activation times of 120 min the R_{CT} increased again to values of about 5.3 kΩ, but is still quite similar to the sensors with an activation time of 60 min. It seems that this activation time is sufficient to fully activate the MPA monolayer. The activated carboxylic acid groups are highly reactive and unstable in aqueous solution. Therefore, the activation time has to be kept as short as possible, otherwise the activated groups can degrade in the aqueous solution over time and the functionality of the sensor could be hampered.

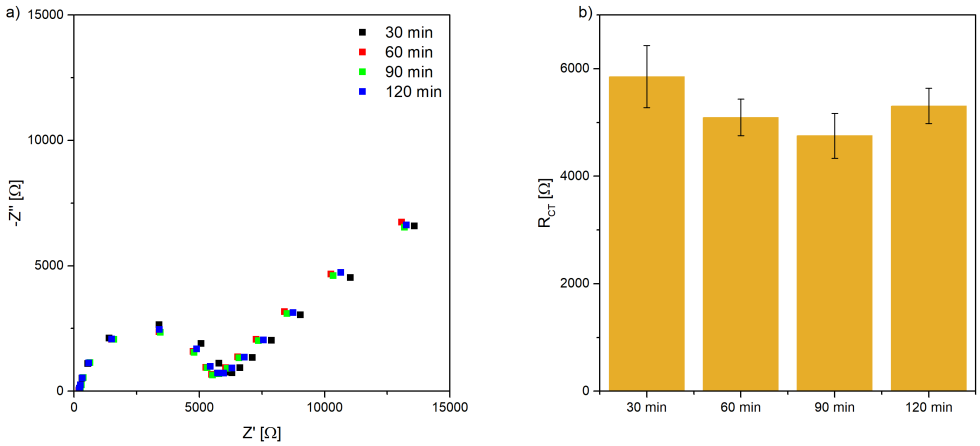

Figure 4.12: Sensor on glass substrate with MPA monolayer, activated for 30 min, 60 min, 90 min, and 120 min with 10 mmol L^{-1} EDC and 10 mmol L^{-1} NHS in MES buffer pH 4.7, measured with 5 mmol L^{-1} ferro-ferricyanide solution in PBS: a) Nyquist plots of the EIS spectra; b) average R_{CT} values of the different WE

4.1.3 Antibody binding

After the activation of the carboxylic acid groups the antibodies were bound to the surface, as illustrated in figure 4.13.

The activated MPA, MUA and mixed MUA-MPOH monolayers were incubated with 30 µL of a 10 µg mL^{-1} cortisol-antibody solution on each WE for 2 h.

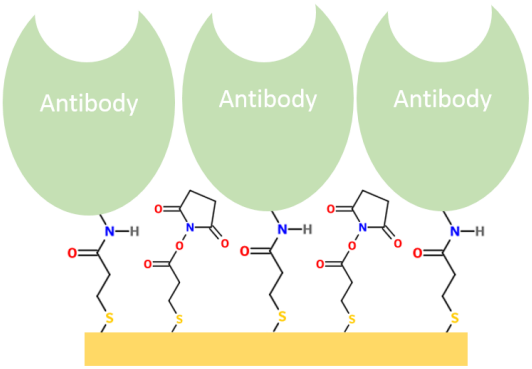

Figure 4.13: Activated MPA monolayer with covalently bound antibodies

The EIS spectra of the sensors with the cortisol antibodies bound to the MPA monolayer are depicted in fig 4.14a. The Nyquist plots of the electrodes only differ slightly from each other. The R_{CT} of the sensors were determined to be about 22 kΩ to 26 kΩ. These values are significantly bigger compared to the R_{CT} of the sensor with the monolayer alone, which were determined to be about 11 kΩ to 13 kΩ. These results indicate, that the binding of the cortisol antibody was successful.

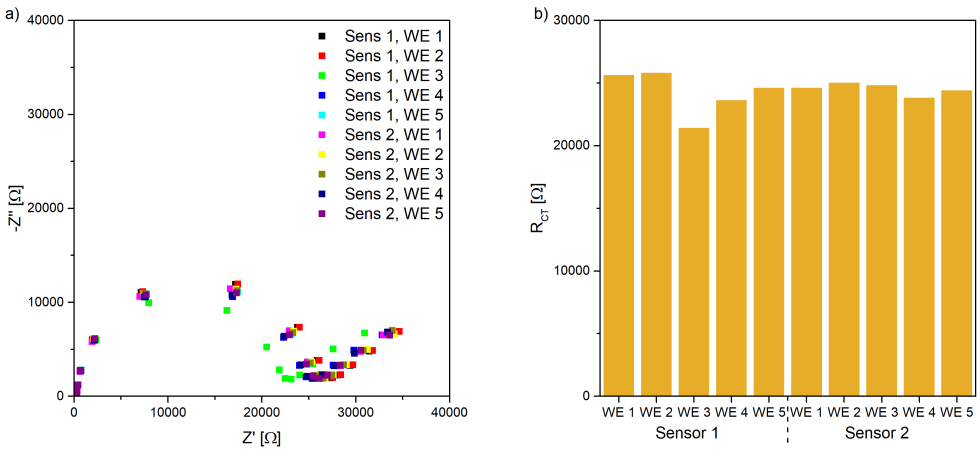

Figure 4.14: Sensor on glass substrate with EDC and NHS activated MPA monolayer, incubated for 2 h with cortisol-Ab, measured with 2.5 mmol L^{-1} ferro-ferricyanide solution in PBS: a) Nyquist plots of the EIS spectra; b) average R_{CT} values of the different WE

The Nyquist plots of the antibodies bound on the MUA-monolayer are depicted in figure 4.15a. The scattering results of the different WE is still noticeable. The R_{CT} of the different sensors, which are depicted in figure 4.15b, range from 60 MΩ to about 115 MΩ. It seems, that the R_{CT} dropped in comparison to the activated MUA monolayer, as depicted in figure 4.10b. The R_{CT} of these sensors was between 80 MΩ and 150 MΩ. The determined resistances of the sensor with the antibody bound to the MUA monolayer are more comparable to the R_{CT} of the sensor with the MUA monolayer alone, which ranged from 80 MΩ to 120 MΩ. Either, the binding of the cortisol antibody was unsuccessful, or all of the measured impedances are within the possible range of variation and can not be utilised to evaluate the success of the functionalisation procedure.

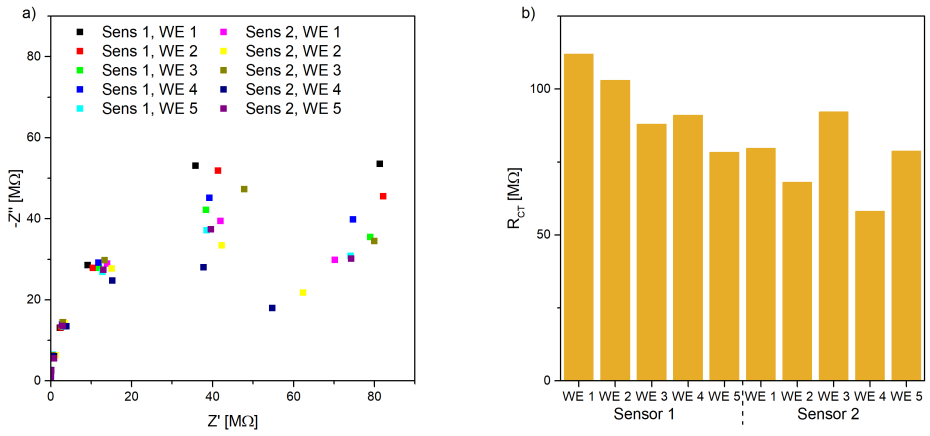

Figure 4.15: Sensor on glass substrate with EDC and NHS activated MUA monolayer, incubated for 2 h with cortisol-Ab, measured with 2.5 mmol L^{-1} ferro-ferricyanide solution in PBS: a) Nyquist plots of the EIS spectra; b) average R_{CT} values of the different WE

The EIS spectra of the mixed MUA-MPOH monolayer with the bound cortisol antibody are depicted in fig 4.16a. The drastic variations in the impedances of the different WE are still observable. Already the formation of the monolayers alone, depicted in figure 4.7, exhibited huge differences. The R_{CT} of the mixed monolayer with the bound antibody range from 3 MΩ to about 21 MΩ, as depicted in figure 4.16b.

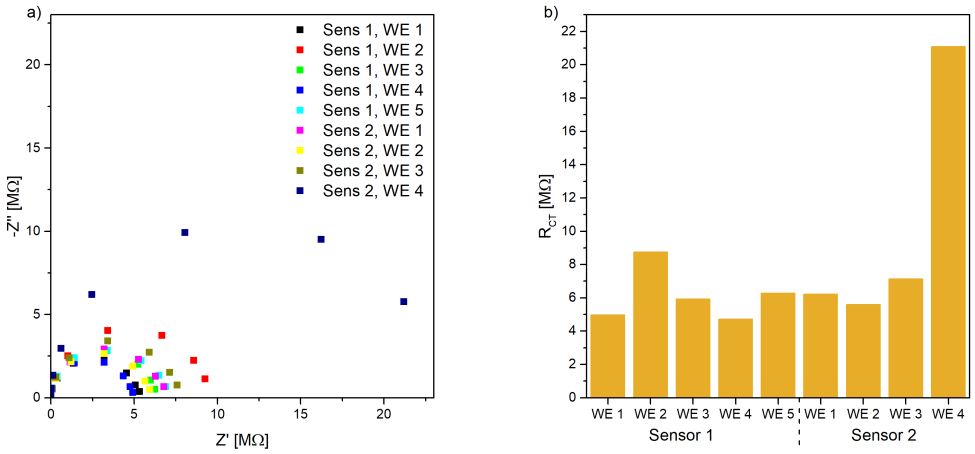

Figure 4.16: Sensor on glass substrate with EDC and NHS activated mixed MUA-MPOH monolayer, incubated for 2 h with cortisol-Ab, measured with 2.5 mmol L^{-1} ferro-ferricyanide solution in PBS: a) Nyquist plots of the EIS spectra; b) average R_{CT} values of the different WE

4.1.4 Blocker binding

After the binding of the antibodies, the remaining activated carboxylic acid groups, which did not bind any antibodies, have to be blocked. After this last functionalisation step the biosensor is finished and is ready for the binding of the antigen. The fully functionalised sensor surface is illustrated in figure 4.17.

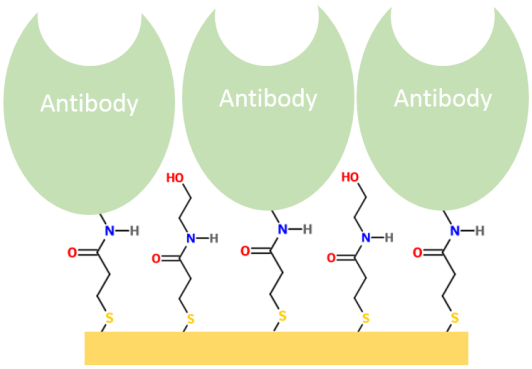

Figure 4.17: MPA monolayer with covalently bound antibodies and ethanolamine as blocker

The sensors were incubated in a 10 % EA solution in PBS for 30 min to block the remaining activated carboxylic acid groups. The Nyquist plots of the fully functionalised MPA based sensors are depicted in figure 4.18a. The spectra of the different WE are very similar and exhibit only small differences from each other. The R_{CT} of these electrodes, which are depicted in figure 4.18b, were determined to be between 18 kΩ and 23 kΩ. It appears that the variation in the R_{CT} increased in comparison to the electrodes with only the MPA monolayer, which are depicted in figure 4.3. Further, the R_{CT} of the sensors appear to have dropped after the binding of the blocker molecule. The sensor prior to the blocking exhibited resistances between 22 kΩ and 26 kΩ. Either the sensors are varying drastically or adsorbed antibodies were removed during the blocking process.

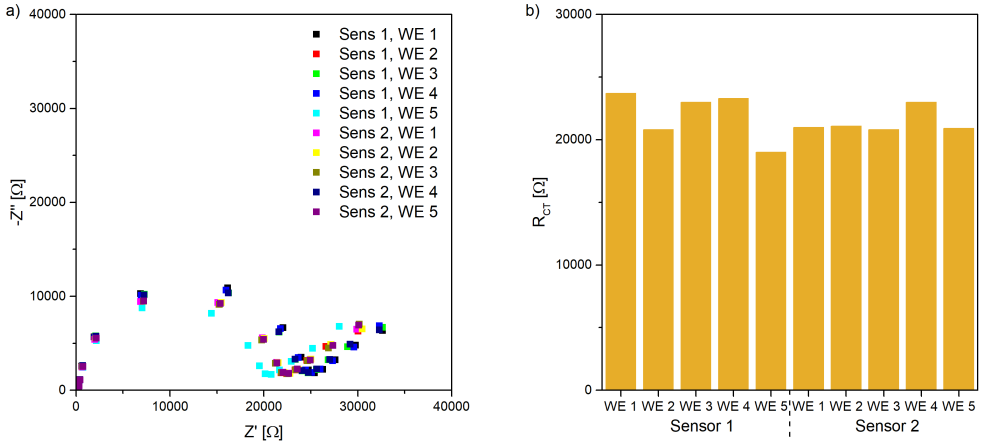

Figure 4.18: Fully functionalised biosensor, MPA/cortisol-Ab/EA, measured with 2.5 mmol L^{-1} ferro-ferricyanide solution in PBS: a) Nyquist plots of the biosensors; b) comparison of the R_{CT} of the fully functionalised biosensor of different WE

In figure 4.19a the EIS spectra of the biosensor with the MUA monolayer after the binding step are depicted. The determined impedance curves of several different sensors, which were functionalised with the same method, are much more comparable with each other. The R_{CT} values, as depicted in figure 4.19b, range from 40 MΩ to 60 MΩ. In all the previous functionalisation steps, the range of the R_{CT} was much wider. There are several possibilities for this result. In the case of the MUA monolayer it is possible that multilayers were present,

which differ from WE to WE and can result in such a wide difference in the R_{CT} values. The activation step, and consequently the antibody binding step, contain highly reactive and unstable functional groups which can hydrolyse in aqueous solution. During the washing steps and the measurement the hydrolysis can occur and widen the range of the determined resistances. After the blocking procedure the sensor should not contain any unstable components any more and should not be effected by the different aqueous solutions. Even with the smaller differences between the WE of the same functionalisation batch, the determined impedances are very high and result in very low currents, which are more difficult to measure correctly in a small POC device. Also, the semicircles are not completely formed in the Nyquist plots which can make the curve fitting more difficult and, therefore, could introduce more variations in the determination of the R_{CT}. Further, with the binding of the antigen the impedances increase even more which would make the previously discussed problems more severe.

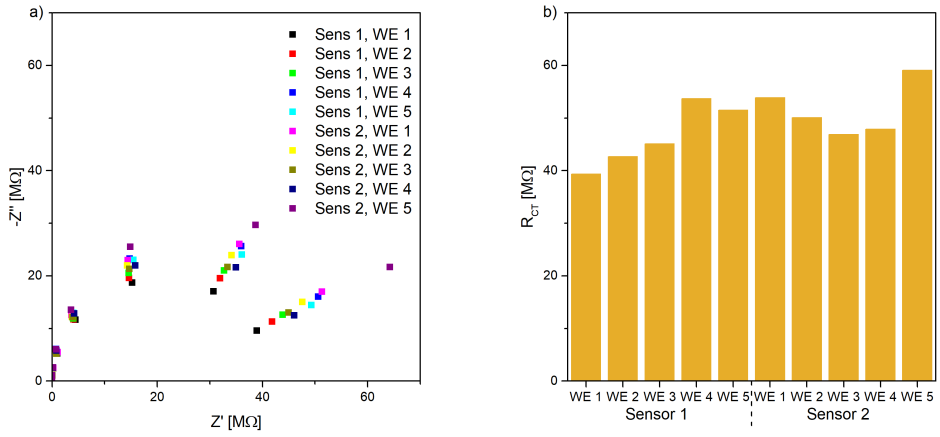

Figure 4.19: Fully functionalised biosensor, MUA/cortisol-Ab/EA, measured with 2.5 mmol L^{-1} ferro-ferricyanide solution in PBS: a) Nyquist plots of the biosensors; b) comparison of the $_{CT}$ of the fully functionalised biosensor of different WE

The Nyquist plots for the mixed MUA-MPOH monolayer after the blocking procedure are depicted in figure 4.20a. With sensors based on this monolayer it is possible to measure the whole semicircle, but the impedances vary too much. The R_{CT} values, as shown in figure 4.20b, can range from 4 MΩ to 17 MΩ. This variation is similar to the results of the previous functionalisation steps and did

not improve after the binding of the blocker. It is very likely that the variation is already introduced during the formation of the mixed monolayer. It is possible, that on some WE more of the short MPOH is bound and, therefore, leads to lower impedances overall. On other sensors the ratio of longer MUA molecules is larger and this leads to sensors with higher impedances. The binding process of the mixed monolayer seems to be random and leads to monolayers with very different electrochemical properties. With the high R_{CT} in the MΩ range and the big variation of the R_{CT} values the biosensors based on the mixed MUA-MPOH monolayer can not be recommended for the application in a POC device.

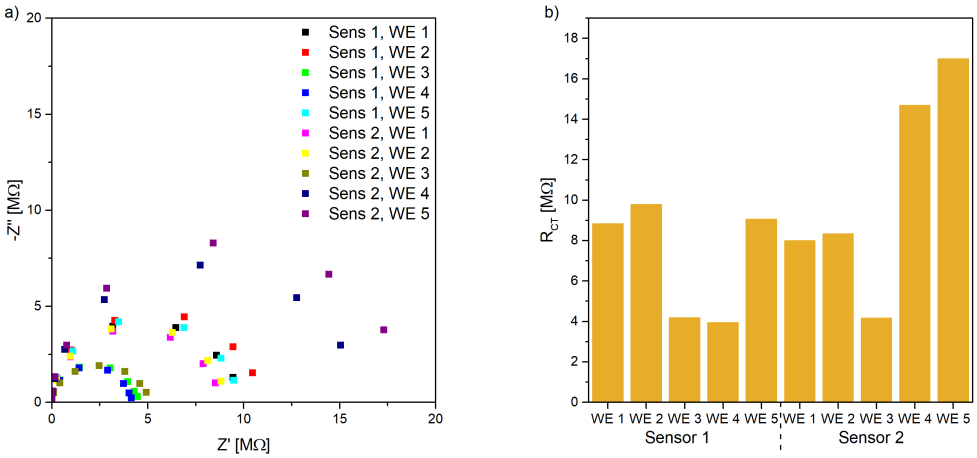

Figure 4.20: Fully functionalised biosensor, MUA-MPOH/cortisol-Ab/EA, measured with 2.5 mmol L^{-1} ferro-ferricyanide solution in PBS: a) Nyquist plots of the biosensors; b) comparison of the R_{CT} of the fully functionalised biosensor of different WE

4.2 Evaluation of two-electrode Cortisol Sensor

The fully functionalised biosensors based on the MPA monolayer were used for the detection of cortisol from buffered solutions. The schematic of the functionalised biosensor binding the antigen is depicted in figure 4.21.

The glass slide sensor consists of five different WE with a MPA/Cortisol-Ab/EA functionalisation. First, the EIS spectrum of each WE before the binding of any antigen was recorded to determine the blank charge transfer resistance

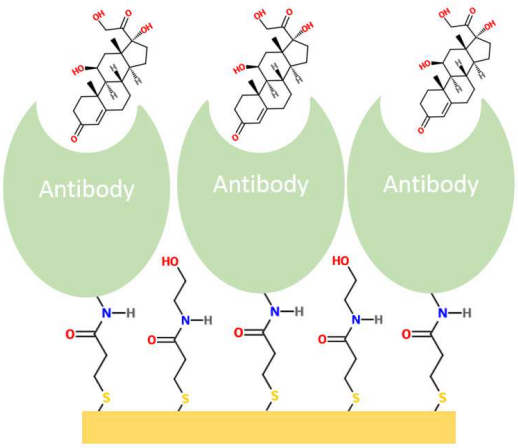

Figure 4.21: Schematics of Cortisol binding on functionalised sensor

R_{CT0}. Next, each of the WE was incubated for 30 min sequentially with increasing cortisol concentrations. The used cortisol concentrations were 1 nmol L^{-1}, 10 nmol L^{-1}, 100 nmol L^{-1}, and 1000 nmol L^{-1}. After the incubation with each standard the EIS spectrum of each working electrode was recorded to determine the response of the biosensor. The recorded EIS spectra of WE 2 are depicted in figure 4.21a. The impedances were the lowest for the blank measurement. After incubation with each buffered cortisol solution, the impedances increased. The curves were fitted according to the Randles circuit depicted in figure 3.7 to determine the corresponding R_{CT}. After the fitting the R_{CT} values were normalised according to equation 12. Then the normalised resistances were plotted against the logarithmic cortisol concentrations of the corresponding buffered standard solutions, as depicted in figure 4.21b. The response of the biosensors to the different cortisol concentrations exhibits a linear correlation.

The Nyquist plots of WE 5 on the same glass slide sensor, which was treated in the same way as the previously described electrode, is depicted in figure 4.23a. The impedances of the blank measurement were the lowest. After the incubation with the 1 nmol L^{-1} cortisol solution the impedances increased significantly in comparison to the blank measurement. The incubation with the 10 nmol L^{-1} cortisol solution also lead to a significant increase, but after this concentration, the cortisol-Ab on the sensor seemed to be completely saturated with cortisol and the impedances did not increase any more by incubating with higher cortisol concentrations. The $R_{CT,norm}$ were plotted against the logarithmic cortisol con-

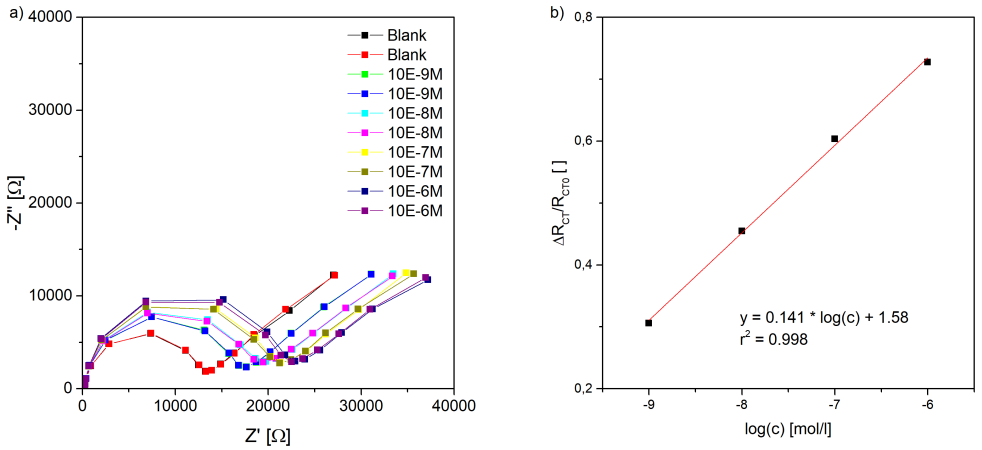

Figure 4.22: WE 2 of biosensor (MPA/cortisol-Ab/EA) after 15 min incubation with PBS buffer, 1 nmol L^{-1}, 10 nmol L^{-1}, 100 nmol L^{-1}, 1000 nmol L^{-1} cortisol standards in PBS, measured with 5 mmol L^{-1} ferro-ferricyanide solution in PBS: a) Nyquist plots; b) calibration curve with $R_{CT,norm}$ plotted against logarithmic cortisol concentration

centration in figure 4.23b. The impedance of the sensor only increased with the first two cortisol concentrations and then stayed nearly the same with the 100 nmol L^{-1} and 1000 nmol L^{-1} cortisol standard.

The response of all five WE on the same glass slide sensor to the different cortisol concentrations are depicted in figure 4.24. All five WE responded very differently to the cortisol standards. WE 1 and 2 responded similarly to the 1 nmol L^{-1} and 10 nmol L^{-1} cortisol solution, but the increase was higher with WE 1 when the electrodes were incubated with higher cortisol concentrations. As discussed previously, WE 5 was completely saturated after the 10 nmol L^{-1} cortisol solution. One reason might be that there are fewer antibodies bound to electrode 5 than to the other electrodes, but this would result in a lower blank value and this value is similar to the blank value of the other electrodes. Another explanation could be the loss of activity of some of the antibodies during the functionalisation or handling of the electrodes, but all five working electrodes are located on the same substrate and they are in close proximity to each other. It is unlikely that all five working electrodes would respond very differently from each other to the same antigen standards when they were all treated in the same way and with the same solutions during the functionalisation step.

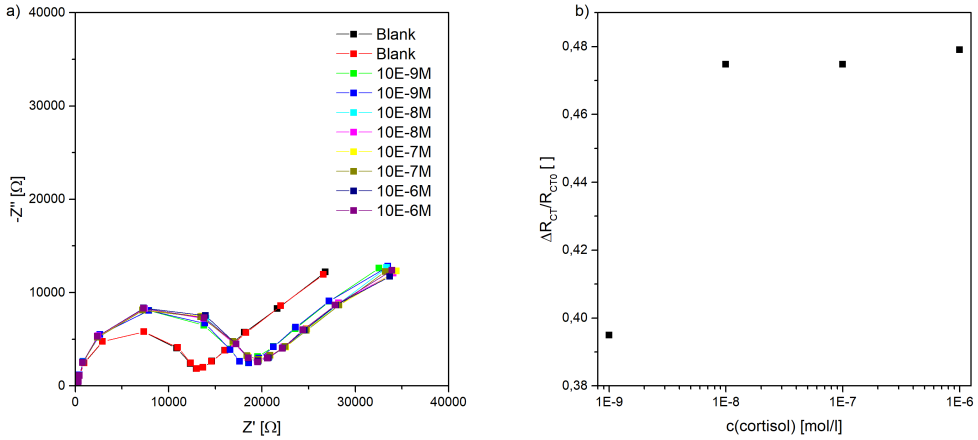

Figure 4.23: WE 5 of biosensor (MPA/cortisol-Ab/EA) after 15 min incubation with PBS buffer, 1 nmol L^{-1}, 10 nmol L^{-1}, 100 nmol L^{-1}, and 1000 nmol L^{-1} cortisol standards in PBS, measured with 5 mmol L^{-1} ferro-ferricyanide solution in PBS: a) Nyquist plots; b) calibration curve with $R_{CT,norm}$ plotted against logarithmic cortisol concentration

As discussed in chapter 4.1 the differences between the different MPA based cortisol biosensors was very small in the same batch and, therefore, similar responses would be expected when the antigen is bound. Another possibility is an influence of the buffer system or the redox-couple on the surface. The redox-couple or the electrolytes in the solution could interact negatively with the functionalisation or even destroy the functionalisation and lead to varying responses.

4.3 Influence of the buffer systems on the EIS measurement

The measurement solution consists of the redox-couple, a solvent and a buffer system. For most biosensors the solvent is water and can not be changed. Other solvents could influence the activity of the receptor molecules and the enzymes on the biosensor negatively. So, only the redox-pair and the buffer system can be exchanged. Several buffer systems were tested which could be used in the measurement solution: PBS, PB-thiocyanate, PB-acetate and PB-sulfate.

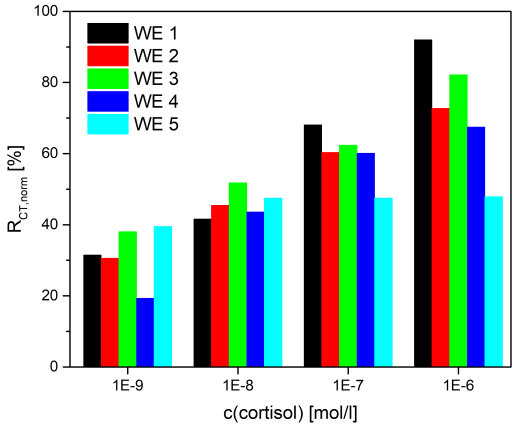

Figure 4.24: Comparison of $R_{CT,norm}$ of five working electrodes to incubation with $1\,nmol\,L^{-1}$, $10\,nmol\,L^{-1}$, $100\,nmol\,L^{-1}$, and $1000\,nmol\,L^{-1}$ cortisol standards in PBS

PBS has been chosen because it is used in most bioassays. PB-thiocyanate, PB-acetate and PB-sulfate are used to provide chloride free phosphate buffer systems. The EIS spectra of the different blank buffer systems were recorded by using cleaned glass slide sensors with a two-electrode setup. The measurement solution used in these cases were the buffer systems in aqueous solutions without a redox-couple. The non-faradaic EIS spectra over time of the different buffer systems were recorded. The Nyquist plots over time for PBS are depicted in figure 4.25a. The impedances decreased over the first few measurements and after about 10 min the EIS spectra remained nearly constant and did not change any more. The EIS spectra over time for the PB-thiocyanate buffer exhibited a similar result, as depicted in figure 4.25b. In the first 8 min the impedances drifted to higher values and then remained nearly constant for the next 18 min of measurement. The EIS spectra of PB-sulfate did not exhibit constant measurements, as depicted in figure 4.26a. The impedances did not reach a stable value even after 28 min of measurement. Also, the EIS spectra of the PB-acetate system did not reach constant impedances, as shown in figure 4.26b. Over the whole 28 min of measurement time the impedances increased continuously and did not reach a constant value. With these measurement results it is obvious, that PB-acetate and PB-sulfate are not suitable buffer systems for impedance measurements. The buffer system PB-thiocyanate exhibited the best results. It reached constant impedances the fastest and exhibited the smallest

variation in the impedance measurements. The measurements with PBS also reached constant values, but the variation of the impedances were much bigger, but PBS contains chloride ions and is mandatory as electrolyte, when a silver-silverchloride reference electrode is used. It can be concluded, that the buffer system PBS does not influence the EIS measurement stability negatively.

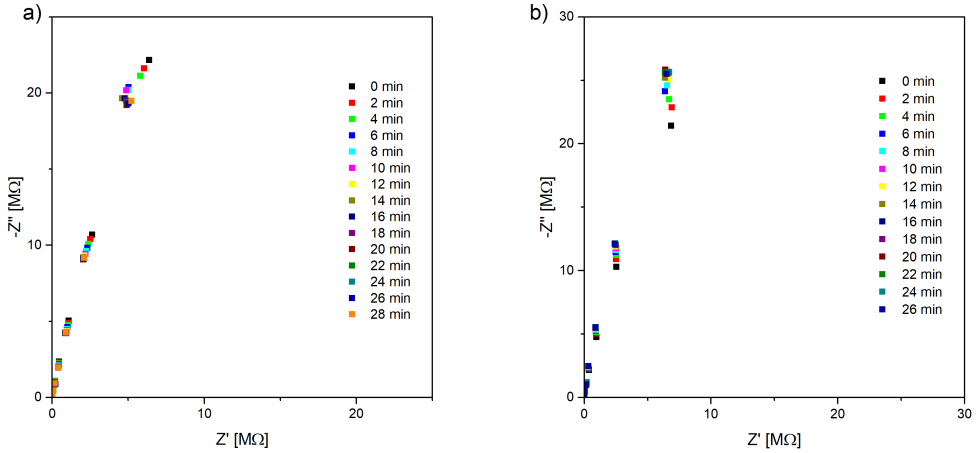

Figure 4.25: Nyquist plots of EIS measurements of glass slide sensors: a) PBS as non faradaic measurement solution; b) PB-thiocyanate as non faradaic measurement solution

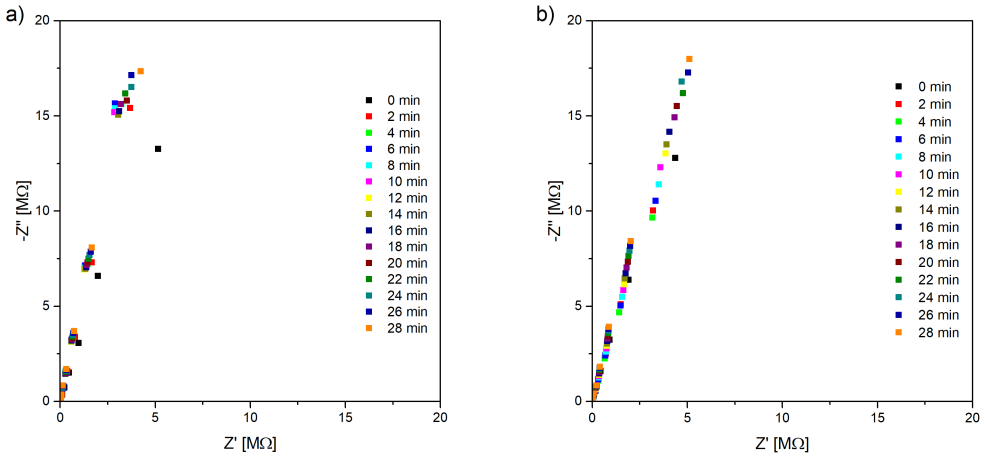

Figure 4.26: Nyquist plots of EIS measurements of glass slide sensors: a) PB-sulfate as non faradaic measurement solution; b) PB-acetate as non faradaic measurement solution

4.4 Limitations of the redox-couple ferro-/ferricyanide

In literature it is mentioned that the redox-couple ferro-/ferricyanide can have a negative influence on the measurement stability and reproducibility in biosensors. A glass slide sensor with five WE was functionalised as previously mentioned with MPA, cortisol-Ab and EA. The EIS spectra of each WE was recorded with eight repeats using 30 µL of a 5 mmol L^{-1} ferro-/ferricyanide solution in PBS as measurement solution. After the measurement the electrodes were washed thoroughly with PBS buffer. The washing buffer was then removed and 30 µL of the previously mentioned ferro-/ferricyanide solution is added and the EIS spectra are recorded. The measurement and washing procedure were repeated four times. The R_{CT} of the gained curves are depicted in figure 4.27. Every measurement series of each WE exhibited similar results. The R_{CT} did not reach a constant value and changed from measurement to measurement. When the EIS spectra were recorded after the washing step, the new measurement series of each WE started with a completely different R_{CT} value. The new starting value does not seem to follow a specific trend as can be observed in figure 4.27. The functionalised sensor was examined using scanning electron microscopy (SEM). The image before the EIS measurements is depicted in figure 4.28a. After the EIS measurements the sensor was washed thoroughly with deionised water and examined with SEM again. As can be seen in figure 4.28b, the surface changed visibly after the contact with the ferro-/ferricyanide solution. Further, the sensor was incubated in the 5 mmol L^{-1} ferro-/ferricyanide solution for seven days. The influence of the measurement solution and its corrosive nature is unambiguously apparent in figure 4.29. A microscopic picture of a working electrode of a glass slide sensor after cleaning with piranha is shown in figure 4.29a. The same WE after the seven days is shown in figure 4.29b. After this extended incubation time nearly the complete 100 nm thick gold layer is removed from the glass slide and only the chromium layer remains. The capture antibodies are anchored to the outer layer of the gold electrodes which were removed over time and render the sensor useless. Any change of the electric properties of the gold electrodes caused by the measurement solution can impair the measurement results and can lead to false positive or false negative measurement results.

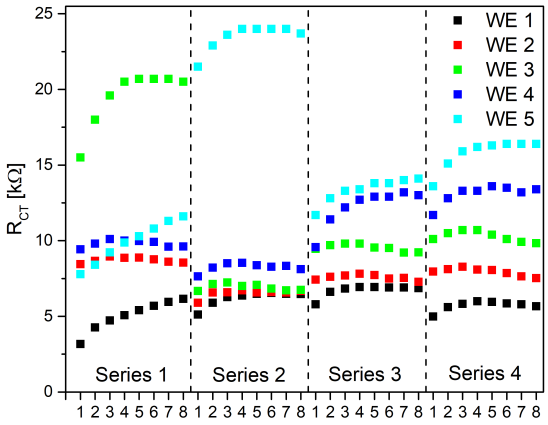

Figure 4.27: R_{CT} of electrodes 1 to 5 over time with 5 mmol L^{-1} ferro-/ferricyanide solution in PBS as measurement solution, four measurement series with washing steps between the measurement series and eight repeats per measurement series

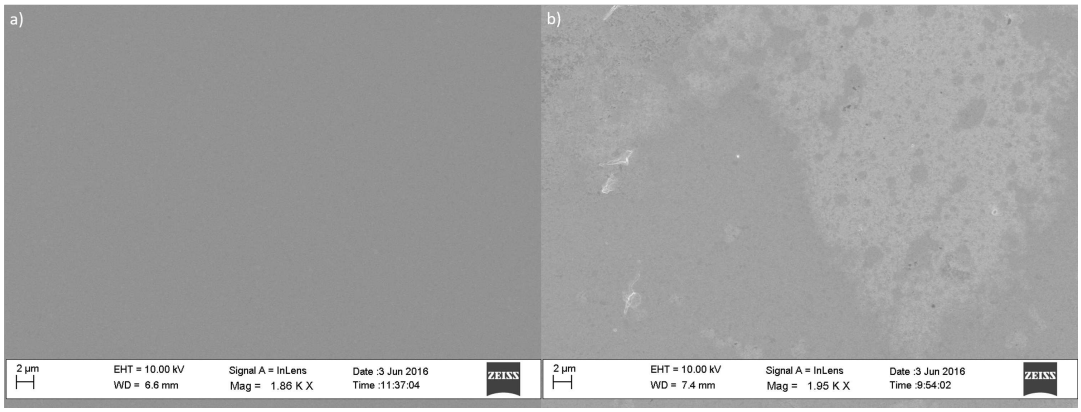

Figure 4.28: SEM images of glass slide sensor: a) WE before contact with ferro-/ferricyanide solution; b) WE after EIS measurements with ferro-/ferricyanide solution

In literature it is stated that the corrosive property of ferro-/ferricyanide is caused by visible light. To counter this problem it is advised to use brown bottle glasses to store the ferro-/ferricyanide measurement solution and perform the measurements in the dark inhibit the corrosion of the electrodes. This method was tested with a 5 mmol L^{-1} ferro-ferricyanide solution in PBS with a glass

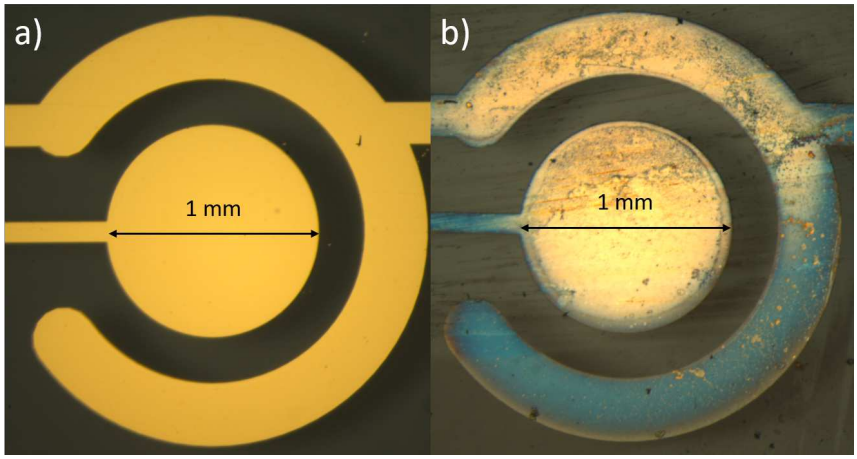

Figure 4.29: Microscopy image of the working electrode of a glass slide sensor: a) before contact with ferro-/ferricyanide solution; b) after 7 d of incubation with ferro-/ferricyanide solution

slide sensor. The recorded EIS spectra over time are depicted in figure 4.30. The measurement solution was prepared in brown glass and the measurement was carried out over 18 min in the dark. The stability of the EIS measurement increased slightly, but the impedances still change from measurement to measurement too much to be useful for a biosensor application.

4.5 Evaluation of redox-systems

4.5.1 Redox-systems with two-electrode setup

For the implementation of a new redox-couple some important requirements have to be met. First, the oxidation and the reduction has to be reversible. Second, the oxidised and the reduced states have to be stable. Third, both states must not undergo a chemical reaction with the surface and the functionalisation. In table 4.1 the different considered redox-couples are listed. To counter the instability of the gold electrodes, induced by the cyanide ligand of the ferro-/ferricyanide redox-couple, a mixture of 5 mmol L^{-1} iron(II) and iron(III) chloride was used for the EIS measurements. The change of the EIS signal was recorded over about 14 min. The evolution of the EIS signal is depicted in figure 4.31a. Over the whole measurement time the impedances increased and after about 14 min the impedance was about double of the initial measurement. This can be attributed to the instability of the iron(II)chloride in aqueous

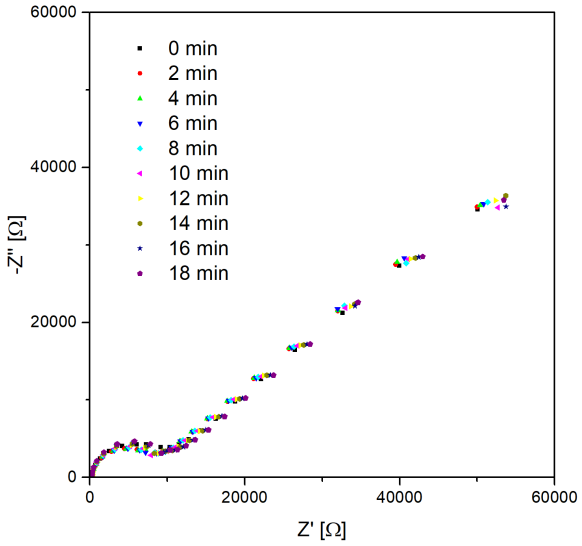

Figure 4.30: Nyquist plots over time of glass slide sensor with 5 mmol L^{-1} ferro-/ferricyanide solution stored in brown glass and measurement with exclusion of light

solutions. Alternatives to the redox-pair ferro-/ferricyanide are scarce because most of stability issues. In most cases, the reduced form is unstable and oxidised by air or humidity continuously. Other inorganic metal redox-couples like europiumchloride (II/III) and hexaammineruthenium(II/III)chloride were discarded immediately because of their standard reduction potential is even lower than iron chloride (II) and can be oxidised easily in aqueous solution. Another problem of iron chloride and europium chloride is that these substances form insoluble salts with phosphates, which would make an application with biological samples and PBS buffer impossible. Other metal ions are not suitable as a redox-probe, because of disproportionation reactions. An example for this would be Cu(I), which immediately disproportionates into Cu(II) and Cu(0). Inorganic, non-metal redox-couples were also considered, such as triiodide and thiosulfate. Both redox-systems are known in literature to dissolve gold and, therefore, they are not suitable for a biosensor application [59, 60].

Redox-couples based on organic substances have the same stability problem. A mixture of 5 mmol L^{-1} hydroquinone-benzoquinone was used on a gold sensor to record the impedance spectrum over time and depicted in the Nyquist plot in figure 4.31b. From measurement to measurement the impedances increase con-

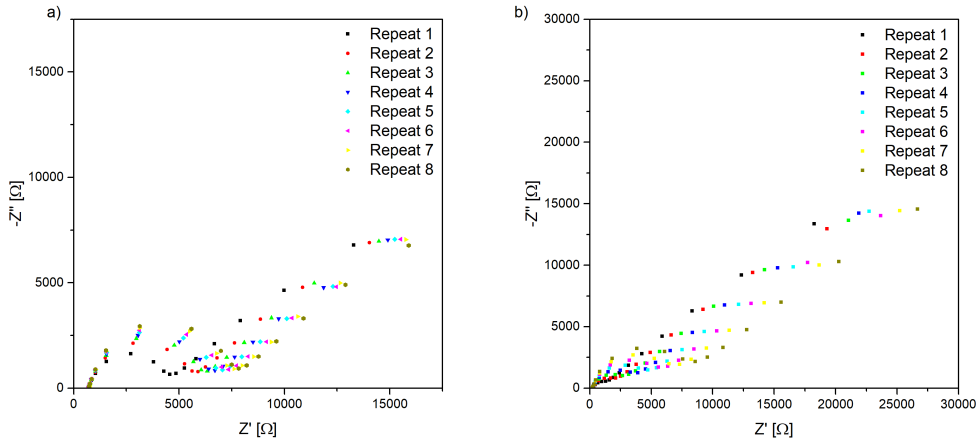

Figure 4.31: Stability of different redox-systems used in a two-electrode setup used for EIS measurements: a) Nyquist plot redox-system iron(III) and iron (II) in concentrations of 5 mmol L^{-1} in 100 mmol L^{-1} aqueous sodiumchloride solution; b) Nyquist plot redox-system benzoquinone and hydroquinone in concentrations of 5 mmol L^{-1} in PBS

tinuously. After the 8th measurement, which corresponds to about 14 min, the measurement solution was removed from the measurement chamber, and a new redox-solution was added. Here we see a small overlap of the 8th measurement of the first series and the 1st measurement of the 2nd series. This may be caused by the different oxidation speeds of the 1,4-benzoquinone in the measurement chamber and the bulk solution in the storage bottle. Naphthoquinone also exhibits similar instabilities in aqueous solutions and was not further considered as redox-couple [61]. Anthroquinone is insoluble in aqueous solutions and unsuitable for a biosensor [62]. Organic redox-couples containing disulfides are also not applicable in biosensors. The reduced form of L-cystine is L-cysteine and has a free thiol group. These free thiol group could possibly bind covalently to the gold surface and change the electrochemical behaviour of the working electrode.

4.5.2 Redox-systems with a three-electrode setup

Alternatives to the redox-pair ferro-/ferricyanide are scarce because most of stability issues. In most cases the reduced form is unstable and is oxidised by air or humidity continuously. Therefore, another strategy was used. A DC-bias is

Table 4.1: Standard electrode potentials of different redox-systems [63, 64]

Substance	E^0 [V]
$[Fe(CN)_6]^{3-} + e^- \rightarrow [Fe(CN)_6]^{4-}$	0.361
$FeCl_3 + e^- \rightarrow FeCl_2$	0.771
$EuCl_3 + e^- \rightarrow EuCl_2$	-0.350
$[Ru(NH_3)_6]^{3+} + e^- \rightarrow [Ru(NH_3)_6]^{2+}$	0.100
$[Ru(NH_3)_5Cl]^{2+} + e^- \rightarrow [Ru(NH_3)_5Cl]^{+}$	-0.042
$I_3^- + 2\ e^- \rightarrow 3\ I^-$	0.536
$S_4O_6^{2-} + 2\ e^- \rightarrow 2\ S_2O_3^{2-}$	0.080
dehydroascorbic acid + 2 e^- → ascorbic acid	0.020
methylene blue + 2 e^- → leuco-methylene blue	0.011
1,4-benzoquinone + 2 e^- → 1,4-hydroquinone	0.699
Naphthoquinone + 2 e^- → Naphthohydroquinone	0.547
Anthraquinone + 2 e^- → Antrahydroquinone	0.401
L-cystine + 2 e^- → L-cysteine	-0.340

applied during the EIS measurement to the sensor. The DC-bias is chosen to reduce the redox-active substance in the solution and generate a redox-couple for the EIS measurement close to the surface of the WE. The suitability of several different organic and inorganic redox-active substances for EIS measurements with DC-bias were tested. The tested substances were: europium(III) chloride, ferricyanide, iron(III) chloride, pentaamminechlororuthenium(III)chloride, hexaammineruthenium(III) chloride, ascorbic acid, methylene blue and 1,4-benzoquinone. In table 4.1 the corresponding standard electrode potentials are listed. As mentioned in chapter 4.5.1, the redox-system has to meet several requirements, and only very few systems, even in an three-electrode setup, can meet these requirements. The problem of the instability of the reduced state can be overcome by the three-electrode setup, but other limitations can still occur with alternative redox-systems. In the case of using europium(III) chloride as redox-active substance the limitation is quite clear. The CV are depicted in figure 4.32a. An unfunctionalised BVT sensor and a 5 mmol L^{-1} europium(III) chloride solution with 100 mmol L^{-1} sodium chloride were used for the measurement. The reduction and oxidation peak are barely identifiable. The maximum of the reduction peak is reached at about −1 V vs. a silver/silverchloride reference electrode. According to literature this reference electrode has a standard reduction potential of −0.36 V vs. a standard hydrogen electrode (SHE). In a 100 mmol L^{-1} sodium chloride solution, the potential of an silver/silverchloride

electrode would be 0.28 V (according to equation 13). So, it can be calculated, that the standard reduction potential of europium(III)chloride is −0.64 V vs. the silver/silverchloride electrode. For the EIS application a DC bias between the reduction peak maximum and the standard reduction potential has to be applied. This is a large potential which has to be applied between the electrodes. A major concern would be the danger of side reactions. Possible side reactions can be the oxidation or reduction of disulfide bridges in the antibodies or enzymes bound to the electrode surface. According to literature the disulfide bridges of proteins are between −0.095 V and −0.47 V vs SHE which corresponds to a potential of −0.437 V and −0.750 V vs. the Ag/AgCl reference electrode [65]. The necessary DC-bias in the EIS measurement for the reduction of the europium(III)chloride is enough to induce side reactions of the analyte molecules and the covalently bound receptor molecules. The EIS measurements were performed at several different DC-biases. The EIS curves were fitted according to the Randles circuit in figure 3.7. The R_{CT} values of these fitted curves are depicted in figure 4.33. The R_{CT} reached a minimum at a DC-bias of about −1 V. At a higher DC-bias the oxidised state is in higher concentrations near the electrode surface and at lower DC-biases the reduced state is available in larger amounts in the vicinity of the electrode surface. Through the production process of the sensor differences of several mV can occur between the WE and the RE. It would be preferable to perform the measurements at higher DC-biases than the determined minimum. This DC-bias is still enough to introduce unwanted side reactions of the analyte and receptor molecules. A further problem is that europium forms insoluble precipitates with phosphates and therefore phosphate-free buffer systems would be necessary. Further, in a long use stability test it was revealed, that the use of europium(III)chloride seems to deteriorate the sensor. Figure 4.32b shows the EIS curve of a sensor with europium(III)chloride as redox-active substance at a DC-bias of −1 V. The sensor was measured several times with the same measurement solution sequentially. The black curve is the first measurement and the red curve the 12th measurement. As it is immediately apparent that the 12th measurement has much more noise at lower frequencies and it was not possible to gain stable measurement results at low frequencies any more. In comparison, the signal of the first measurement was less noisy and only the last point is off by a small margin. With all these results europium(III)chloride can not be recommended as an alternative to the ferro-/ferricyanide redox-system.

$$E_{Ag/AgCl} = E^0_{Ag/AgCl} - 0,059 \cdot log(c_{Cl^-}) \tag{13}$$

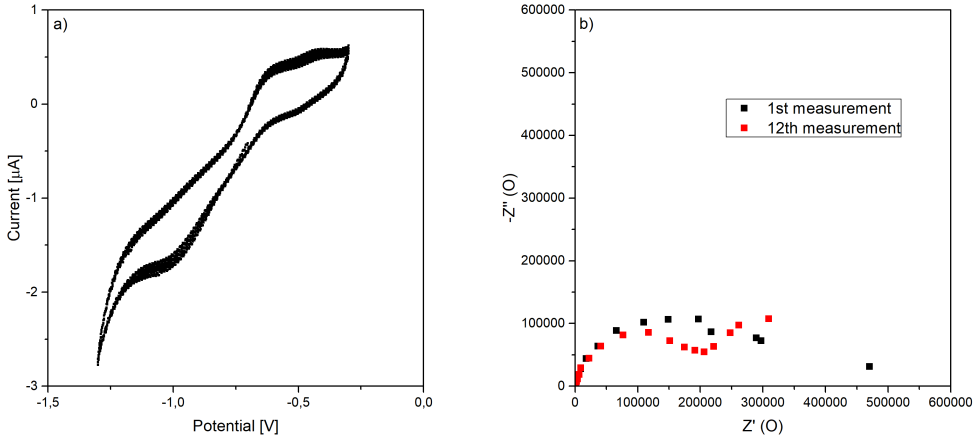

Figure 4.32: Electrochemical measurements of cleaned gold electrodes with a measurement solution containing 5 mmol L^{-1} $EuCl_3$ in 100 mmol L^{-1} NaCl: a) CV over time; b) EIS spectra over time, −1 V DC-bias

Hexacyanoferrate(II) and (III) can perform a ligand exchange with the water and can release cyanide into the solution under the influence of light [66]. Therefore, it was tested to only use hexacyanoferrate(III) in a three-electrode setup. Also, the measurement solution was stored in a brown bottle and the measurement was performed in the dark, to further reduce the release of cyanide. A 5 mmol L^{-1} potassiumhexacyanoferrate(III) solution in PBS was used for the electrochemical measurements. The CV measurements, shown in figure 4.34a, did not reveal any improvement in comparison to the two-electrode setup with hexacyanoferrate(II) and (III) in the solution. The CV increased continuously over the whole measurement period. As can be clearly seen in figure 4.34a the reduction peak current decreased during the measurement continuously and did not reach a stable value over the measurement time. The EIS measurements were performed at a DC-bias of −30 mV and the EIS spectra of the measurement over time are depicted in figure 4.34b. The impedances were unstable over the whole measurement period and did not reach a stable value. Using a brown bottle and performing the measurements under exclusion of light did not

improve the measurement stability in any way. Ferrocyanide can be discarded completely as a stable redox-system in EIS biosensors.

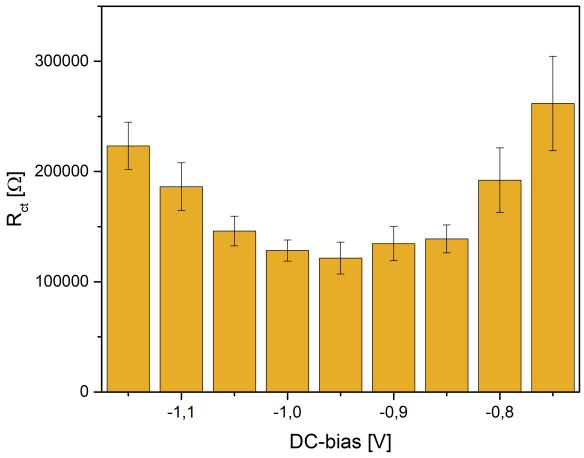

Figure 4.33: Dependency of the R_{CT} on the DC-bias from −1.15 V to −0.75 V using a 5 mmol L^{-1} $EuCl_3$ solution

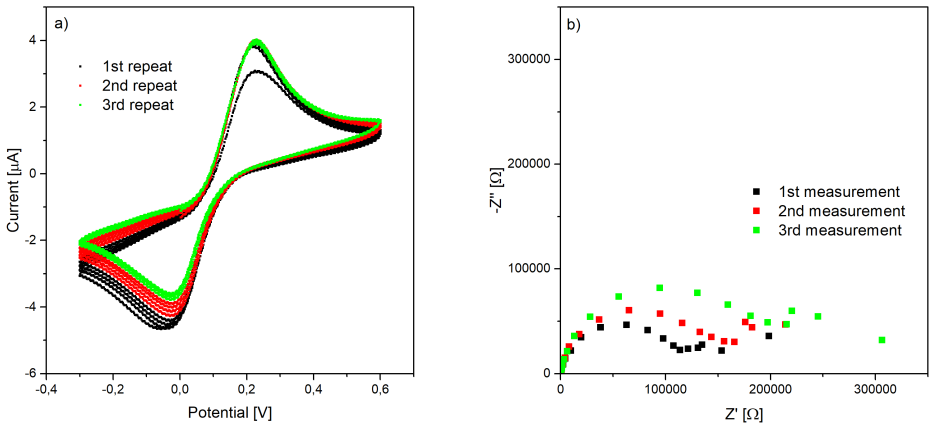

Figure 4.34: Electrochemical measurements of cleaned gold electrodes with a measurement solution containing 5 mmol L^{-1} hexacyanoferrate(III) in PBS: a) CV over time; b) EIS spectra over time, −30 mV DC-bias

Further, pentaamminechlororuthenium(III) chloride was used as redox-active substance in the measurement solution for the three-electrode sensor. For the measurements the redox-substance was used in a concentration of 5 mmol L^{-1}

in PBS. The CVs are depicted in figure 4.35a. It is immediately apparent that the CVs reach a stable value after four cycles. The oxidation peak was at −320 mV and the maximum of the reduction peak was at −460 mV. According to table 4.1 the standard reduction potential of pentaamminechlororuthenium(III) is at −42 mV vs. NHE. The CV measurement was performed with the redox-substance in PBS buffer which has a chloride concentration of 139.7 mmol L^{-1}. The potential difference between a silver/silverchloride reference electrode and a NHE is at this chloride concentration 273 mV according to equation 13. So the pentaamminechlororuthenium(III) has a standard reduction potential of −310 mV versus the silver/silverchloride reference electrode. The EIS measurements were performed with the same measurement solution with a DC-bias of −370 mV. The EIS measurement revealed a good stability of the measurement and the recorded EIS spectra did not drift at all. The only possible limitation of this redox-substance could be the necessary DC-bias for the EIS measurement. The DC bias for the EIS measurements is low enough to not induce any possible reductions of sulfide bridges in the analytes and receptor molecules, but a lower DC-bias would be preferable to reduce the danger of possible side reactions even further.

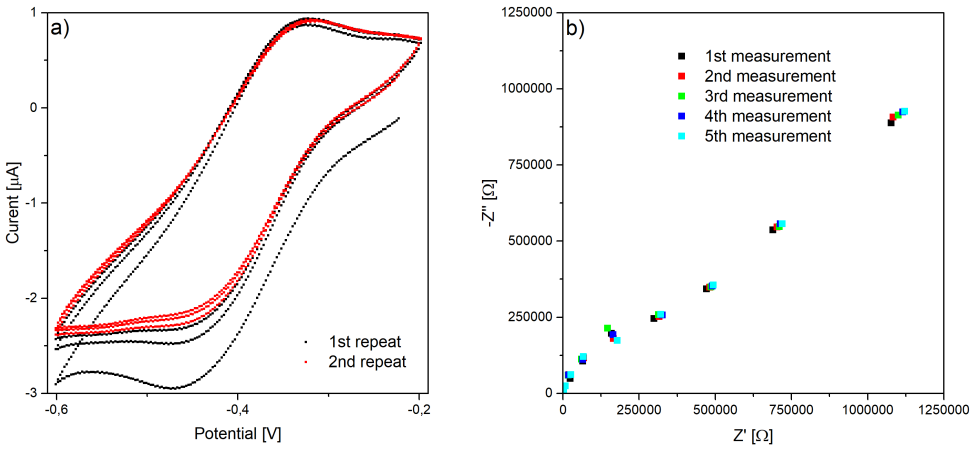

Figure 4.35: Electrochemical measurements of cleaned gold electrodes with a measurement solution containing 5 mmol L^{-1} pentaamminechlororuthenium(III) in PBS: a) CV over time; b) EIS spectra over time, −370 mV DC-bias

The tests of the redox-substance hexaammineruthenium(III) were promising.

This substance was used in a concentration of 10 mmol L^{-1} in PBS. The cyclic voltammograms are depicted in figure 4.36a. Already after the first cycle a stable measurement is reached and no drifts can be observed. The reduction peak was at −270 mV and the oxidation peak at −180 mV. In table 4.1 the standard reduction potential is described to be about 100 mV vs. NHE. Using the Nernst equation for the silver/silverchloride reference electrode, the standard reduction potential versus this reference electrode is about −160 mV. The EIS measurements were performed at this reduction potential and with a hexaammineruthenium(III) of 10 mmol L^{-1}. The determined impedances are stable over the multiple measurements and do not exhibit any drift. With these first results hexaammineruthenium(III) seems to be a suitable alternative to ferro-/ferricyanide.

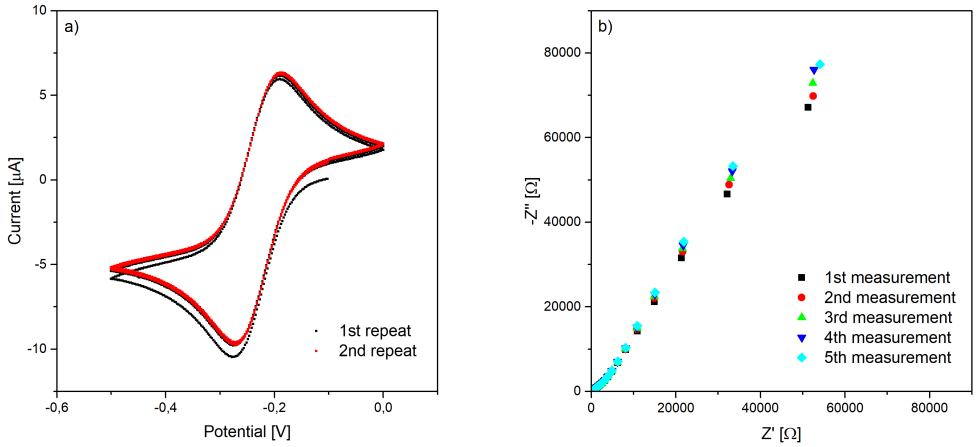

Figure 4.36: Electrochemical measurements of cleaned gold electrodes with a measurement solution containing 10 mmol L^{-1} hexaammineruthenium(III) in PBS: a) CV over time; b) EIS spectra over time, −160 mV DC-bias

The usability of ascorbic acid in electrochemical measurements was tested by using a 5 mmol L^{-1} ascorbic acid solution in PBS buffer. The CV are shown in figure 4.37. The CV depicts a big oxidation peak at about 800 mV and only a very small reduction peak at about −500 mV. Further, the peak area of the reduction peak decreased from cycle to cycle and shifted continuously. This indicates that the reduction of the ascorbic acid is irreversible and, therefore, renders this substance unusable as an redox-system for a biosensor based on EIS.

The EIS measurements confirm this assumption, as can be seen in the Nyquist plot in figure 4.37b. The determined impedances increased from measurement to measurement. Additionally, it is not possible to gain any stable impedance values at low frequencies. As shown in figure 4.37b, the impedances measured at low frequencies on the right edge of the curve do not follow the progression of the EIS curve any more. This limitation renders ascorbic acid unusable as an alternative redox-system to ferro-/ferricyanide.

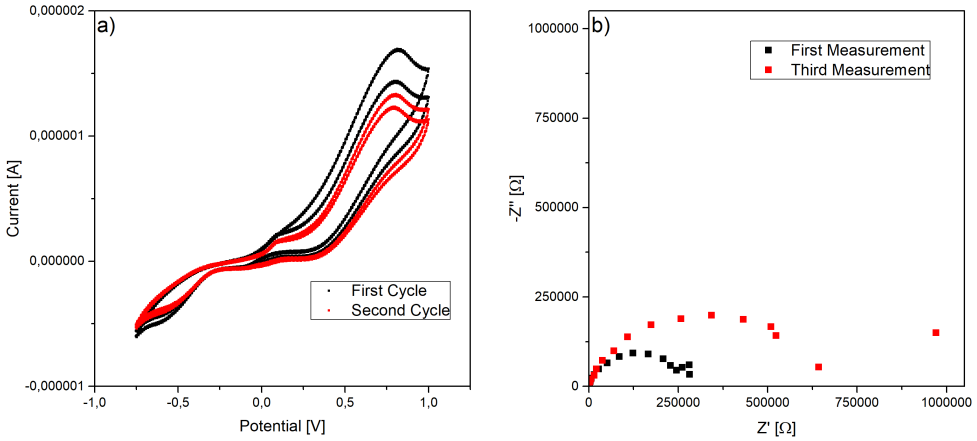

Figure 4.37: Electrochemical measurements of cleaned gold electrodes with a measurement solution containing 5 mmol L^{-1} ascorbic acid in PBS: a) CV over time; b) EIS spectra over time, −300 mV DC-bias

The CV and EIS measurements for methylene blue as redox-substance seemed promising. As depicted in the CV in figure 4.38a, the curves reached stability after a few cycles and remained stable. The maximum of the oxidation peak was at −245 mV and of the reduction peak at −285 mV. In literature the standard reduction potential is noted to be at 10 mV versus NHE. When silver/silverchloride is used as RE, this potential is shifted to −260 mV according to equation 13. This corresponds with the half-potential of the measurement which is −265 mV in the CV measurement. The oxidation peak was very sharp in the CV and the reduction peak is very broad. The EIS spectra were recorded using a 5 mmol L^{-1} methylene blue solution in PBS with a DC-bias of −265 mV. The spectra are depicted in figure 4.38b. The measured impedances were very low and the semicircle are barely visible. A very small drift is noticeable, but the shift over time is much lower than in other redox-systems. When the same

sensor was used multiple times or over longer times with methylene blue the RE was coloured slightly blue. Using lower concentrations of methylene blue did not improve this situation. Even with concentration of 0.1 mmol L^{-1} methylene blue the reference electrode gained a blue hue. In single use biosensors methylene blue could be used as redox-substance.

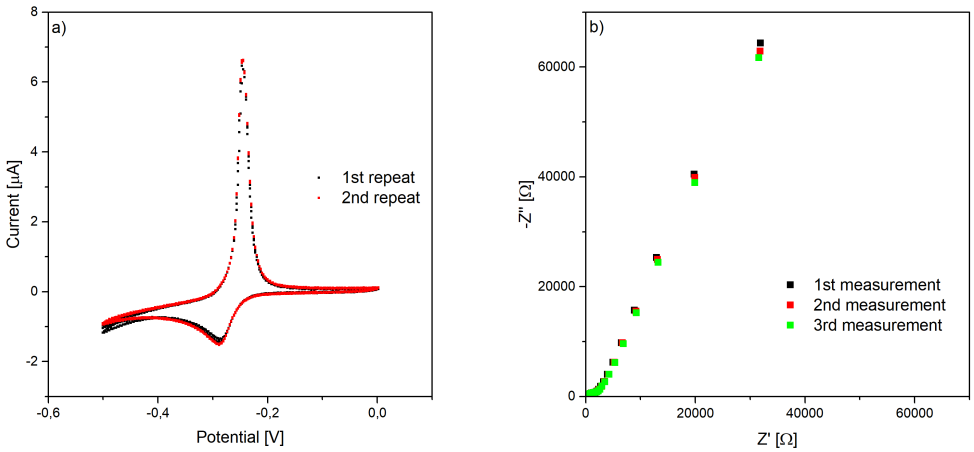

Figure 4.38: Electrochemical measurements of cleaned gold electrodes with a measurement solution containing 5 mmol L^{-1} methylene blue in PBS: a) CV over time; b) EIS spectra over time, −265 mV DC-bias

The redox-substance 1,4-benzoquinone can undergo two reduction and oxidation steps. In the first reduction step benzoquinone is reduced to the unstable radicale semiquinone with a single electron transfer process. Next, the semiquinone is further reduced to hydroquinone. In aqueous solution this reduction occurs only as a single two electron step and the 1,4-benzoquinone is reduced directly to 1,4-hydroquinone. Only in aprotic solutions the semiquinone reduction step is stable long enough to appear in the cyclic voltammetry [67]. A 5 mmol L^{-1} 1,4-benzoquinone solution in PBS was used for the electrochemical measurements. The CV are depicted in figure 4.39a. The maximum of the reduction peak was at −240 mV and of the oxidation peak at −140 mV. Similar results are shown in literature [68]. The form of the CV and the position of the reduction and oxidation peak is very dependent on the solvent and buffer. As shown in figure 4.39a, the CV did not remain stable after multiple repeats. This drift can also be observed in the EIS measurements. The Nyquist

plots of the EIS spectra with the same 5 mmol L^{-1} 1,4-benzoquinone solution in PBS at a DC-bias of −200 mV are depicted in figure 4.39b. The impedances increased from measurement to measurement and did not reach stability. Another limitation of 1,4-benzoquinone is its toxicity. There are other non-toxic quinones available, but with the unstable results of 1,4-benzoquinone, these other quinones were not considered as alternative redox-active substances.

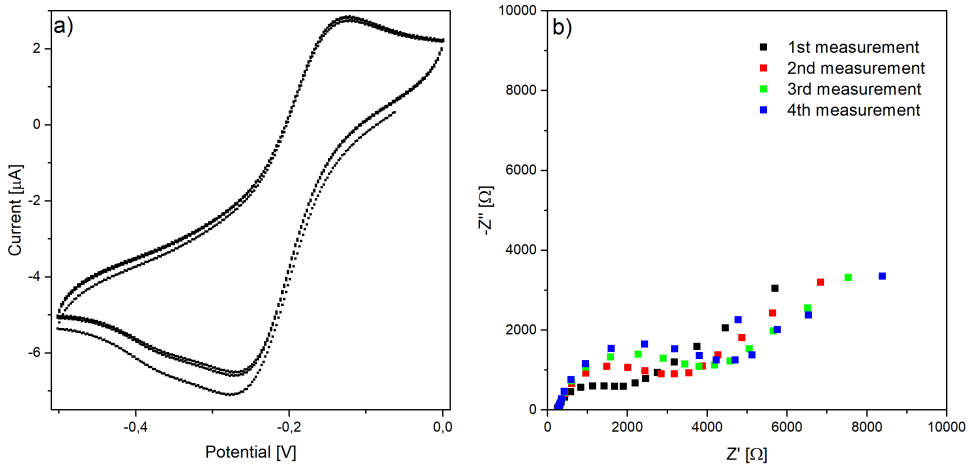

Figure 4.39: Electrochemical measurements of cleaned gold electrodes with a measurement solution containing 5 mmol L^{-1} 1,4-benzoquinone in PBS: a) CV over time; b) EIS spectra over time, −200 mV DC-bias

The results of the tested redox-substances are listed in table 4.2. Europium(III) chloride, ferricyanide, iron(III) chloride, ascorbic acid and 1,4-benzoquinone are not suitable redox-systems. These substances were not stable in the CV and the EIS measurements. Methylene blue exhibited only a minor drift in the EIS spectra and over longer measurement times methylene blue seemed to adsorb on the reference electrode. Even with these limitations methylene blue could be used in a single use POC biosensor, but more suitable reference-substances are available. Pentaamminechlororuthenium(III) exhibited stable CV and only a barely noticeable drift in the EIS spectra. Even with this limitation it could be used in a biosensor. The best results were obtained by using hexaammineruthenium(III) as the redox-active substance. There were no noticeable drifts in the CV and the EIS spectra. This could make hexaammineruthenium(III) the perfect candidate in a biosensor. Further tests with this redox-active substances were performed and the results are discussed in chapter 4.5.3.

Table 4.2: Overview of different redox-active substances with a three-electrode setup

Substance	Suitability	Comments
$EuCl_3$	No	Colour of reference electrode and working electrode changes over time; unstable CV and EIS; precipitates with phosphates
$[Fe(CN)_6]^{3-}$	No	Unstable CV and EIS
$FeCl_3$	No	Precipitates with phosphates
$[Ru(NH_3)_5Cl]^{2+}$	Yes	Stable CV; only very small drift in EIS spectras
$[Ru(NH_3)_6]^{3+}$	Yes	Stable CV and EIS
ascorbic acid	No	Unstable CV and EIS; irreversible reduction
methylene blue	Maybe	very slow colour change of reference electrode; only small instability
1,4-benzoquinone	No	Unstable CV and EIS

4.5.3 Examination of Hexaammineruthenium(III)

A first evaluation of different redox-probes applied in an EIS measurement with DC-bias revealed hexaammineruthenium(III) as the most promising candidate. The oxidised form is stable in aqueous solution. The redox-couple does not undergo any chemical reactions with the electrode surface and the functionalisation. The biggest influence on the in-situ production of the redox-couple during the EIS measurements has the DC-bias itself. In figure 4.40 the influence of the DC-bias on the R_{CT} is depicted. The R_{CT} decreases with lowering the DC-bias. This is caused by the concentration ratio of the reduced and oxidised form. At a DC-bias of 160 mV, the oxidised form is available at higher concentrations. When the DC-bias is lowered further, the concentration of the reduced state increases. At a DC-bias of about −270 mV the R_{CT} reaches a minimum because the concentration of reduced and oxidised state of the redox-active substance is the same. Lowering the DC-bias further leads to a rise of the R_{CT} because the concentration of the reduced state increases further and is then larger than the concentration of the oxidised state. As stated in chapter 4.5.2 the standard reduction potential against the silver/silverchloride reference electrode

is about −160 mV. For EIS measurements a DC-bias of at least −160 mV is recommended for biosensor. The influence of the DC-bias on the $R_{CT,norm}$ in the range from −150 mV to −170 mV in steps of 1 mV is depicted in figure 4.40a. In the area of −160 mV to −170 mV the change is nearly linear. An error of 1 mV in the DC-bias only changes the R_{CT} by about 2 %. An instability of the constant DC-bias would only have a very small influence on the EIS measurement. When a DC-bias between −150 mV and −160 mV is used, the influence would be significantly larger. Close to −150 mV the change in the R_{CT} would be about 6 %. Overall the DC-bias should be kept as low as possible, because at a DC-bias of about −340 mV disulfide bridges can be reduced and the bound receptor molecules could loose their activity. A DC-bias of −160 mV is recommended because it is sufficiently low to not induce any unwanted side reactions and the possible error of the R_{CT} caused by an instability of the DC-bias is as low as possible.

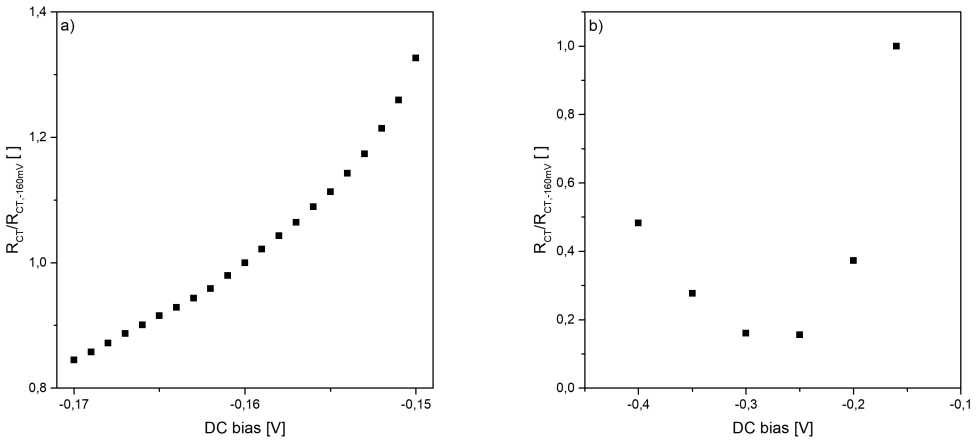

Figure 4.40: Relative change in the R_{CT} with small variation of DC-bias

For the stability test of the hexaammineruthenium(III) a fully functionalised sensor was used for the CV and the EIS measurements. The results of the CV measurements are depicted in figure 4.41a. The CV was recorded over 40 min. After 20 min the CV did not change any more. The CV of fully functionalised biosensor using ferro-/ferricyanide as redox-couple are depicted in figure 4.42a. Even after 30 min of measurement time the CV changed continuously and did not reach stable values. The impedance spectra of fully functionalised biosensors

using hexaammineruthenium(III) were stable nearly immediately and did not change significantly over time as depicted in figure 4.41b. Even after 18 min of measurement the spectra remained stable and did not drift to higher or lower values. When the redox-couple ferro-ferricyanide was used, the impedance drifted continuously to higher values over time and did not reach a constant value, as shown in figure 4.42b.

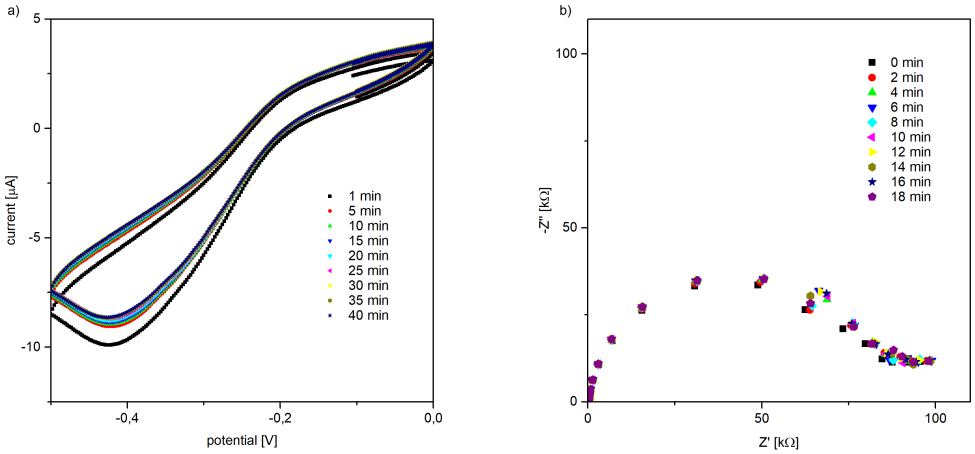

Figure 4.41: Stability measurements of 10 mmol mL^{-1} hexaammineruthenium(III)chloride in PBS with fully functionalised screen-printed biosensor (MUA/Fc-IgG-Ab/EA): a) CV over time; b) Nyquist plots over time with −160 mV DC-bias

Further, a sensor with gold electrodes was incubated for seven days in the 10 mmol L^{-1} hexaammineruthenium(III) chloride solution in PBS to observe the long time influence of the measurement solution. The microscopic image of the working and counter electrode of the glass slide sensor before the incubation in the hexaammineruthenium(III) solution is depicted in figure 4.43a. Even after seven days no change of the gold electrodes was visible, as shown in figure 4.43a. Applying hexaammineruthenium(III) with a DC-bias of −160 mV improved the stability of the EIS measurements significantly. Also, the new measurement solution did not interfere with the functionalisation and did not corrode the electrode structures.

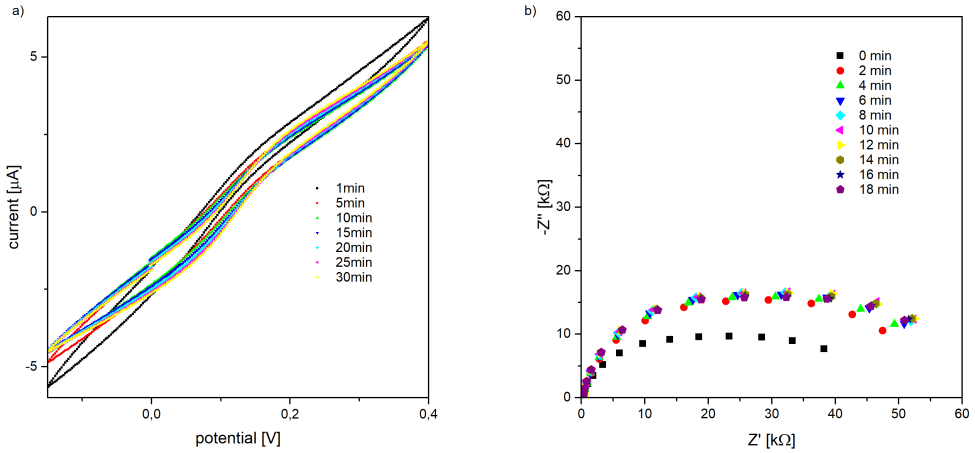

Figure 4.42: Stability measurements of 10 mmol mL^{-1} ferro-ferricyanide in PBS with fully functionalised screen-printed biosensor (MUA/Fc-IgG-Ab/EA): a) CV over time; b) Nyquist plots over time without DC-bias

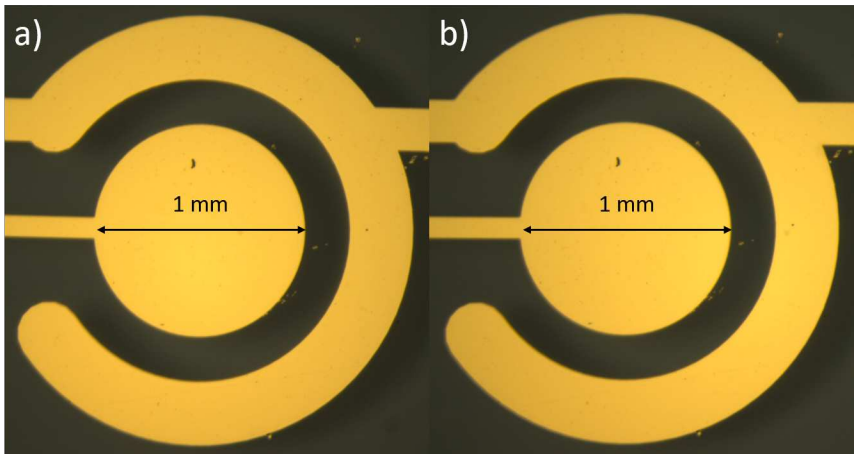

Figure 4.43: Microscopy image of glass slide sensor: a) before incubation with 10 mmol mL^{-1} hexaammineruthenium(III)chloride in PBS; b) after seven days of incubation with 10 mmol mL^{-1} hexaammineruthenium(III)chloride in PBS

4.6 Monolayer functionalisation of different three-electrode sensors

4.6.1 Three-electrode sensor on ceramic substrate

Using hexaammineruthenium(III) with DC-bias for EIS measurements requires a three-electrode sensor. The previously used glass sensor only has a two-

electrode setup which consists of a gold WE and gold CE. Therefore, a commercially available screen-printed three-electrode sensor on ceramic substrate was used for the functionalisation process. All EIS measurements were performed using hexaammineruthenium(III) as a mediator and the working electrode was kept at a DC-polarisation of −160 mV. The EIS spectra for the unfunctionalised sensor is depicted in figure 4.44. Two different sensors were measured in triplicates. The R_{CT} values of both sensors were quite low with about 400 Ω. After the functionalisation with MPA from aqueous solution, as mentioned in chapter 4.1.1, the impedances increased, as depicted in figure 4.44b. The R_{CT} only doubled to about 800 Ω. With the two-electrode sensor with ferro-ferricyanide the increase was much larger. This difference may be caused by the use of hexaammineruthenium(III) which has a positive charge. The monolayer consists of MPA which has a pKa 4.34. The measurement solution has a pH value of 7.4 and at this pH the acid will be completely dissociated and the monolayer has a negative charge. When ferro-ferricyanide is used as redox-couple, the negative charge of the redox-couple and of the monolayer will repel each other and increase the R_{CT}. When hexaammineruthenium(III) is used, the positive charge of the redox-active substance and the negative charge of the monolayer attract each other and can lead to a decrease of the impedances.

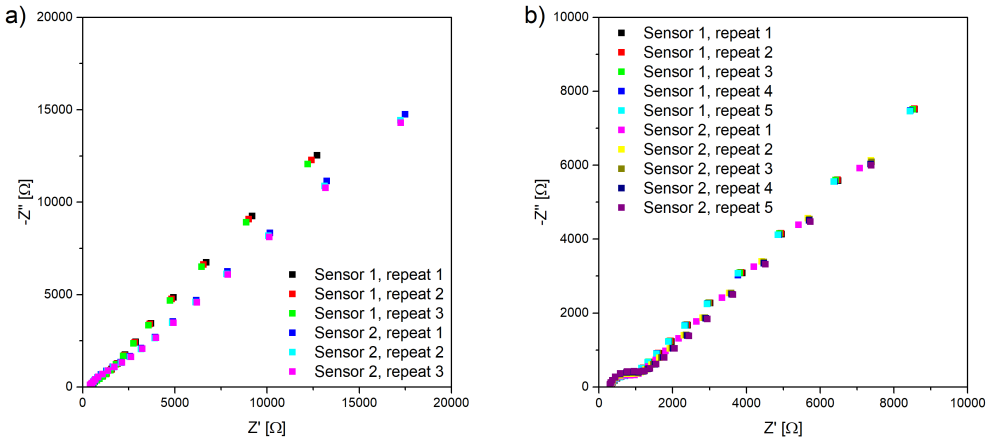

Figure 4.44: Nyquist plots of three-electrode sensor on ceramic substrate, measurement with 10 mmol mL^{-1} hexaammineruthenium(III)chloride in PBS and −160 mV DC-bias: a) sensor after cleaning b) sensor with MPA monolayer

To increase the R_{CT}, thiolic-acids with longer alkane chains have been used, such as MUA and MHDA. The Nyquist plots of sensors functionalised with MUA are depicted in figure 4.45a. Four different sensors were functionalised with a 10 mmol L^{-1} solution with 95 % ethanol as solvent for 16 h. The sensors were measured with three repeats each. The repeats of each sensor were nearly identical and varied only by a small amount. The R_{CT} of the sensors with the MUA monolayer, figure 4.45b, increased significantly to values in the range of 3000 Ω to 9000 Ω in comparison to the clean gold surface. It is immediately observable that the R_{CT} can vary from functionalised unit to unit. One reason for this variation can the formation of multilayers, which form differently on each electrode. Further, the variation can be caused by the electrode material. The used sensors on the ceramic substrate are produced via screen-printing. As mentioned in chapter 2.3 the screen-printing paste consists of the electrode material and different organic components to make the paste printable. Residues of the organic compounds, which remain after the temperature process, or differences in the roughness of the electrode surface can lead to variations in the formed monolayers on the WE.

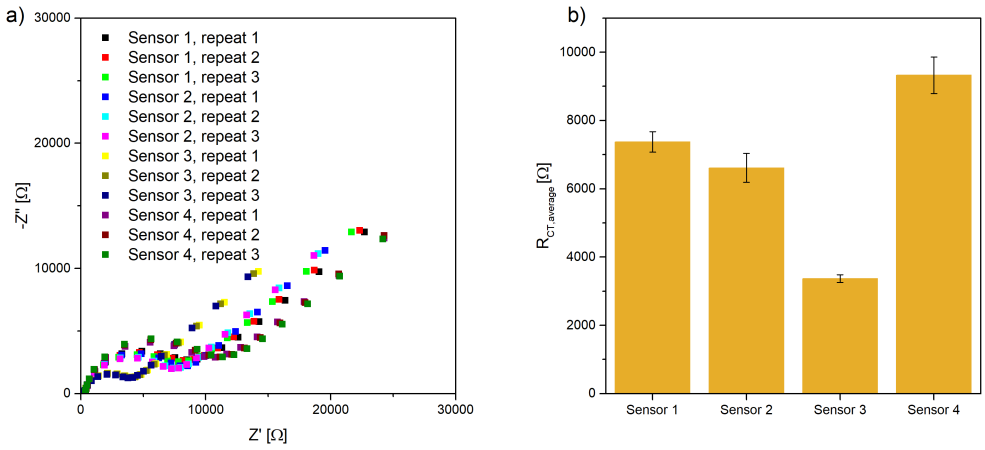

Figure 4.45: Three-electrode sensor on ceramic substrate with MUA monolayer, measured with 10 mmol mL^{-1} hexaammineruthenium(III) chloride in PBS and −160 mV DC-bias: a) Nyquist plot of the EIS spectra; b) average R_{CT} values of the different WE

When monolayers with even longer alkane chains are used, the impedances of the sensor increase even further. The EIS spectra of the sensors modified with MHDA are depicted in figure 4.46a. Each of the sensors was measured

with three repeats. The repeats of a sensor were all nearly identical and only differ slightly from each other, but the fitted curves resulted in varying R_{CT} values. The average R_{CT} values of each sensor are depicted in figure 4.46b. The impedances of ranged from about 28 kΩ to 38.6 kΩ. The standard deviation for sensor 1 was the highest with 6.5 kΩ. The Nyquist plots in figure 4.46a have a very different form in comparison to EIS spectra of the MUA monolayer. The minimum of the impedances at low frequencies is not clearly noticeable any more and the imaginary part of the impedances increases continuously after the maximum of the semicircle. This hampers the curve fitting of the EIS spectra and increases the variation in the calculated R_{CT}.

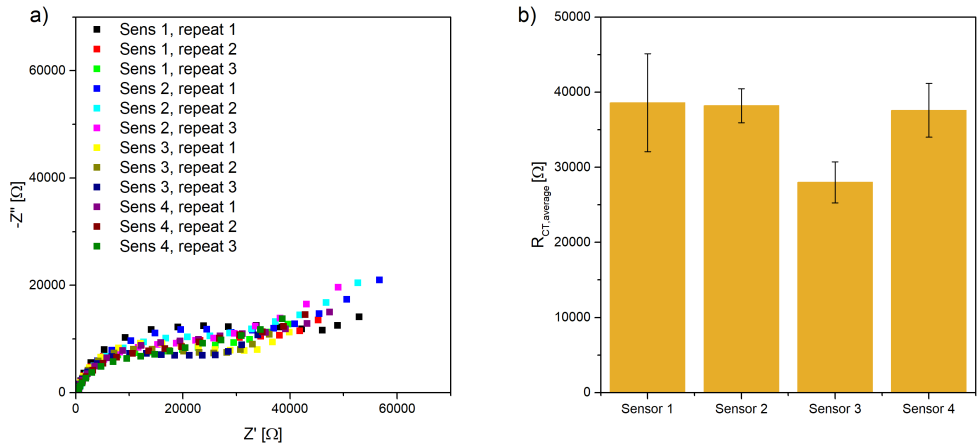

Figure 4.46: Three-electrode sensor on ceramic substrate with MHDA monolayer, measured with 10 mmol mL^{-1} hexaammineruthenium(III) chloride in PBS and −160 mV DC-bias: a) Nyquist plot of the EIS spectra; b) average R_{CT} values of the different WE

Different mixed monolayers were also tested to reduce the drastic increase of the impedances of a homogeneous monolayer consisting of long alkane chains. The tested monolayers were mixtures of MUA with BT, DT and UT. The EIS spectra of the mixed monolayer MUA-BT are depicted in figure 4.47a. The measurements of two sensors with the same functionalisation measured with three repeats each are depicted. The repeats of each sensor are nearly identical. Also, the electrochemical behaviour of both sensors is similar. The determined impedances are larger than the impedances of the clean gold surface and the MPA monolayer, but smaller than the impedances of the homogeneous MUA monolayer. The mixed monolayer of MUA and DT resulted in larger imped-

ances, as depicted in the Nyquist plots in figure 4.47b. Two sensors are shown and each of them was measured three times. Each of the repeats is nearly identical, but the impedances of both sensors are very different from each other. As discussed in chapter 4.1.1, the functionalisation of mixed monolayers can lead to varying monolayers. The impedances of the MUA-DT monolayer seem to be higher than of the MUA-BT monolayer, but still lower than of the MUA monolayer. The alkane chain of DT is longer by six carbon atoms than the BT which leads to a thicker monolayer and, therefore, to higher impedances.

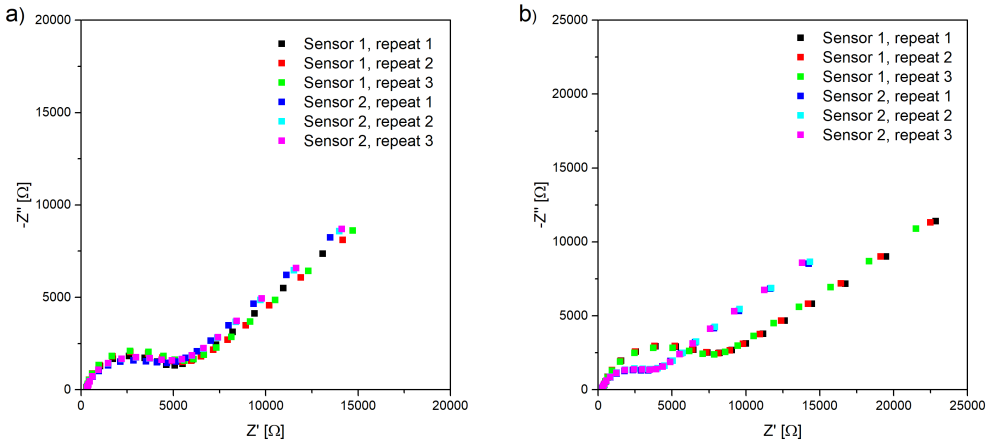

Figure 4.47: Nyquist plots of three-electrode sensor on ceramic substrate, measurement with 10 mmol mL^{-1} hexaammineruthenium(III)chloride in PBS and −160 mV DC-bias: a) sensor with mixed MUA-BT monolayer b) sensor with mixed MUA-DT monolayer

The Nyquist plots of the EIS spectra of the mixed monolayer MUA-UT are depicted in figure 4.48. The determined impedances of these sensors are very similar to the results of the sensors with the mixed MUA-DT monolayer. The repeats of each sensor are nearly identical and the impedances of the monolayer are very different form sensor to sensor. The similarities between the MUA-UT and the MUA-DT monolayer can be explained by the similarities of the thickness of both mixed monolayers. The alkane chain of UT is only longer by one carbon atom which leads to a very similar thickness and electrochemical behaviour of the functionalised sensor. The impedances of the MUA-UT monolayer are only slightly larger than of the MUA-DT monolayer, but still lower than of the homogeneous MUA monolayer.

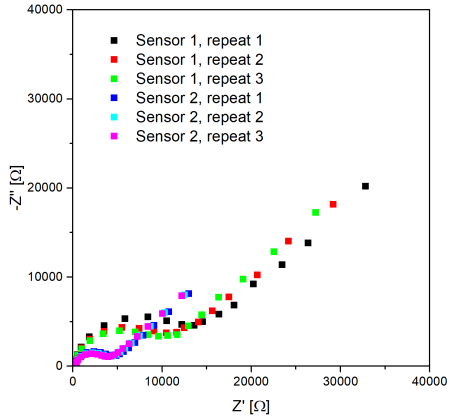

Figure 4.48: Nyquist plots of three-electrode sensor on ceramic substrate with MUA-UT monolayer, measurement with 10 mmol mL^{-1} hexaammineruthenium(III)chloride in PBS and −160 mV DC-bias

4.6.2 Three-electrode sensor on glass substrate

The in chapter 4.1 mentioned sensors on a glass substrate were used for this functionalisation, after a silver/silverchloride reference electrode was added. The EIS spectra of the cleaned gold electrodes prior to any functionalisation are depicted in the Nyquist plots in figure 4.49a. The determined impedances are very low and the R_{CT} of the gold electrodes is only about 100 Ω. The semicircle is barely noticeable as shown in the close up in figure 4.49b.

The functionalisation with MPA was not utilised for the electrodes on the glass and PET substrate because of the results of the fully functionalised MPA based biosensors as will be discussed in chapter 4.7.1. The sensor was incubated with 10 mmol L^{-1} MUA for 16 h, 18 h and 20 h to optimise the monolayer functionalisation. The EIS spectra of the sensor on the glass substrate with 16 h of incubation time are depicted in figure 4.50a. The measured impedances vary from WE to WE. Similar behaviour of the MUA monolayer after the monolayer functionalisation was also observed with the two-electrode sensor and the three-electrode sensor on the ceramic substrate. The R_{CT} values were determined by curve fitting to be between 9.3 kΩ and 17.0 kΩ kOhm as depicted in figure 4.50b. In comparison, the R_{CT} values of the monolayer after 18 h of incubation time were determined to be 15.1 kΩ and 23.7 kΩ, as depicted in figure 4.51a. Initially it appears that the formation of the monolayer was not finished after the 16 h

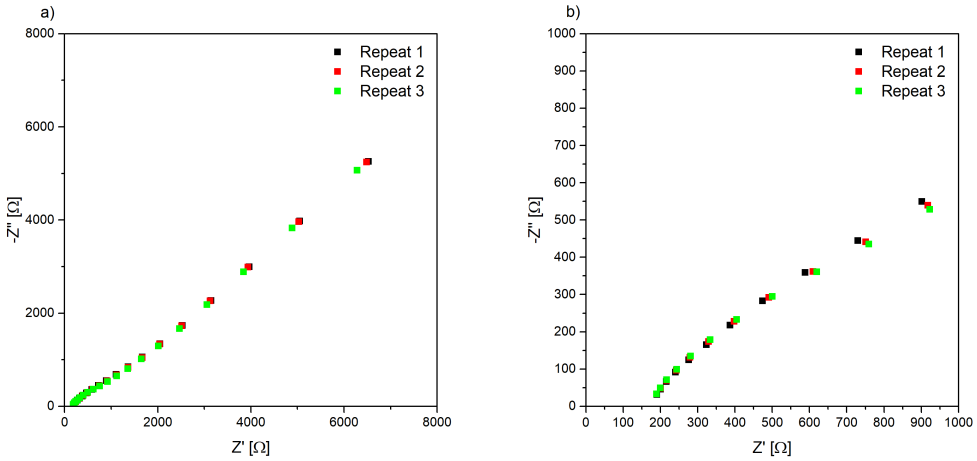

Figure 4.49: Nyquist plots of three-electrode sensor on glass substrate without functionalisation, measurement with 10 mmol mL^{-1} hexaammineruthenium(III)chloride in PBS and −160 mV DC-bias

of incubation time and got more dense with the longer incubation time, but the R_{CT} values of the sensor after 20 h, shown in figure 4.51b, contradict this conclusion. The R_{CT} values of the five functionalised WE were determined to be between 7.1 kΩ and 21.1 kΩ. With these results it is more likely, that the variation of R_{CT} value is caused by differences in the formation of the mono- or possible multilayers and not influenced at all by the incubation time. It seems that the 16 h of incubation time are sufficient for the monolayer formation.

4.6.3 Three-electrode sensor on PET substrate

To examine the functionalisation process on the PET substrate, the EIS spectrum of the clean gold electrode were recorded. The impedances were very low with values of about 100 Ω, as can be observed in figure 4.52. The CV of the gold electrode was recorded to observe the electrochemical behaviour of the PET based sensor further. As shown in figure 4.52a, the measurement did not reveal any side reactions or unexpected behaviour of the sensor.

The sensor was functionalised with a MUA monolayer from a 0.1 mmol L^{-1} solution with different formation times of 16 h, 18 h, 20 h and 40 h. The EIS spectra of these sensors are depicted in figure 4.53a. The longer the incubation time was, the higher the determined impedances of the sensor became. The R_{CT} of the sensor after 16 h was determined to be 1.1 kΩ and increased after the 40 h

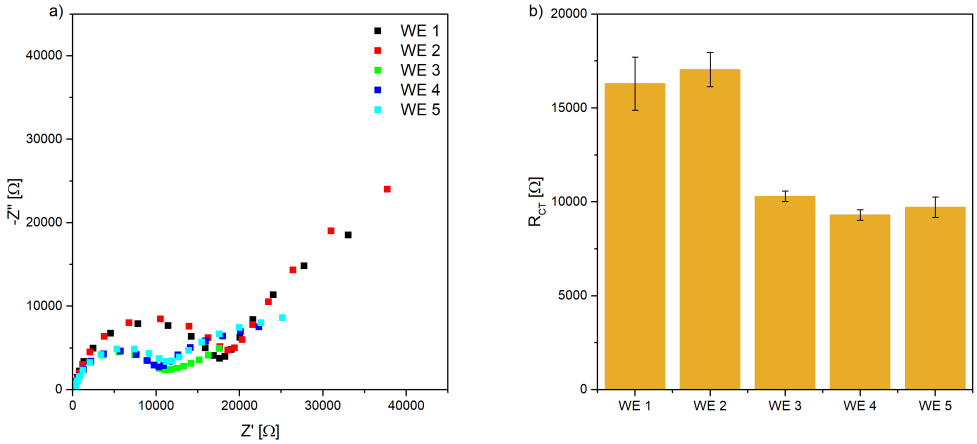

Figure 4.50: Three-electrode sensor on glass substrate with MUA monolayer after 16 h of incubation time, measured with 10 mmol mL^{-1} hexaammineruthenium(III) chloride in PBS and −160 mV DC-bias: a) Nyquist plot of the EIS spectra; b) average R_{CT} values of the different WE

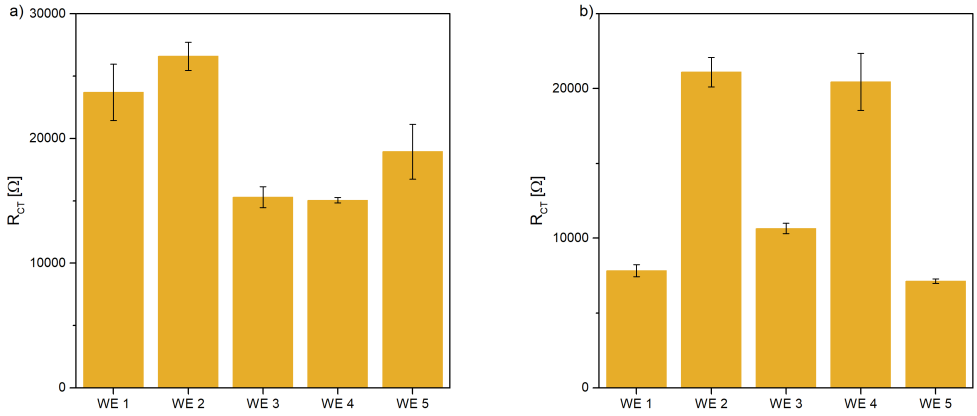

Figure 4.51: Average R_{CT} values of the different WE of three-electrode sensor on glass substrate with MUA monolayer with different incubation times, measured with 10 mmol mL^{-1} hexaammineruthenium(III) chloride in PBS and −160 mV DC-bias: a) average R_{CT} values after 18 h of incubation; b) average R_{CT} values after 20 h of incubation

to about 6 kΩ as shown in figure 4.56a. This indicates, that either the incubation time or the MUA concentration is insufficient to form the SAM. Increasing the MUA concentration to 1 mmol L^{-1} increased the impedances further. In

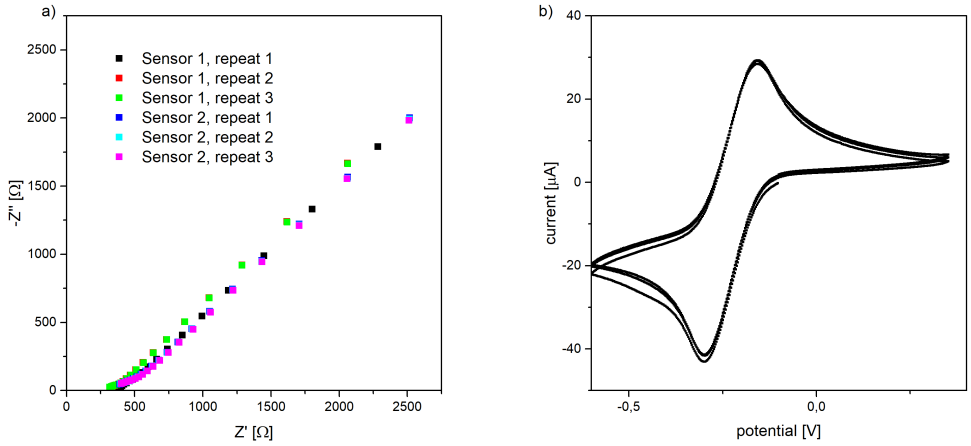

Figure 4.52: Three-electrode sensor on PET substrate with cleaned gold surface, measured with 10 mmol mL^{-1} hexaammineruthenium(III) chloride in PBS: a) Nyquist plot of the EIS spectra with −160 mV DC-bias; b) CV measurement

figure 4.53b the EIS curves of two PET based sensors with a monolayer formed from 1 mmol L^{-1} MUA for 16 h are shown. Both sensors did provide a R_{CT} of about 5 kΩ, but the offset from zero, the solution resistance, was very different from each other.

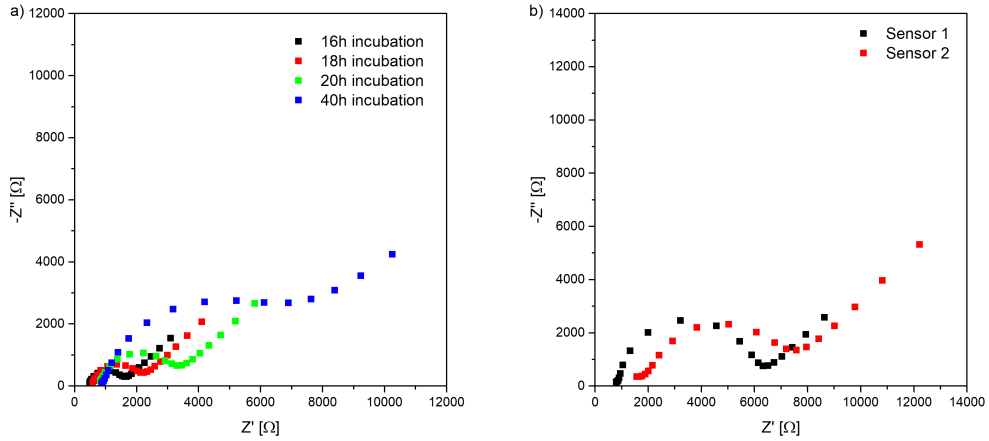

Figure 4.53: EIS spectra of three-electrode sensor on PET substrate measured with 10 mmol mL^{-1} hexaammineruthenium(III) chloride in PBS and −160 mV DC-bias: a) functionalised with 0.1 mmol L^{-1} MUA for 16 h, 18 h, 20 h, and 40 h; b) sensors functionalised with 1 mmol L^{-1} MUA solution for 16 h

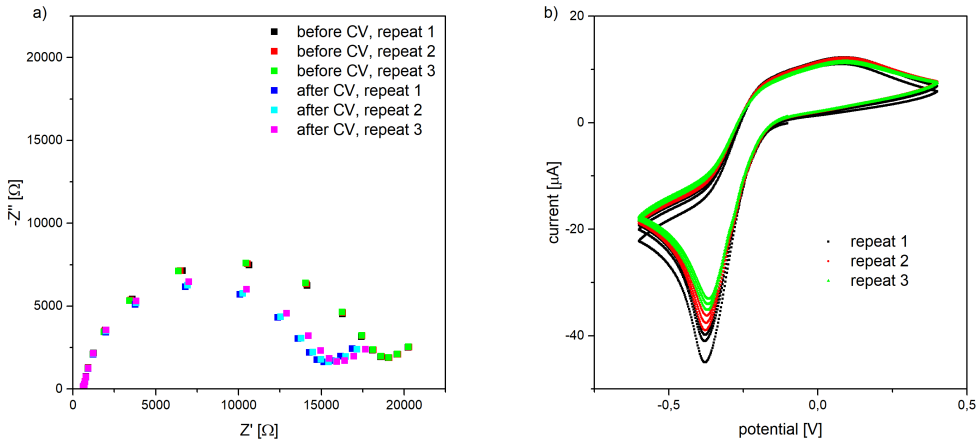

Figure 4.54: Three-electrode sensor on PET substrate with MUA monolayer, measured with 10 mmol mL^{-1} hexaammineruthenium(III) chloride in PBS: a) Nyquist plot of the EIS spectra with −160 mV DC-bias and minimal changes before and after CV measurement; b) CV changes over measurement time

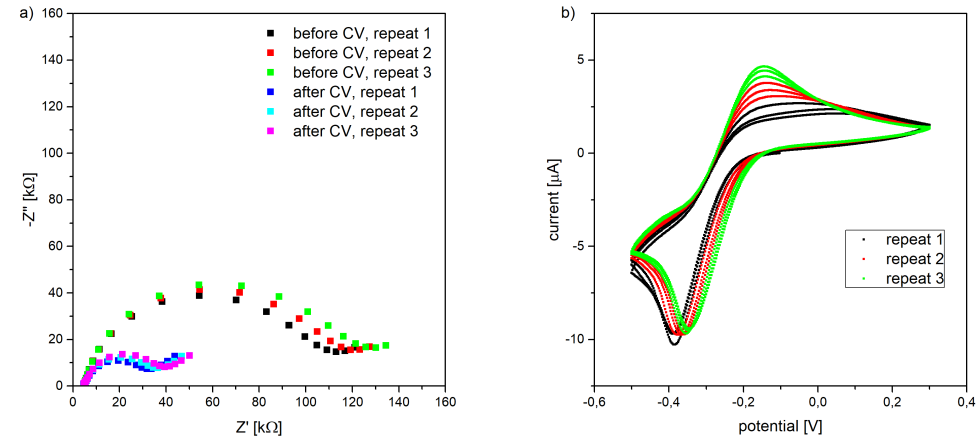

Figure 4.55: Three-electrode sensor on PET substrate with MUA monolayer, measured with 10 mmol mL^{-1} hexaammineruthenium(III) chloride in PBS: a) Nyquist plot of the EIS spectra with −160 mV DC-bias and significant changes before and after CV measurement; b) CV changes over measurement time

The R_{CT} value of the sensors after 16 h in a 1 mmol L^{-1} MUA solution was lower than the sensor with the MUA layer formed from a 0.1 mmol L^{-1} MUA solution for 40 h. To ensure a dense formation of the MUA monolayer the sensor

was incubated with a 10 mmol L^{-1} MUA solution for 16 h. The EIS spectras of the sensor are depicted in figure 4.54. The impedances of the sensor were recorded before and after a CV measurement. The R_{CT} was about 17.3 kΩ before and 14.1 kΩ after the CV measurement. This indicates that neither the 40 h incubation with 0.1 mmol L^{-1} MUA nor the 16 h incubation with 1 mmol L^{-1} MUA were sufficient to form a dense monolayer. Also, the change of the R_{CT} value before and after the CV measurement indicate, that something changes with the electrode system. A corrosion of the electrode system can be disregarded because of the previous tests of the redox-system in chapter 4.5.3. When the CV of the sensor is recorded, as depicted in figure 4.54b, the reduction peak decreases which would rather indicate an increase of the R_{CT}. An error of the washing step in between measurements which led to an accumulation of the redox-couple on the electrode is more likely to be the cause of the small measurement differences. But in other cases the differences between the EIS measurements before and after the CV can be more severe for the sensors on the PET substrate, as depicted in figure 4.55a. The repeats of the EIS measurements drifted during the measurement itself and the impedances decreased drastically after the CV measurement. It can be observed in figure 4.55b that the peak position of the reduction peak changed its position with each measurement. Additionally, the peak height of the oxidation peak increased continuously. The first repeat was more closely in its form to the CV of the PET based sensor with the MUA monolayer in figure 4.54a. After the third repeat the form of the CV resembled the CV curve of the cleaned gold surface in figure 4.52b. This would indicate that something was adsorbed on the gold surface during the functionalisation step and desorbed during the CV measurement. It is possible, that some additives from the PET substrate dissolve during the functionalisation procedure and adsorb on the gold electrodes and cause these differences between the PET based sensors of the same batch. This problem renders the sensor on the PET substrate unusable. A change of the PET substrate or use of a different flexible substrate could avoid this problem.

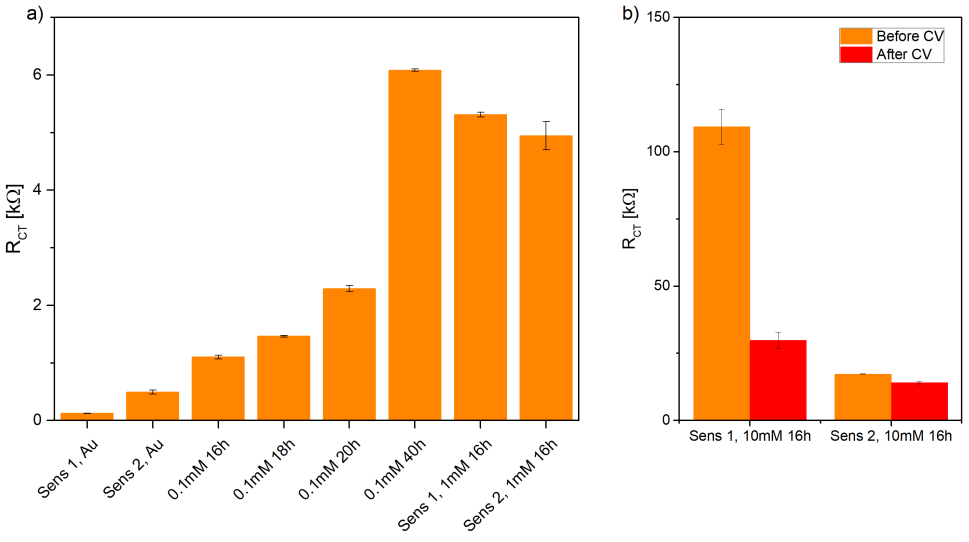

Figure 4.56: R_{CT} values of differently functionalised PET based sensors: a) sensor with gold surface, functionalised with 0.1 mmol L^{-1} MUA for 16 h/18 h/20 h/40 h and functionalised with 1 mmol L^{-1} MUA for 16 h; b) R_{CT} values of two different PET based sensors functionalised with 10 mmol L^{-1} MUA for 16 h before and after CV measurement

4.7 Evaluation functionalisation protocols of three-electrode biosensors

4.7.1 Biosensors on ceramic substrate

The ceramic based sensors with the different monolayers, which were mentioned in chapter 4.6.1, were fully functionalised. They were activated with 10 mmol L^{-1} EDC and 10 mmol L^{-1} NHS for 1 h. Further, the Fc-IgG-Ab was bound to the surface and the remaining activated carboxylic acid groups were blocked with EA. After the functionalisation the blank impedances were recorded with a 10 mmol L^{-1} hexaammineruthenium(III) solution in PBS at a DC-bias of −160 mV. After this, the different biosensors were incubated for 30 min with a 1 mg L^{-1} IgG solution. This concentration is in the range of the expected IgG concentration in a human saliva sample. The response of the biosensor with MPA as the basis of the functionalisation is depicted in figure 4.57a. The impedances increased only barely. The $R_{CT,norm}$ was only 0.08. In com-

parison the MUA based biosensor had a considerably larger increase. The EIS spectrum of the biosensor increased after the incubation with the bufferd IgG standard, as depicted in figure 4.57b. The determined $R_{CT,norm}$ was 0.61, which is nearly 8 times higher than the response of the MPA based sensor.

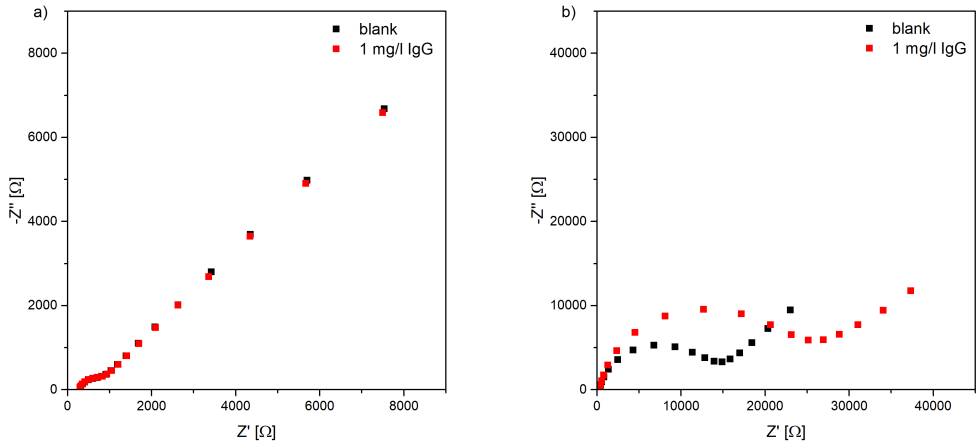

Figure 4.57: Nyquist plots of a fully functionalised three-electrode sensor on ceramic substrate, measurement with 10 mmol mL^{-1} hexaammineruthenium(III) chloride in PBS and −160 mV DC-bias: a) MPA as basis of the functionalisation; b) MUA as basis of the functionalisation

The response to the buffered IgG solution of the fully functionalised biosensors based on mixed monolayers was also tested. The EIS spectra of the biosensor with the mixed MUA-BT layer before and after the binding of the antigen are depicted in the Nyquist plots in figure 4.58a. The increase of the impedances is only barely noticeable. The normalised increase is only about 0.06 with a standard deviation of 0.04. It is likely, that there is no increase at all and the deviation is only caused by the variation of the measurement. In the case of the biosensor with the mixed monolayer MUA-DT as basis for the functionalisation the increase is a little bit bigger, as depicted in the Nyquist plots in figure 4.58b, but $R_{CT,norm}$ was only 0.1 which is not very much in comparison to the biosensor based on the MUA monolayer.

The increase of the length of the mixed MUA-UT monolayer improved the response of the biosensor, as can be seen in figure 4.59a. The change of the R_{CT} before and after the binding process is clearly noticeable. The normalised increase is much bigger than the other mixed monolayers with 0.19, but it is

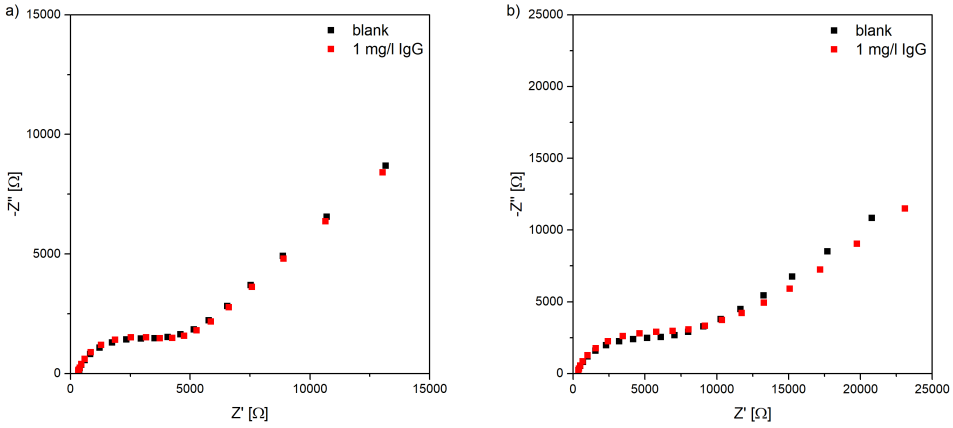

Figure 4.58: Nyquist plots of a fully functionalised three-electrode sensor on ceramic substrate, measurement with 10 mmol mL^{-1} hexaammineruthenium(III) chloride in PBS and −160 mV DC-bias: a) MUA-BT as basis of the functionalisation; b) MUA-DT as basis of the functionalisation

still three times lower than the response of the biosensor based on the MUA monolayer. The sensor based on the MHDA monolayer has a similar response to the binding of the IgG as the sensor based on the MUA-UT monolayer, as can be seen in the Nyquist plot in figure 4.59b. The $R_{CT,norm}$ is 0.18, but the form of the EIS spectrum made the curve fitting difficult, as was discussed in chapter 4.6.1. With this difficulty, the standard deviation of the response was also about 0.18, which renders the biosensor based on the MHDA monolayer completely useless.

All the $R_{CT,norm}$ values of the biosensors based on the different monolayers are summarised in figure 4.60. It is immediately obvious that the best result was achieved with the MUA based biosensor which reached a response of about 0.61. The biosensors based on the MPA, the mixed MUA-BT and MUA-DT monolayer had the lowest responses and were barely noticeable. Increasing the thickness of the MUA monolayer by five carbon atoms to MHDA worsened the response of the biosensor and only increased the variation of the impedance measurements. With these results the only viable choice of biosensors is the one based on the MUA monolayer.

To optimise the response of the MUA based biosensor, different EDC and NHS concentrations were tested. The remaining steps in the functionalisation

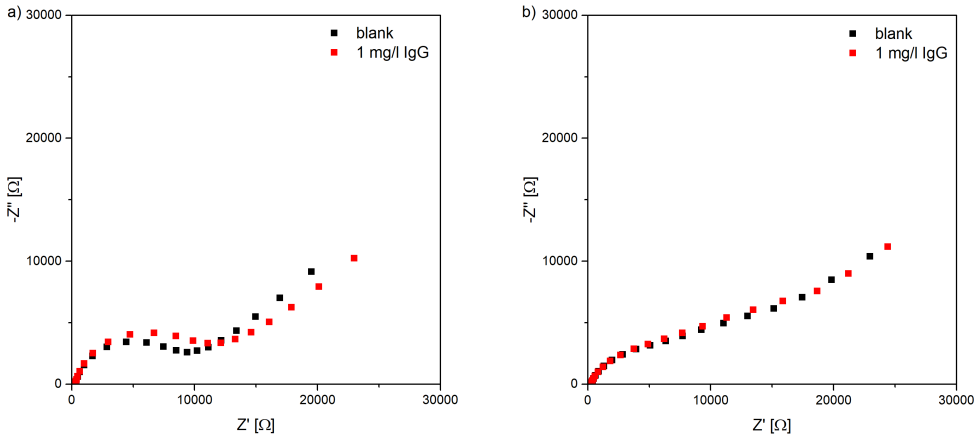

Figure 4.59: Nyquist plots of a fully functionalised three-electrode sensor on ceramic substrate, measurement with 10 mmol mL^{-1} hexaammineruthenium(III) chloride in PBS and −160 mV DC-bias: a) MUA-UT as basis of the functionalisation; b) MHDA as basis of the functionalisation

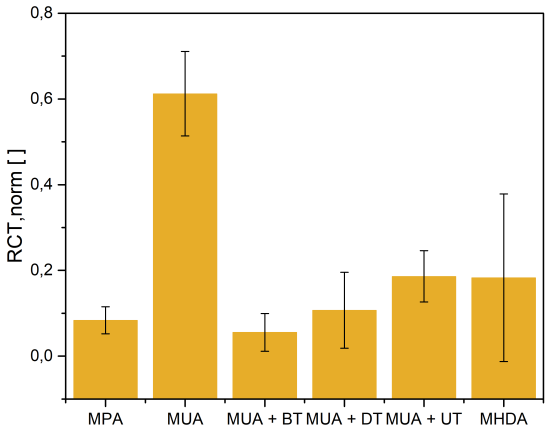

Figure 4.60: Comparison of $R_{CT,norm}$ values to incubation with 1 mg L^{-1} IgG standard of sensors on ceramic substrate with functionalisation based on different monolayers

process, the binding of the antibody and blocking of the remaining activated carboxylic acid groups, were kept the same. In figure 4.61a the EIS spectra of the blank measurement and the response of a MUA based biosensor, which was activated with EDC and NHS concentration of 5 mmol L^{-1} each for 1 h, to

a 1 mg L^{-1} IgG solution are depicted. The impedances of the sensor increased significantly after the incubation. The $R_{CT,norm}$ was 0.43. Which is more than the biosensors based on the mixed monolayer, MPA or MHDA, but is still lower than the activation of the MUA monolayer with an EDC and NHS concentration of 10 mmol L^{-1}. Increasing the EDC and NHS concentration more to 25 mmol L^{-1} each worsened the response of the biosensor as can be seen in figure 4.61b. After the binding of the antigen the impedances increased only by a very small amount. The $R_{CT,norm}$ was 0.19 which is only about a third of the initially used functionalisation procedure of the MUA based biosensor.

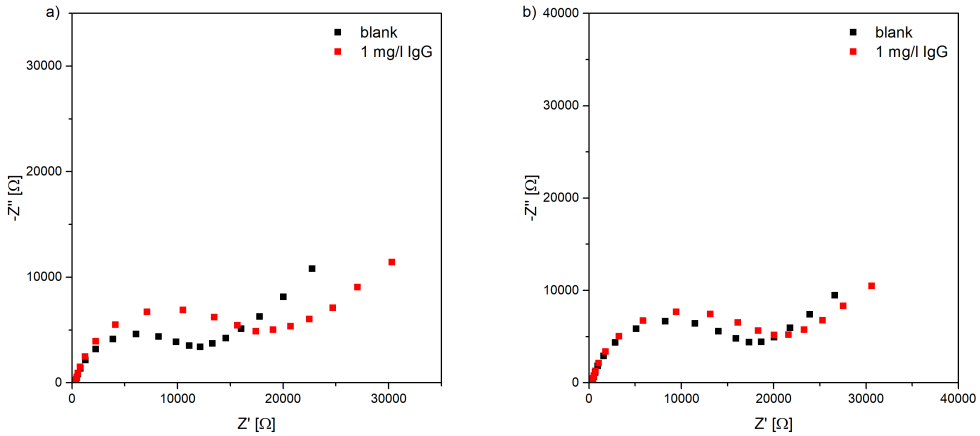

Figure 4.61: Nyquist plots of a fully functionalised three-electrode sensor on ceramic substrate, MUA/Fc-IgG-Ab/EA, measurement with 10 mmol mL^{-1} hexaammineruthenium(III) chloride in PBS and −160 mV DC-bias: a) sensor activation with 5 mmol L^{-1} EDC and NHS; b) sensor activation with 25 mmol L^{-1} EDC and NHS

Increasing the EDC and NHS concentration worsened the response even more. The Nyquist plots of biosensors with a 100 mmol L^{-1} EDC and NHS concentration are depicted in figure 4.62a and EIS spectra of a sensor activated with a concentration of 250 mmol L^{-1} are depicted in figure 4.62b. In both cases the increase is much lower. For the activation with 100 mmol L^{-1} the $R_{CT,norm}$ was 0.15. The sensors which were activated with a EDC and NHS concentration of 250 mmol L^{-1} did not increase at all after the incubation with the IgG standard.

The responses of the different functionalisation protocols of the MUA based biosensors are summarised in figure 4.63. The highest response was reached when the functionalisation protocol with 10 mmol L^{-1} EDC and 10 mmol L^{-1}

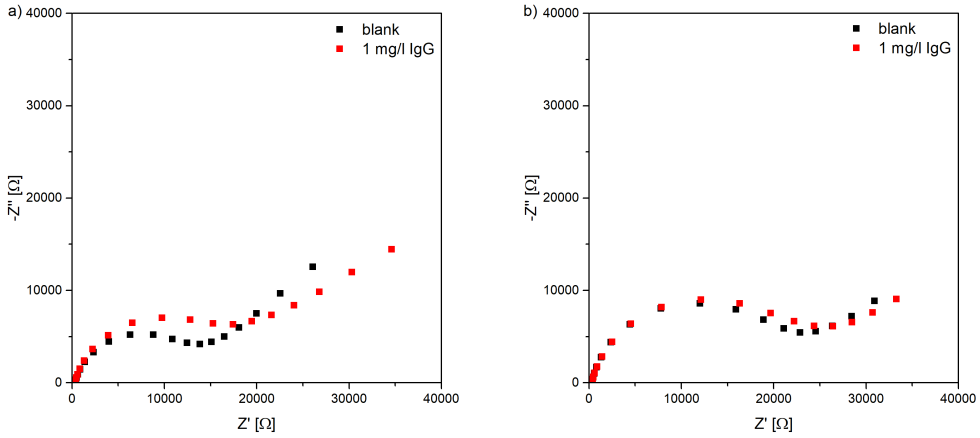

Figure 4.62: Nyquist plots of a fully functionalised three-electrode sensor on ceramic substrate, MUA/Fc-IgG-Ab/EA, measurement with 10 mmol mL^{-1} hexaammineruthenium(III) chloride in PBS and −160 mV DC-bias: a) sensor activation with 100 mmol L^{-1} EDC and NHS; b) sensor activation with 250 mmol L^{-1} EDC and NHS

NHS was used. Increasing the EDC and NHS concentration worsened the response of the biosensor. At a EDC and NHS concentration of 250 mmol L^{-1} the biosensor did not respond in any way when the sensors were incubated with the 1 mg L^{-1} IgG solution. When carboxylic acid groups are activated with EDC and NHS, side reactions can occur at high concentrations which can inactivate the functional groups and hinder the binding of the receptor molecule. In the case of this measurement series it appears, that the inactivation takes place when EDC and NHS concentrations larger than 10 mmol L^{-1} are used. At lower concentrations, the carboxylic acid groups are not fully activated and also worsen the binding capacity of the biosensor which already occurs at a EDC and NHS concentration of 5 mmol L^{-1}.

4.7.2 Biosensor on glass substrate

For the MUA based biosensors on a glass substrate, the activation protocol was investigated again. In figure 4.64a the EIS spectra of a biosensor activated with a 10 mmol L^{-1} EDC and 10 mmol L^{-1} NHS solution are depicted. After the incubation with the 1 mg L^{-1} IgG solution, the bound antigen increased the impedances significantly. The $R_{CT,norm}$ reached a value of 0.63 with a very low standard deviation of 0.003. Increasing the EDC and NHS concentration in

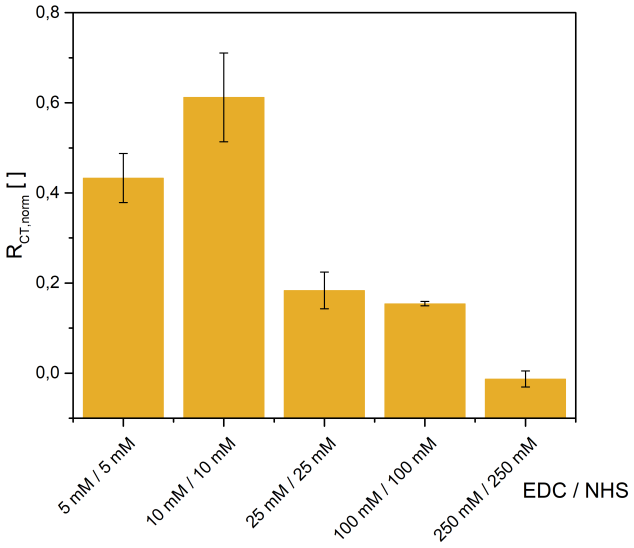

Figure 4.63: $R_{CT,norm}$ responses of three-electrode ceramic based sensors, functionalisation MUA/Fc-IgG-Ab/EA, with different EDC and NHS concentrations used in the activation step

the functionalisation protocol to 25 mmol L^{-1} each worsened the response of the biosensor as shown in figure 4.64b. The response of the sensor was lowered by about two thirds to a $R_{CT,norm}$ of 0.19.

When the EDC and NHS concentration was increased further, the response of the sensors turned out even worse. The EIS spectra before and after the incubation with the IgG standard for the biosensors activated with 50 mmol L^{-1} EDC and NHS are depicted in figure 4.65a and for the sensor which was activated with 100 mmol L^{-1} EDC are depicted in figure 4.65b.

The $R_{CT,norm}$ values of the different functionalisation protocols are summarised in figure 4.66. The results of this test series are very similar to the test results of the ceramic based biosensors. The highest response was achieved with a 10 mmol L^{-1} EDC and NHS concentration of about 0.63. The sensors responded less with an increase of the EDC and NHS concentration. At a concentration of 100 mmol L^{-1} EDC and NHS the response decreased to 0.036.

4.7.3 Biosensor on PET substrate

The PET based sensors with the MUA monolayer were also fully functionalised as the glass or ceramic based ones. The carboxylic acid groups were activated

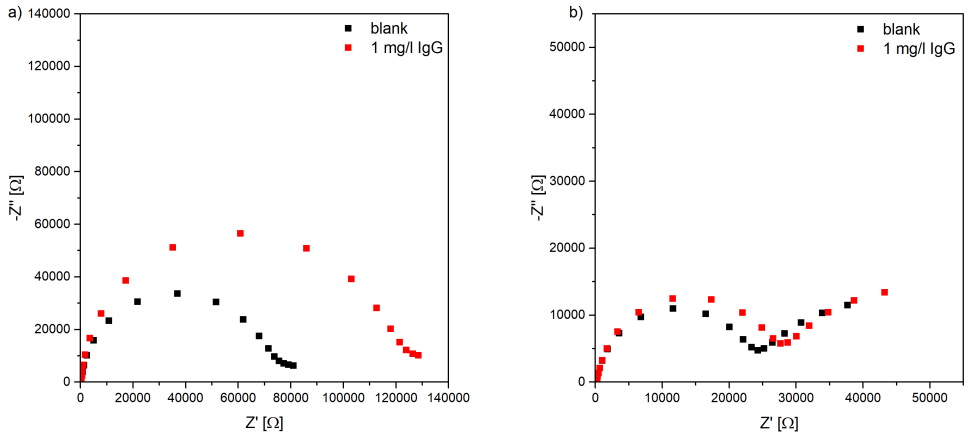

Figure 4.64: Nyquist plots of a fully functionalised three-electrode sensor on glass substrate, MUA/Fc-IgG-Ab/EA, measurement with 10 mmol mL^{-1} hexaammineruthenium(III) chloride in PBS and −160 mV DC-bias: a) sensor activation with 10 mmol L^{-1} EDC and NHS; b) sensor activation with 25 mmol L^{-1} EDC and NHS

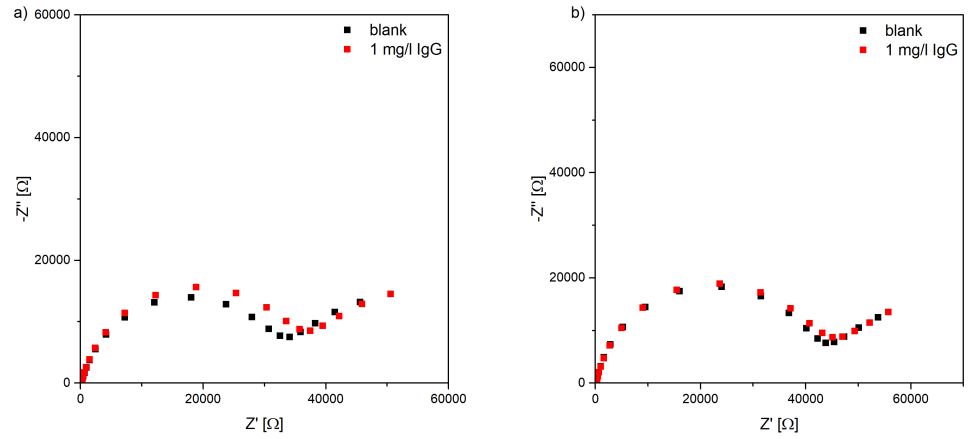

Figure 4.65: Nyquist plots of a fully functionalised three-electrode sensor on glass substrate, MUA/Fc-IgG-Ab/EA, measurement with 10 mmol mL^{-1} hexaammineruthenium(III) chloride in PBS and −160 mV DC-bias: a) sensor activation with 50 mmol L^{-1} EDC and NHS; b) sensor activation with 100 mmol L^{-1} EDC and NHS

with different EDC and NHS concentrations to optimise the functionalisation procedure. Subsequently, the IgG-Ab was bound to the surface and the remain-

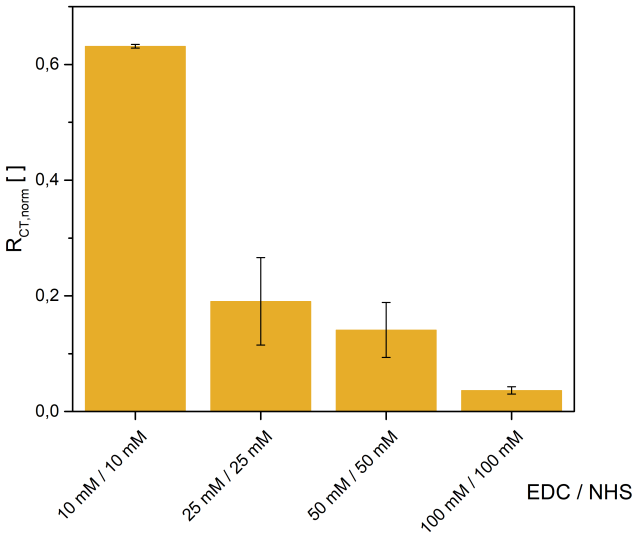

Figure 4.66: $R_{CT,norm}$ responses of three-electrode glass based sensors, functionalisation MUA/Fc-IgG-Ab/EA, with different EDC and NHS concentrations used in the activation step

ing activated functional groups were blocked with EA. First, the functionalisation protocol with a 10 mmol L^{-1} EDC and NHS concentration was tested. The EIS spectra before and after the incubation with a 1 mg L^{-1} IgG solution are depicted in figure 4.67a. The impedances after the binding of the antigen increased only barely. The $R_{CT,norm}$ was only determined to be 0.18 which is more than three times lower than the response of the best ceramics or glass based biosensor. Increasing the concentration of EDC and NHS to 25 mmol L^{-1} did not improve the response at all, as can be observed in the EIS spectra in figure 4.67b. After the binding of the antigen the $R_{CT,norm}$ was only 0.11.

Further increasing the concentration of EDC and NHS for the activation to 50 mmol L^{-1} or 100 mmol L^{-1} made the response of the sensor to the incubation with the 1 mg L^{-1} IgG standard even worse. The EIS spectrum changed only a little bit in the case of the activation with 50 mmol L^{-1}, as shown in figure 4.68a. With a concentration of 100 mmol L^{-1} EDC and NHS the increase of the impedances was barely noticeable as depicted in figure 4.68b. With a $R_{CT,norm}$ of 0.08 and a standard deviation of 0.06, the sensor is completely unsuitable for the application in a POC device.

The response of the sensors which were activated with EDC and NHS con-

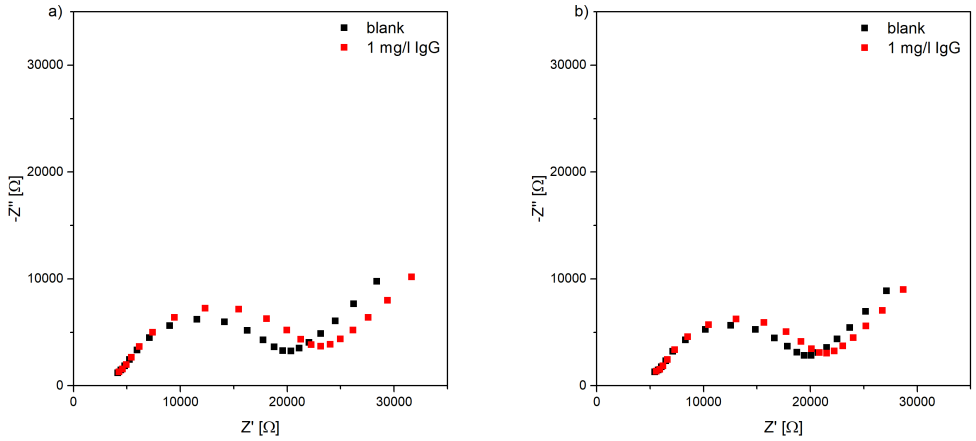

Figure 4.67: Nyquist plots of different functionalisation protocols used for PET based biosensors before (black) and after incubation with a $1\,\mathrm{mg\,L^{-1}}$ IgG solution (red), measured with $10\,\mathrm{mmol\,L^{-1}}$ hexaammineruthenium(III) with $-160\,\mathrm{mV}$ DC-bias: a) sensor activated with $10\,\mathrm{mmol\,L^{-1}}$ EDC and NHS solution; b) sensor activated with $25\,\mathrm{mmol\,L^{-1}}$ EDC and NHS solution

centrations of $10\,\mathrm{mmol\,L^{-1}}$, $25\,\mathrm{mmol\,L^{-1}}$, $50\,\mathrm{mmol\,L^{-1}}$ and $100\,\mathrm{mmol\,L^{-1}}$ are compared in figure 4.69. The best response was achieved with a concentration of $10\,\mathrm{mmol\,L^{-1}}$ EDC and NHS during the activations step. The $R_{CT,norm}$ was 0.18 with a very small standard deviation of 0.004. Increasing the EDC and NHS concentration for the activation step did not improve the response of the sensor. The sensor activated with $25\,\mathrm{mmol\,L^{-1}}$ EDC and NHS had only a response of 0.11. Using $50\,\mathrm{mmol\,L^{-1}}$ EDC and NHS had a similar response with 0.14. With an EDC and NHS concentration of $100\,\mathrm{mmol\,L^{-1}}$ the worst response was recorded with an $R_{CT,norm}$ of 0.08. Increasing the EDC and NHS concentration worsened the response and also increased the standard deviation of the sensors. The standard deviation for the sensor with the $100\,\mathrm{mmol\,L^{-1}}$ EDC and NHS activation was the highest with 0.06 which is almost as high as the response itself. Only the functionalisation protocol with the $10\,\mathrm{mmol\,L^{-1}}$ activation step had a usable result, but the response is still lower than the sensors based on glass or ceramic substrate.

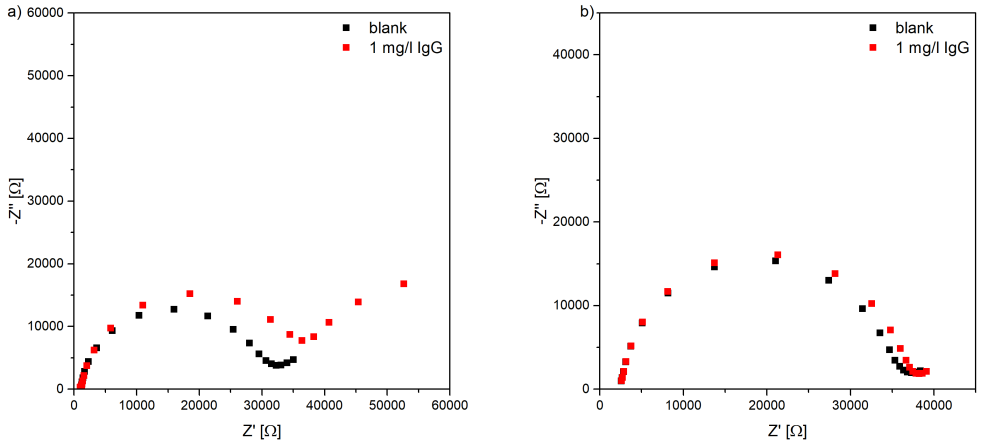

Figure 4.68: Nyquist plots of different functionalisation protocols used for PET based biosensors before (black) and after incubation with a $1\,\mathrm{mg\,L^{-1}}$ IgG solution (red), measured with $10\,\mathrm{mmol\,L^{-1}}$ hexaammineruthenium(III) with $-160\,\mathrm{mV}$ DC-bias: a) sensor activated with $50\,\mathrm{mmol\,L^{-1}}$ EDC and NHS solution; b) sensor activated with $100\,\mathrm{mmol\,L^{-1}}$ EDC and NHS solution

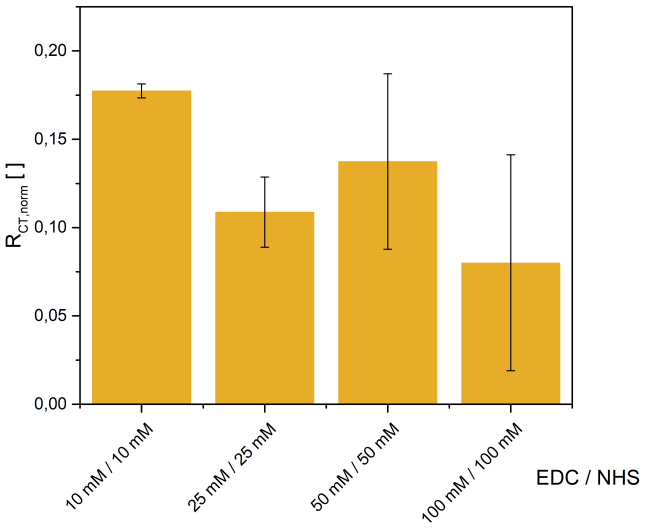

Figure 4.69: $R_{CT,norm}$ responses of three-electrode PET based sensors, functionalisation MUA/Fc-IgG-Ab/EA, with different EDC and NHS concentrations used in the activation step

4.7.4 Comparison of of biosensors on different substrates

The response of the biosensors on the ceramic, glass and PET substrate to the incubation with the $1\,\mathrm{mg\,L^{-1}}$ IgG solution are summarised in figure 4.70.

Overall, the best results were achieved with an EDC and NHS concentration of 10 mmol L^{-1}. With higher concentrations the response was lower and was close to zero at an EDC and NHS concentration of 100 mmol L^{-1} for most substrates. The activation of carboxylic acid groups with carbodiimides can lead to side reactions which inactivate the functional groups. At high concentrations these negative side reactions occur more often and lower the yield of activated carboxylic acid groups. The best yield was achieved at a concentration of 10 mmol L^{-1}. Comparing the response of the different substrates it is apparent that the biosensor on the PET substrates exhibited the smallest response to the IgG standard. Even in the best case of the tested functionalisation protocols the response was only 0.18 which is about three times lower than the response of the biosensors based on ceramic or glass substrate. It is possible that constituents of the PET substrate inhibit the functionalisation procedure. Taking the results of the CV of the MUA monolayer on the PET based biosensor in chapter 4.6.3 into account it is possible that some of the additives of the PET substrate are dispersed on the gold surface and inhibit the formation of a dense SAM and therefore, a functional biosensor. With the current level of response to the 1 mg L^{-1} IgG solution the biosensor on the PET substrate is not suitable for an POC device. Other PET substrates have to be tested which do not lead to this behaviour, or other flexible substrates have to be used. The responses of the biosensors on the ceramic and glass substrate are very similar. Both sensor types have a response of about 0.6. The standard deviation of the ceramic based sensor was bigger with a value of 0.098 in comparison to the sensor on the glass substrate with a deviation of 0.003. The gold electrodes on the ceramic substrate were produced by the company BVT in a screen-printing process and the electrodes on the glass substrate were deposited in the lab with TVD. It is possible that the bigger variation is caused by the difference of the electrode deposition process. For the screen-printing organic additives are used for the printing. In an annealing step the additives are removed, but it is possible that residues are still left behind which can impede the performance of the sensor.

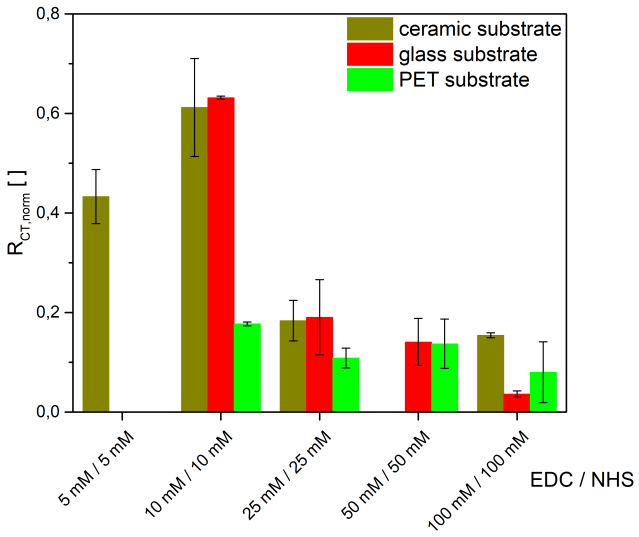

Figure 4.70: $R_{CT,norm}$ responses of three-electrode sensors on PET, ceramic or glass substrates, functionalisation MUA/Fc-IgG-Ab/EA, with different EDC and NHS concentrations used in the activation step

4.8 Three-electrode cortisol sensor

4.8.1 Measurement of buffered cortisol solutions

The biosensors on the ceramic substrate from the previous chapter were also functionalised with cortisol specific antibodies instead of human-IgG specific antibodies. All other parts of the functionalisation protocol, such as the MUA monolayer, EA as blocker, and the 10 mmol L^{-1} EDC and NHS solution for the activation, were kept the same. First, the blank value of the biosensor was determined and then the sensor was incubated with PBS buffered cortisol solutions. The sensor was incubated with cortisol concentrations ranging from 1 pmol L^{-1} to 1 µmol L^{-1}. The biosensor was incubated for 15 min with each concentration and after the binding process the EIS spectrum was determined. The EIS spectra of the biosensor are depicted in figure 4.71a. The impedances had the lowest values in the case of the blank measurement. After the incubation with the 1 pmol L^{-1} cortisol concentration, the impedances increased only slightly. In the concentration range from 10 pmol L^{-1} to 100 nmol L^{-1} the sensor response was linear to the logarithm of the concentration, as depicted in the calibration curve in figure 4.71b. At a concentration of 1 µmol L^{-1} the impedances

did not increase any more and the sensor seemed to be saturated. In human saliva the cortisol concentration of a healthy individual is reported in literature to be between 2.7 nmol L^{-1} and 3 nmol L^{-1} [20].

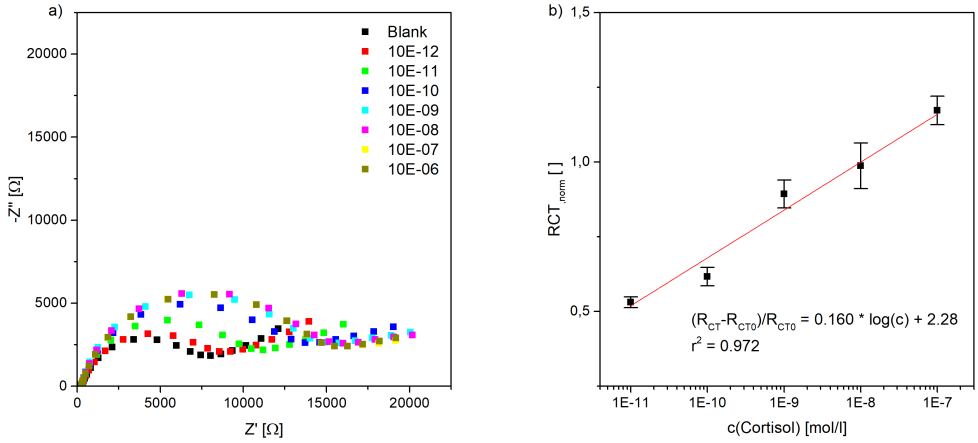

Figure 4.71: Three-electrode sensor on ceramic substrate, functionalisation MUA/cortisol-Ab/EA, EIS measurement with 10 mmol L^{-1} hexaammineruthenium(III) in PBS with −160 mV DC-bias: a) Nyquist plots of blank measurement and after incubation with cortisol standards; b) calibration curve of the sensor with $R_{CT,norm}$ plotted against the logarithmic cortisol concentration

4.8.2 Cross-reactivity of three-electrode cortisol sensor

Further, the cross reactivity of the cortisol sensor is of great importance. In saliva a lot of different hormones are available which could possibly bind to the sensor and lead to a false positive measurement result. To test specificity the cortisol sensor was incubated with 1 nmol L^{-1} solutions of progesterone and prednisone. Progesterone is a sex hormone and present in concentrations of 0.38 nmol L^{-1} in human saliva [20]. The EIS spectra before and after the incubation with a 1 nmol L^{-1} buffered progesterone solution are depicted in figure 4.72a. It seems that a small amount of the progesterone bound to the surface and increased the R_{CT} by 0.11. When the sensor was incubated with a 1 nmol L^{-1} solution of prednisone, which is a synthetic hormone and not naturally available in saliva, the impedances of the sensor also increased by a small amount, as can be observed in figure 4.72b. In both cases the increase is relat-

ively small in comparison to the incubation with a 1 nmol L^{-1} cortisol solution as depicted in the Nyquist plot in figure 4.73a. The $R_{CT,norm}$ of all three tests are compared in figure 4.73b. The response to cortisol is about 5 times higher with a value of 0.53 in comparison to progesterone and prednisone. The cross reactivity is relatively small in comparison to the expected concentrations of cortisol in saliva, which is about ten times higher than the concentration of progesterone.

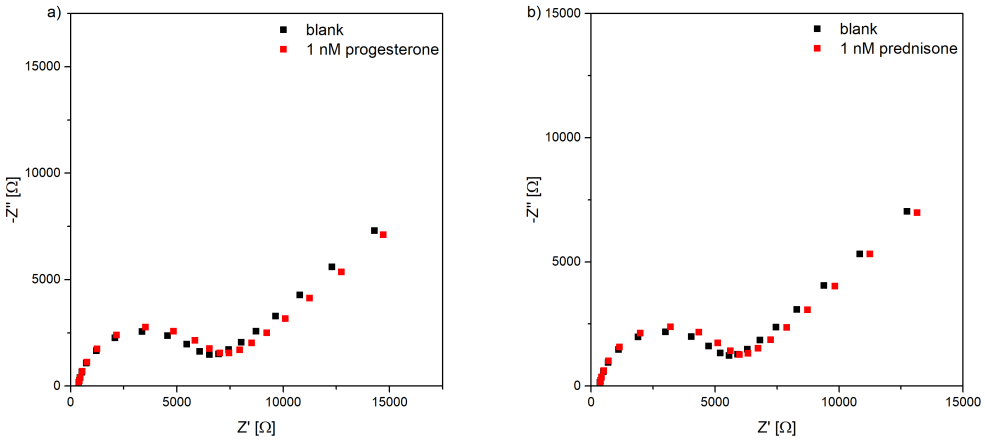

Figure 4.72: Cross reactivity test of three-electrode cortisol sensor, functionalisation MUA/cortisol-Ab/EA, measurement with 10 mmol L^{-1} hexaammineruthenium(III) in PBS with −160 mV DC-bias: a) response to incubation with 1 nmol L^{-1} progesterone; b) response to incubation with 1 nmol L^{-1} prednisone

4.9 Three-electrode IgG sensor

4.9.1 Comparison of IgG sensors

The discussed functionalisation procedure for IgG with 10 mmol L^{-1} EDC and NHS on the ceramic and glass substrate from chapter 4.7 was tested with different buffered IgG solutions and the results were compared. First, several biosensors on the ceramic substrate from the same batch were used for the measurements. This means that each sensor was incubated with the same solutions in parallel and was handled in the same way. After the functionalisation procedure the EIS spectrum of each biosensor prior to the incubation with the IgG

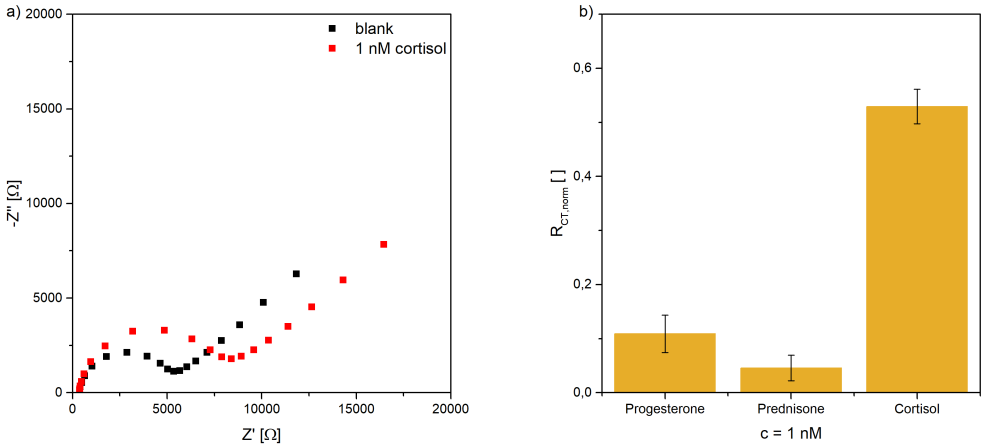

Figure 4.73: Cross reactivity test of three-electrode cortisol sensor, functionalisation MUA/cortisol-Ab/EA, measurement with 10 mmol L^{-1} hexaammineruthenium(III) in PBS with −160 mV DC-bias: a) response to incubation with 1 nmol L^{-1} ; b) comparison of the $R_{CT,norm}$ of the cortisol sensor of the cross reactivity test

standards was recorded. Next, the sensors were incubated for 30 min with IgG standards with IgG concentrations ranging from 0.0113 mg L^{-1} to 113 mg L^{-1}. The recorded EIS spectra of a ceramic based IgG-sensor are depicted in figure 4.74a. The determined impedances of the blank measurement were the lowest and increased after the incubation with each IgG standard. The R_{CT} values were gained via curve fitting, normalised and plotted against the logarithmic IgG concentration of the standards. The $R_{CT,norm}$ values increased linearly as shown in figure 4.74b. In human saliva samples of healthy individuals IgG concentrations of about 1 mg L^{-1} IgG are expected. The response of these samples would be in the middle of the calibration curve and, therefore, measurable with the developed sensor platform.

As mentioned, several ceramic based sensors of the same functionalisation batch were used for the detection of IgG in buffered standard solutions. However, the response results were very different from sensor to sensor. In figure 4.75 the response of four functionalised biosensors on ceramic substrate from the same batch after incubation with 11.3 mg L^{-1} IgG solution are depicted. The $R_{CT,norm}$ was determined to be 2.8 for the sensor with the highest response and 0.11 for the sensor with the lowest response. The difference in the response to the IgG standards can have several reasons. It could be that the cleaning of

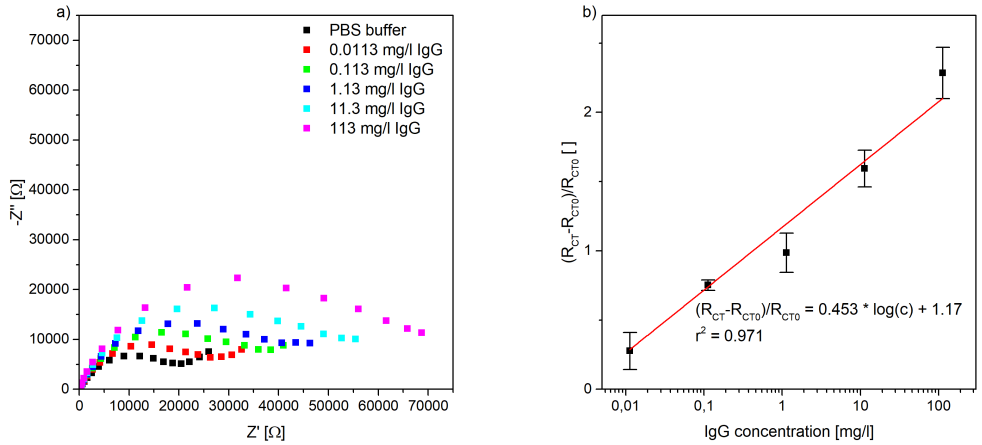

Figure 4.74: Three-electrode sensor nr. 2 on ceramic substrate, functionalisation MUA/Fc-IgG-Ab/EA, EIS measurement with 10 mmol L^{-1} hexaammineruthenium(III) in PBS with −160 mV DC-bias: a) Nyquist plots of blank measurement and after incubation with IgG standards; b) calibration curve of the sensor with $R_{CT,norm}$ plotted against the logarithmic IgG concentration with the response of each concentration measured in triplicates on the same sensor

the ceramic based sensors is insufficient and it does not form a dense monolayer for the subsequent functionalisation steps. If this was true, there would be measurable differences in the EIS spectra of gold electrodes after the cleaning process, but all ceramic based sensors exhibited R_{CT} of about 400 Ω as depicted in figure 4.44a. Another possibility is that the screen-printed electrodes have differences in the surface roughness or variations in the electrochemically active surface areas. These differences could have been introduced by the screen-printing process itself and could have led to the large differences in the functionalisation and the response of the sensor. Sensors on the ceramic substrate had already significant differences after the monolayer functionalisation as shown in chapter 4.6.1. Further, these intra-batch variation of the response to IgG standards were observed less in the case of the biosensors on the glass substrate.

Five WE which were deposited with TE on the glass substrate were functionalised with the IgG specific antibodies in the same way as the electrodes on the ceramic substrate. The glass based biosensors were also incubated with 11.3 mg L^{-1} IgG standards. The determined $R_{CT,norm}$ values are compared in

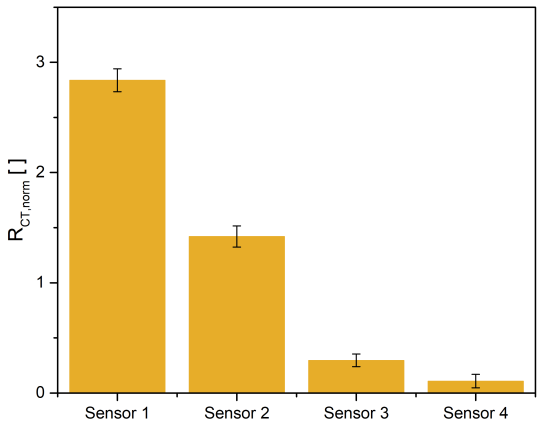

Figure 4.75: $R_{CT,norm}$ values of IgG specific sensors on ceramic substrate after incubation with 11.3 mg L^{-1} IgG

figure 4.76. The intra-batch variation is much lower in the case of the electrodes on the glass substrate. Four of the five sensors exhibited a response of about 1.2. The response of one sensor was only halve of the others with 0.6. The thin-film electrodes on the glass slide sensor seem to have a much lower variation and are much more comparable. It is possible that the difference in the response can be lowered by an automated functionalisation. Several of the steps of the functionalisation procedure are done by pipetting the solutions onto the individual working electrodes. From electrode to electrode differences in the handling can occur and can have a drastic influence on the performance of the sensor.

Further, from batch to batch the response of the sensor can vary a lot. In figure 4.77 a fully functionalised sensor on glas substrate from batch A is compared to another sensor from a different batch B. Four of the five working electrodes on the glass slide were incubated with different buffered IgG standards with concentrations ranging from 0.05 mg L^{-1} to 50 mg L^{-1}. The fifth electrode was incubated with a 1:10 diluted saliva sample. The standard curve of the sensor from batch A is depicted in figure 4.77a and of the sensor from batch B in figure 4.77b. The calibration curves of both batches are completely different from each other. The slope of the linear curve of batch A is 1.37 and of batch B it is about halve with 0.66. Even with all these differences the calculated IgG concentration of the saliva sample is very similar. In batch A the concentration in the undiluted saliva sample was calculated to be 2.4 mg L^{-1} and in batch B

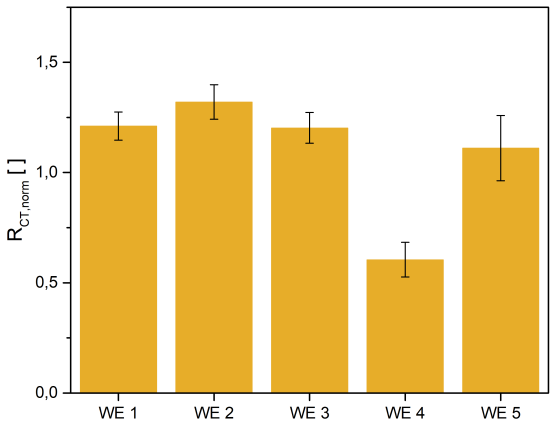

Figure 4.76: $R_{CT,norm}$ values of IgG specific sensors on glass substrate after incubation with 11.3 mg L^{-1} IgG

1.3 mg L^{-1}. This shows that at least in case of a manual laboratory production level for each batch of sensors the calibration curve has to be determined and using the calibration curve from a different batch leads to completely wrong results.

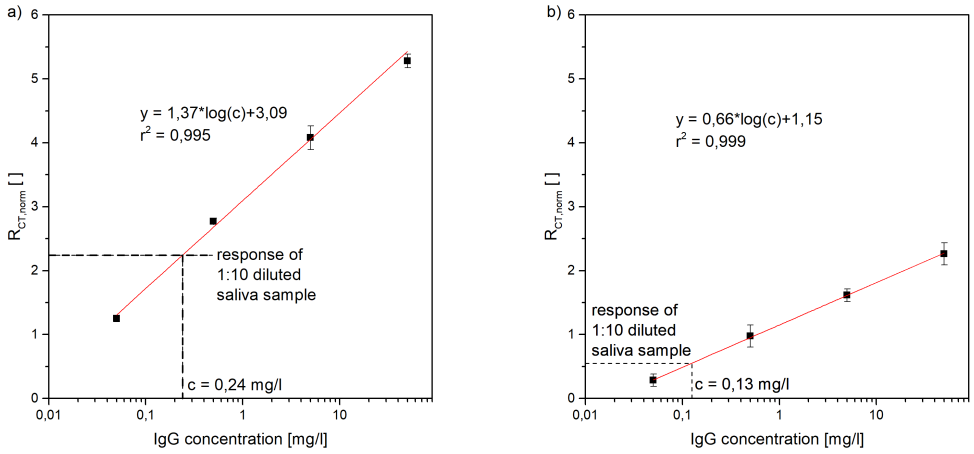

Figure 4.77: Comparison of calibration curves of different glass based biosensor batches, a) IgG sensor from batch 1; b) IgG sensor from batch 2

Table 4.3: Sample and standard layout on well plate for the ELISA

	1	2	3
A	$100\,\mathrm{ng\,mL^{-1}}$	$100\,\mathrm{ng\,mL^{-1}}$	Saliva diluted 1:100
B	$50\,\mathrm{ng\,mL^{-1}}$	$50\,\mathrm{ng\,mL^{-1}}$	Saliva diluted 1:100
C	$25\,\mathrm{ng\,mL^{-1}}$	$25\,\mathrm{ng\,mL^{-1}}$	Saliva diluted 1:1000
D	$12.5\,\mathrm{ng\,mL^{-1}}$	$12.5\,\mathrm{ng\,mL^{-1}}$	Saliva diluted 1:1000
E	$6.25\,\mathrm{ng\,mL^{-1}}$	$6.25\,\mathrm{ng\,mL^{-1}}$	-
F	$3.125\,\mathrm{ng\,mL^{-1}}$	$3.125\,\mathrm{ng\,mL^{-1}}$	-
G	$1.5625\,\mathrm{ng\,mL^{-1}}$	$1.5625\,\mathrm{ng\,mL^{-1}}$	-
H	blank	blank	-

4.9.2 Measurement of saliva sample with EIS-sensor and ELISA

A 1:10 diluted human saliva sample has been analysed by using functionalised sensors on a glass substrate from two different batches. The measurements with the sensor from batch A resulted in an IgG concentration of the undiluted saliva sample of $2.4\,\mathrm{mg\,L^{-1}}$ IgG, as depicted in the standard curve in figure 4.77a. The analysis with the sensor from batch B determined that the saliva sample had an IgG concentration of $1.3\,\mathrm{mg\,L^{-1}}$.

To verify the results of the IgG sensors, the saliva sample was also analysed with a commercially available ELISA kit for total human IgG. The measurement procedure was performed exactly as stated in the manual and summarised in chapter 3.10. The layout of samples on the ELISA plate was as shown in table 4.3. The absorption in the well plates were recorded with a plate reader. The differences of the absorption values at 450 nm and 570 nm were calculated and plotted against the IgG concentrations, as depicted in figure 4.78. Through the data points a logistics curve is fitted, and shows a good correlation. The absorption values of the saliva samples were used to calculate the IgG concentration of the undiluted saliva sample, which corresponds to $2.7\,\mathrm{\mu g\,mL^{-1}}$ IgG. The mean values of IgG sensors and the ELISA kit are different, but within the same magnitude. A two-sample t-test was performed to find out if there is a significant difference between the results of the EIS-sensors and the ELISA-test. Equal variances of the two samples were assumed. With a significance level of 0.05 the two mean values are not different from each other. So the results of the electrochemical IgG sensors from both batches are comparable to a standard ELISA kit.

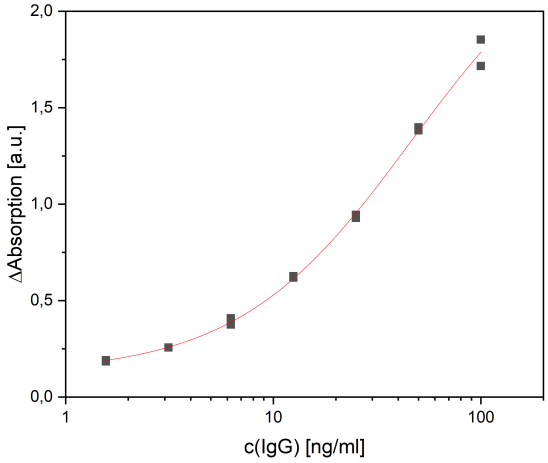

Figure 4.78: ELISA standard curve

4.9.3 Comparison of measurement chambers

Previous measurements were all performed with the working electrodes in individual measurement chambers, as depicted in figure 3.6. A concern was, if there is an influence on the different working electrodes, when all working electrodes share the same chamber and the same measurement solution. An electrode holder was designed with one big measurement chamber for all five working electrodes, as depicted in figure 4.79. First, CVs of the sensors in the small and the big measurement chambers were recorded. In figure 4.80a the CV of the sensor with five individual chambers and in figure 4.80c the CV of the sensor with one big measurement chamber is shown. The CVs are quite comparable. There are no additional peaks or other possible influences from the other working electrodes in the big measurement chamber. The only obvious difference is the height of the measured peak current and the position of the peak maxima. These can be attributed to the the larger volume of the solution and a different current density distribution. Also, the EIS measurement of the functionalised sensor did not reveal a negative influence of the one big chamber on the measurement. Figure 4.80b shows the EIS spectra of a sensor with five individual measurement chamber. First, the blank value was recorded and than the working electrodes 1 to 5 were incubated for 30 min each with the same buffered IgG standards with increasing concentrations. In the case of the single big measurement chamber, the blank values of the electrodes were recorded. Next, the

sensor was incubated with the buffered IgG samples one after the other with increasing IgG concentrations. The EIS spectra of one of the working electrodes is depicted in figure 4.80d. The measured impedances increased with the concentration of the IgG. No influence of the other working electrodes in the single measurement chamber is apparent.

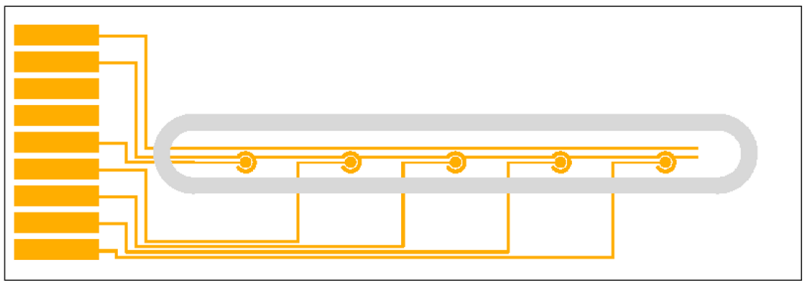

Figure 4.79: Sensor layout with one big measurement chamber for all working electrodes

4.10 Waste management of biosensors

The use of the biosensors for POC testing at home for individuals can lead to a big amount of waste. The test with the biosensor has to be done at least once per day to make meaningful decisions for the training. Even better would be multiple measurements per day to see the overall development of the different biomarker concentrations over the course of the day. Additionally, measurements before and after a training session can be done to get information about the training intensity and the affect of the training on the body. For each of this tests a new sensor has to be used. There are several reasons for the single use of the sensor. First and foremost is the hygiene. The sensor is in contact with human saliva samples. Even when the sensor is washed, pathogens could remain on the sensors and reusing the POC device could facilitate the transmission of diseases. Further, the end user at home would have to perform the washing of the sensor to remove the bound antigen from the sensor. In most cases the user is not sufficiently trained and wrong handling of the device can lead to damages of the surface and the functionalisation. These damages can have different effects. Either, the sensor is completely broken and does not give any results any more, or the sensor gives wrong information about the fitness, health or stress

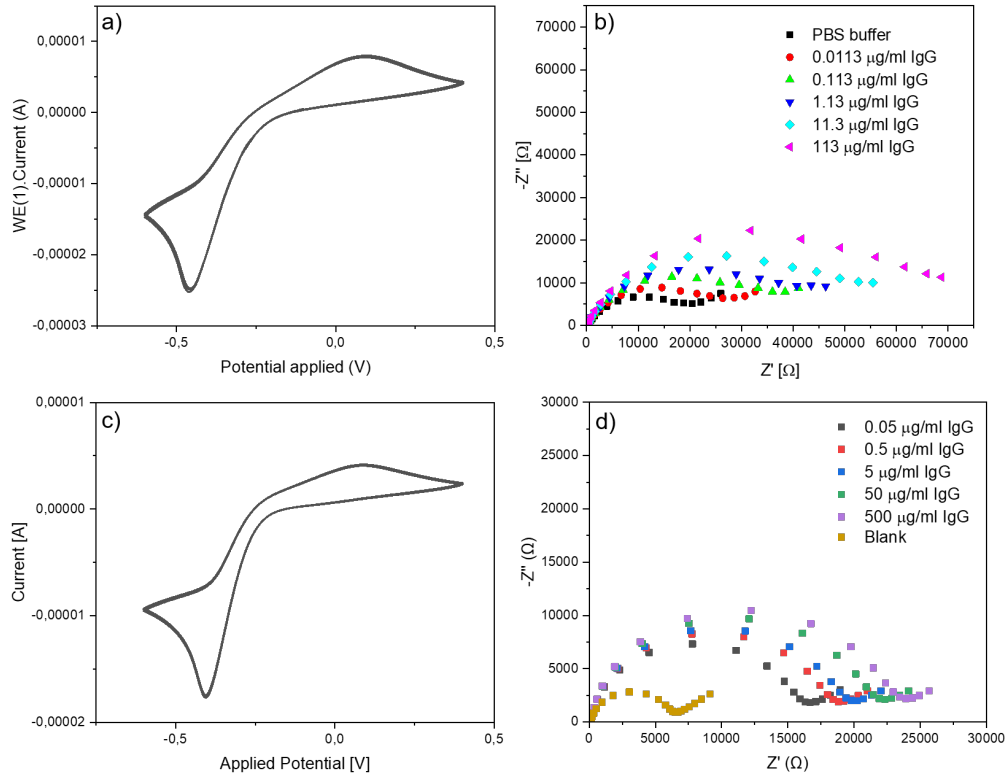

Figure 4.80: Comparison of CV and EIS measurements when using five small measurement chambers or one big measurement chamber; a) CV with small measurement chambers; b) EIS of sensor with different IgG concentrations in small measurement chambers; c) CV with one big measurement chamber; d) EIS of sensor with different IgG concentrations in one big measurement chamber

status of the user. This could lead to wrong decisions in the training plan and could be very damaging for the health of the user and must be avoided. The collection and centralised cleaning of the sensors would also not be a feasible method. First, because of the afore mentioned health concerns. Second, the functionalisation is not very stable in ambient conditions over extended periods of time. The antibodies or enzymes on the sensor can loose their functionality over time and the results of the regenerated sensor would be dubious. Also, it was reported in literature that the sensors can loose up to 50 % of their initial signal response after the regeneration process [46].

Instead of regenerating the whole functionalised sensor or completely recycling the whole sensor, only the functionalisation on the electrodes could be removed.

The choice of the cleaning method would be the most important concern. Using very aggressive cleaning methods, such as piranha solution or oxygen plasma, could damage other components of the sensor. When polymers or paper are used as substrate or a polymer layer is used for passivation of the electric conductors, they can be destroyed by the afore mentioned cleaning procedures. Using softer cleaning procedures could be insufficient and residues of the previous functionalisation would remain on the electrodes. This would hinder the new functionalisation of the sensor and impede the sensitivity of the new biosensor.

The safest way to ensure the functionality of the sensor would be a recycling of the materials of the sensor. Noble metals are only deposited on the sensor in small amounts, but they can still be recycled in the same procedures as other electronic waste. The substrate of the electronics has the largest share in the volume of the waste of the biosensor and is therefore the biggest concern in the recycling process. The recycling of ceramics is hardly in use. Ceramics are shredded and can only be reused for the production of coarse ceramics or as filling material in road construction for example. PET and glass are both materials which are recycled in large quantities in recycling facilities, but PET is harder to recycle when mixed with other polymer based waste. The recycling process is then solvent based and is much more energy consuming. Recycling glass needs also larger amounts of energy because of the high temperatures during the production process. The use of a more environmentally friendly and sustainable substrate, such as paper, would be a great advantage for a single use POC test.

5 Summary

Different functionalisation methods were tested to develop a cortisol sensitive two-electrode biosensor on a glass substrate. Of all the tested monolayers MPA emerged to be the most suitable basis for the two-electrode sensor with ferro-/ferricyanide as redox-couple in the EIS measurement solution. The formed MUA monolayer was too dense and increased the measured impedances too much. The density of the mixed MUA-MPOH monolayer varied too much and lead to varying impedances of the sensor. The activation of the surface functionalisation with 10 mmol L^{-1} EDC and NHS for 60 min lead to reproducible results. The fully functionalised sensor had a good linear response to cortisol in the range of 1 nmol L^{-1} to 1 µmol L^{-1}. It was observed that the sensors, which were functionalised in the same batch, had completely different responses to the same cortisol concentrations from one another. This would make the batch calibration of the sensors impossible and prevent the application of the sensor in a POC device. As possible influence of the intra-batch variation an essential part of the commonly used measurement solution has been identified. The PBS buffer solution was tested and did not reveal any changes in the electrochemical properties of the sensor. It turned out that the redox-couple ferro-/ferricyanide lead to changes of the properties of the electrodes. When the same sensor was washed in between EIS measurements, the impedances changed completely. Further, SEM pictures of the sensor before and after EIS measurements revealed morphology changes of the gold electrodes. When the gold electrodes were incubated for an extended time period in the ferro-/ferricyanide solution, the gold electrodes dissolved and the chromium adhesion layer remained. Alternative redox-cuples were hard to find, because of the instability of the reduced state of most redox-active substances. Iron(III)/(II) and 1,4-benzoquinon and hydroquinone were tested. In both cases the reduced state was slowly oxidised in the aqueous solution during the EIS measurement. This resulted in a continuous drift of the EIS spectra over the whole measurement period. To counter this

stability issue another method was proposed: the use of a three-electrode setup and EIS measurement with a DC-bias. A suitable DC-bias is applied and the oxidised redox-active substance is reduced. Both, the reduced and the oxidised state, are now available close to the working electrode. By applying the alternating current, the equilibrium is pushed to the reduced or oxidised state and the impedances are determined. Several redox-active substances were considered: ferricyanide, europium(III), iron(III), pentaamminechlororuthenium(III), hexaammineruthenium(III), ascorbic acid, methylene blue and 1,4-benzoquinone. Ferricyanide was discarded because it still caused instabilities and corroded the gold electrodes. Europium seemed to damage the working electrodes. After several EIS measurements the determined impedances became unstable and the noise in the EIS spectra increased. Further, europium can not be used in PBS buffer because it forms insoluble precipitates with the phosphate. Because iron(III) can also form insoluble salts with phosphates it was not considered any further. The redox-reaction of ascorbic acid seems to be irreversible and can not be used in the EIS measurement. Methylene blue exhibited only slight stability issues. Over extended measurement periods the RE obtained a slight blue hue and the EIS spectrum changed slightly. In a single-use application this redox-active substance could be applied. 1,4-Benzoquinone exhibited stability issues in the CV and EIS measurements. Additionally, the substance is poisonous and, therefore, not suitable for a POC device. Pentaamminechlororuthenium(III) only showed minor EIS instabilities similar to methylene blue. Hexaammineruthenium(III) displayed great stability in the CV and EIS measurements. Extended test of hexaammineruthenium(III) in the EIS measurement at a DC-bias of $-160\,\mathrm{mV}$ revealed that the determined R_{CT} was stable over a measurement period of 18 min. Three different three-electrode sensors were tested: thin-film electrodes on PET and glass and additionally screen-printed electrodes on ceramic substrate. The functionalisation of the sensors was carried out with different monolayers. The tested monolayers were: MPA, MUA, MHDA, MUA-BT, MUA-DT, and MUA-UT. The sensors were functionalised with IgG specific antibodies. The best responses were achieved with sensors based on the MUA monolayer. Sensors with MUA monolayers on all three substrate types were activated with different EDC and NHS concentration to optimize the functionalisation protocol. The tested EDC and NHS concentrations ranged from $5\,\mathrm{mmol\,L^{-1}}$ to $250\,\mathrm{mmol\,L^{-1}}$. The response of the functionalised

sensors to a buffered 1 mg L^{-1} IgG solution was tested. This revealed, that the best results were achieved with a functionalisation protocol utilising a EDC and NHS concentration of 10mM. Additionally, the sensors on the PET substrate had a $R_{CT,norm}$ of only 0.18, which is about three times lower than the response of the biosensors on the ceramic or glass substrate. The difference in the response is maybe caused by additives in the PET substrate which dissolve during the functionalisation procedure and can adsorb on the gold electrodes. Tests after the formation of the MUA monolayer on the gold electrodes on the PET substrate revealed, that in the case of PET based sensors with high impedances, that the impedances can decrease drastically after a CV measurement. The CV indicate that the electrochemical properties of the sensor slowly change over time and their electrochemical behaviour resembles more closely the cleaned gold electrodes on the PET substrate. A cortisol specific biosensor on ceramic substrate was functionalised in the same way as the optimised IgG biosensor with the only difference that instead of the IgG specific antibody a cortisol specific antibody was attached. The cortisol immunosensor exhibited a linear range from 10 pmol L^{-1} to 100 pmol L^{-1}. The cross-reactivity of the sensor was tested with progesterone and prednisone. After the binding of progesterone the response was 0.11 and the response with prednisone was 0.08. The response to the same concentration of cortisol is about 5 times higher. The IgG-biosensors on the ceramic and glass substrate were used to establish a calibration curve. The IgG-sensors on the ceramic substrate exhibited a linear response in the range from 0.0113 mg L^{-1} to 113 mg L^{-1}, but the test of multiple ceramic based sensors revealed, that the sensors from the same batch can response very differently from one another to the same IgG standards. The response of four sensors from the same batch to a 11.3 mg L^{-1} IgG solution can range from 0.11 to 2.8. This variation is maybe caused by the screen-printed electrodes of the sensors on the ceramic substrate. The screen-printed electrodes require organic additives for the printing process. Residues of these organic substances can interfere with the functionalisation process greatly and lead to drastic differences between the sensors of the same batch. In the case of the thin-film gold electrodes on the glass substrate these differences were not that drastic. A test of five different sensors from the same batch revealed, that 4 of 5 sensors were nearly identical. One of the sensors had only halve the response of the other five sensors. The range of possible scatter is much smaller. The difference of the glass based

sensors is maybe caused by possible errors in the functionalisation procedure. All the required solutions are pipetted onto the electrodes by hand. An automatisation of the functionalisation procedure could prevent these differences of the sensors on the glass substrate completely. Still, differences between batches of the glass sensor are considerable. The calibration curve of sensors on the glass substrate from two different batches were compared. The linear range of both sensor was from $0.05\,\mathrm{mg\,L^{-1}}$ to $50\,\mathrm{mg\,L^{-1}}$. The slope of the sensors of batch A was 1.37 and the slope of batch B was 0.66. With sensors from both batches the concentration of a saliva sample was determined. The result of batch A was a concentration of $2.4\,\mathrm{mg\,L^{-1}}$ and of batch B was $1.3\,\mathrm{mg\,L^{-1}}$. The results were compared to a commercially available ELISA kit. The result of the kit was a concentration of $2.7\,\mathrm{mg\,L^{-1}}$ IgG in the undiluted saliva sample. A two-sample t-test with assumed equal variances was performed to compare the results of the electrochemical sensor with the ELISA kit. The test revealed that with a significance level of 0.05 the results of the EIS sensors are not different from the result of the ELISA kit. For the previous tests each of the working electrodes had their own measurement chamber and did not share the measurement solution with one another. In a POC device all the electrodes will share the same measurement volume. A different sensor holder was designed with a single measurement chamber for all five working electrodes. The sensor was incubated with IgG standards and the results were compared to a sensor with five separate measurement chambers. There were no identifiable differences between both types of measurement chambers.

6 Outlook

To overcome the problem of the low response of the PET based biosensor other flexible substrates have to be tested. It is possible that other PET foils do not interfere with the formation of the monolayer. Use of completely different flexible substrates, such as cellophane or paper, can sustain a working immunosensor with a high response. Additionally, the functionalisation procedure has to be tested with the remaining biomarkers myoglobin, H-FABP and lactate. The cortisol or IgG antibodies have to be replaced by a myoglobin or H-FABP specific antibody and the response of the sensors have to be tested. Only changing the last production step of the antibody attachment and keeping the functionalisation procedure the same already worked for the IgG and cortisol antibody. It is expected that it could also work for myoglobin and the H-FABP antibody. Lactate has to be detected with the help of an enzymatic reaction and the electrochemical method for this types of reaction is usually chronoamperometry. The sensor concept has to be tested for this type of electrochemical detection. Finally, the functionalised electrodes have to be connected to the microchip, which works as a potentiostat and impedance meter, and the functionality has to be examined. After these tests the development of a complete concept for a demonstrator which can be used by an untrained user will be possible.

Bibliography

[1] WKO. *Der Fitness-Markt in Österreich*, (accessed March 14, 2020).

[2] Friedrich Schneider and Elisabeth Dreer. *Zwischenbericht - Volkswirtschaftliche Analyse der Prävention von Burnout*, (accessed March 20, 2020).

[3] Eun-Hyung Yoo and Soo-Youn Lee. Glucose biosensors: an overview of use in clinical practice. *Sensors*, 10(5):4558–4576, 2010.

[4] Luyun Jiang. *Biomedical Diagnostics at Point-of-Care 2019-2029: Technologies, Applications, Forecasts*, (accessed April 31, 2020).

[5] Djordje Bozovic, Maja Racic, and Nedeljka Ivkovic. Salivary cortisol levels as a biological marker of stress reaction. *Medical archives (Sarajevo, Bosnia and Herzegovina)*, 67(5):374–377, 2013.

[6] Janice M. Yoshizawa, Christopher A. Schafer, Jason J. Schafer, James J. Farrell, Bruce J. Paster, and David T. W. Wong. Salivary biomarkers: toward future clinical and diagnostic utilities. *Clinical microbiology reviews*, 26(4):781–791, 2013.

[7] Robert M. Califf. Biomarker definitions and their applications. *Experimental biology and medicine (Maywood, N.J.)*, 243(3):213–221, 2018.

[8] Josef Finsterer. Biomarkers of peripheral muscle fatigue during exercise. *BMC musculoskeletal disorders*, 13:218, 2012.

[9] Gonzalo Palacios, Raquel Pedrero-Chamizo, Nieves Palacios, Beatriz Maroto-Sánchez, Susana Aznar, and Marcela González-Gross. Biomarkers of physical activity and exercise. *Nutricion hospitalaria*, 31 Suppl 3:237–244, 2015.

[10] Mitch D. VanBruggen, Anthony C. Hackney, Robert G. McMurray, and Kristin S. Ondrak. The relationship between serum and salivary cortisol

levels in response to different intensities of exercise. *International journal of sports physiology and performance*, 6(3):396–407, 2011.

[11] Matias Brodsgaard Grynderup, Henrik Albert Kolstad, Sigurd Mikkelsen, Johan Hviid Andersen, Jens Peter Bonde, Henriette Normolle Buttenschon, Anette Kaergaard, Linda Kaerlev, Reiner Rugulies, Jane Frolund Thomsen, Marianne Agergaard Vammen, Ole Mors, and Ase Marie Hansen. A two-year follow-up study of salivary cortisol concentration and the risk of depression. *Psychoneuroendocrinology*, 38(10):2042–2050, 2013.

[12] Masato Furuhashi and Gökhan S. Hotamisligil. Fatty acid-binding proteins: role in metabolic diseases and potential as drug targets. *Nature reviews. Drug discovery*, 7(6):489–503, 2008.

[13] Paola Brancaccio, Giuseppe Lippi, and Nicola Maffulli. Biochemical markers of muscular damage. *Clinical chemistry and laboratory medicine*, 48(6):757–767, 2010.

[14] Saad Abdul Rehman, Zohaib Khurshid, Fayez Hussain Niazi, Mustafa Naseem, Hamed Al Waddani, Haafsa Arshad Sahibzada, and Rabia Sannam Khan. Role of salivary biomarkers in detection of cardiovascular diseases (cvd). *Proteomes*, 5(3), 2017.

[15] Jonathan B. Wittenberg and Beatrice A. Wittenberg. Myoglobin function reassessed. *The Journal of experimental biology*, 206(Pt 12):2011–2020, 2003.

[16] Vladimir V. Klimov. *From Basic to Clinical Immunology*. 1st ed. 2019 edition, 2019.

[17] Daniel E. Furst. Serum immunoglobulins and risk of infection: how low can you go? *Seminars in arthritis and rheumatism*, 39(1):18–29, 2009.

[18] Nathália Matos-Gomes, Marilise Katsurayama, Fabiano Hiromichi Makimoto, Linda Luciana Oliveira Santana, Edijane Paredes-Garcia, Maria Alice d'Avila Becker, and Maria Cristina Dos-Santos. Psychological stress and its influence on salivary flow rate, total protein concentration and iga, igg and igm titers. *Neuroimmunomodulation*, 17(6):396–404, 2010.

[19] R. Segura, C. Javierre, J. L. Ventura, M. A. Lizarraga, B. Campos, and E. Garrido. A new approach to the assessment of anaerobic metabolism: measurement of lactate in saliva. *British journal of sports medicine*, 30(4):305–309, 1996.

[20] Shoko Konishi, Eleanor Brindle, Amanda Guyton, and Kathleen A. O'Connor. Salivary concentration of progesterone and cortisol significantly differs across individuals after correcting for blood hormone values. *American journal of physical anthropology*, 149(2):231–241, 2012.

[21] Eleni Topkas, Patricia Keith, Goce Dimeski, Justin Cooper-White, and Chamindie Punyadeera. Evaluation of saliva collection devices for the analysis of proteins. *Clinica chimica acta; international journal of clinical chemistry*, 413(13-14):1066–1070, 2012.

[22] Sabesan Mythili. Salivary heart fatty acid binding protein - a novel biomarker of myocardial damage. *Journal of Oral Hygiene & Health*, 02(04), 2014.

[23] Thomas Shpitzer, Gideon Bahar, Raphael Feinmesser, and Rafael M. Nagler. A comprehensive salivary analysis for oral cancer diagnosis. *Journal of cancer research and clinical oncology*, 133(9):613–617, 2007.

[24] Rajesh, V. Sharma, V. K. Tanwar, S. K. Mishra, and A. M. Biradar. Electrochemical impedance immunosensor for the detection of cardiac biomarker myogobin (mb) in aqueous solution. *Thin Solid Films*, 519(3):1167–1170, 2010.

[25] Miraida Pagán, Dámaris Suazo, Nicole Del Toro, and Kai Griebenow. A comparative study of different protein immobilization methods for the construction of an efficient nano-structured lactate oxidase-swcnt-biosensor. *Biosensors & bioelectronics*, 64:138–146, 2015.

[26] Sunil K. Arya, Ganna Chornokur, Manju Venugopal, and Shekhar Bhansali. Dithiobis(succinimidyl propionate) modified gold microarray electrode based electrochemical immunosensor for ultrasensitive detection of cortisol. *Biosensors and Bioelectronics*, 25(10):2296–2301, 2010.

[27] Dana Stan, Carmen-Marinela Mihailescu, Rodica Iosub, Mihaela Savin, Baciu Ion, and Raluca Gavrila. *Development of an Immunoassay for Impedance-Based Detection of Hear-Type Fatty Acid Binding Protein: 15 - 17 Oct. 2012, Sinaia, Romania*. IEEE, Piscataway, NJ, 2012.

[28] Mahmoud Amouzadeh Tabrizi, Mojtaba Shamsipur, and Ali Mostafaie. A high sensitive label-free immunosensor for the determination of human serum igg using overoxidized polypyrrole decorated with gold nanoparticle modified electrode. *Materials science & engineering. C, Materials for biological applications*, 59:965–969, 2016.

[29] Florinel-Gabriel Banica. *Chemical sensors and biosensors: Fundamentals and applications*. Wiley, Wiley, 1. publ edition, 2012.

[30] Andrzej Lasia. *Electrochemical Impedance Spectroscopy and its Applications*. Springer New York, New York NY, 2014.

[31] Parikha Mehrotra. Biosensors and their applications - a review. *Journal of oral biology and craniofacial research*, 6(2):153–159, 2016.

[32] Daniel R. Thévenot, Klara Toth, Richard A. Durst, and George S. Wilson. Electrochemical biosensors: recommended definitions and classification1international union of pure and applied chemistry: Physical chemistry division, commission i.7 (biophysical chemistry); analytical chemistry division, commission v.5 (electroanalytical chemistry).1. *Biosensors and Bioelectronics*, 16(1-2):121–131, 2001.

[33] Honglan Qi, Chen Wang, and Ning Cheng. Label-free electrochemical impedance spectroscopy biosensor for the determination of human immunoglobulin g. *Microchimica Acta*, 170(1-2):33–38, 2010.

[34] K. Yokoyama, K. Sode, E. Tamiya, and I. Karube. Integrated biosensor for glucose and galactose. *Analytica Chimica Acta*, 218:137–142, 1989.

[35] Petr Skládal. Advances in electrochemical immunosensors. *Electroanalysis*, 9(10):737–745, 1997.

[36] Bambang Kuswandi and Ali A. Ensafi. Perspective—paper-based biosensors: Trending topic in clinical diagnostics developments and commercialization. *Journal of The Electrochemical Society*, 167(3):037509, 2020.

[37] Yusheng Wang, Xiaoqi Wang, Wei Lu, Qingpan Yuan, Yourong Zheng, and Bo Yao. A thin film polyethylene terephthalate (pet) electrochemical sensor for detection of glucose in sweat. *Talanta*, 198:86–92, 2019.

[38] Lee M. Fischer, Maria Tenje, Arto R. Heiskanen, Noriyuki Masuda, Jaime Castillo, Anders Bentien, Jenny Émneus, Mogens H. Jakobsen, and Anja Boisen. Gold cleaning methods for electrochemical detection applications. *Microelectronic Engineering*, 86(4-6):1282–1285, 2009.

[39] F. L. Almeida and S. G. Santos-Filho. Surface activation of gold electrodes using electrochemical conditioning. In *2013 Symposium on Microelectronics Technology and Devices (SBMicro)*, pages 1–5.

[40] Yung-Sen Lin. A surface analysis on oxygen plasma-cleaned gold pattern-plated substrates for wire bondability. *Surface and Coatings Technology*, 173(1):47–57, 2003.

[41] Jing Kang and Paul A. Rowntree. Gold film surface preparation for self-assembled monolayer studies. *Langmuir : the ACS journal of surfaces and colloids*, 23(2):509–516, 2007.

[42] J. Christopher Love, Lara A. Estroff, Jennah K. Kriebel, Ralph G. Nuzzo, and George M. Whitesides. Self-assembled monolayers of thiolates on metals as a form of nanotechnology. *Chemical Reviews*, 105(4):1103–1170, 2005.

[43] Greg T. Hermanson. *Bioconjugate Techniques*. Elsevier/AP, Amsterdam, 3rd ed. edition, 2013.

[44] Emine Yorganci and Erol Akyilmaz. Alkaline phosphatase based amperometric biosensor immobilized by cysteamine-glutaraldehyde modified self-assembled monolayer. *Artificial cells, blood substitutes, and immobilization biotechnology*, 39(5):317–323, 2011.

[45] Muammer Kaya. *Electronic waste and printed circuit board recycling technologies*. The Minerals, Metals & Materials Series. Springer, Cham, Switzerland, 2019.

[46] J. A. Goode, J. V. Rushworth, and P. A. Millner. Biosensor regeneration: A review of common techniques and outcomes. *Langmuir : the ACS journal of surfaces and colloids*, 31(23):6267–6276, 2015.

[47] Christie A. Canaria, Jonathan So, James R. Maloney, C. J. Yu, Jeffrey O. Smith, Michael L. Roukes, Scott E. Fraser, and Rusty Lansford. Formation and removal of alkylthiolate self-assembled monolayers on gold in aqueous solutions. *Lab on a chip*, 6(2):289–295, 2006.

[48] T. H. Silva, A. C. M. Castro, F. C. Valente Neto, M. M. N. S. Soares, D. S. de Resende, and A. C. S. Bezerra. Recycling ceramic waste as a raw material in sanitary ware production. *Cerâmica*, 65(375):426–431, 2019.

[49] Hans Martens and Daniel Goldmann. *Recyclingtechnik: Fachbuch für Lehre und Praxis*. Springer Vieweg, Wiesbaden, 2. auflage edition, 2016.

[50] S. Vogt, Q. Su, C. Gutierrez-Sanchez, and G. Noll. Critical view on electrochemical impedance spectroscopy using the ferri/ferrocyanide redox couple at gold electrodes. *Analytical chemistry*, 88(8):4383–4390, 2016.

[51] A. Bogomolova, E. Komarova, K. Reber, T. Gerasimov, O. Yavuz, S. Bhatt, and M. Aldissi. Challenges of electrochemical impedance spectroscopy in protein biosensing. *Analytical chemistry*, 81(10):3944–3949, 2009.

[52] Jaroslav Lazar, Christoph Schnelting, Evelina Slavcheva, and Uwe Schnakenberg. Hampering of the stability of gold electrodes by ferri-/ferrocyanide redox couple electrolytes during electrochemical impedance spectroscopy. *Analytical chemistry*, 88(1):682–687, 2016.

[53] M. Dijksma, B. A. Boukamp, B. Kamp, and W. P. van Bennekom. Effect of hexacyanoferrate(ii/iii) on self-assembled monolayers of thioctic acid and 11-mercaptoundecanoic acid on gold. *Langmuir*, 18(8):3105–3112, 2002.

[54] S. Syed. Recovery of gold from secondary sources—a review. *Hydrometallurgy*, 115-116:30–51, 2012.

[55] David Geoffrey Wild and Rhys John. *The immunoassay handbook: Theory and applications of ligand binding, ELISA and related techniques*. Elsevier, Amsterdam, 4th ed. edition, 2013.

[56] Hua Wang, Shengfu Chen, Lingyan Li, and Shaoyi Jiang. Improved method for the preparation of carboxylic acid and amine terminated self-assembled monolayers of alkanethiolates. *Langmuir*, 21(7):2633–2636, 2005.

[57] Ralf Arnold, Waleed Azzam, Andreas Terfort, and Christof Wöll. Preparation, modification, and crystallinity of aliphatic and aromatic carboxylic acid terminated self-assembled monolayers. *Langmuir*, 18(10):3980–3992, 2002.

[58] Dana Stan, Carmen-Marinela Mihailescu, Rodica Iosub, Carmen Moldovan, Mihaela Savin, and Ion Baciu. Electrochemical studies of homogeneous self-assembled monolayers versus mixed self-assembled monolayers on gold electrode for "label free" detection of heart fatty acid binding protein. *Thin Solid Films*, 526:143–149, 2012.

[59] San Yee Khaing, Yuichi Sugai, and Kyuro Sasaki. Gold dissolution from ore with iodide-oxidising bacteria. *Scientific Reports*, 9(1):4178, 2019.

[60] M.G Aylmore and D.M Muir. Thiosulfate leaching of gold—a review. *Minerals Engineering*, 14(2):135–174, 2001.

[61] Ouarda Brahmia and Claire Richard. Phototransformation of 1,4-naphthoquinone in aqueous solution. *Photochemical & photobiological sciences : Official journal of the European Photochemistry Association and the European Society for Photobiology*, 2(10):1038–1043, 2003.

[62] William M. Haynes, editor. *CRC handbook of chemistry and physics: A ready-reference book of chemical and physical data*. CRC Press, Boca Raton and London and New York, 97th edition edition, 2017.

[63] Cynthia G. Zoski. *Handbook of electrochemistry*. Elsevier, Amsterdam, 2007.

[64] William Mansfield Clark. *Oxidation-reduction Potentials of Organic Systems*. The Williams & Wilkins Company, Baltimore, 1960.

[65] Tyler J. Bechtel and Eranthie Weerapana. From structure to redox: The diverse functional roles of disulfides and implications in disease. *Proteomics*, 17(6), 2017.

[66] B. M. Chadwick and A. G. Sharpe. Transition metal cyanides and their complexes. volume 8 of *Advances in Inorganic Chemistry and Radiochemistry*, pages 83–176. Elsevier, 1966.

[67] Partha Sarathi Guin, Saurabh Das, and P. C. Mandal. Electrochemical reduction of quinones in different media: A review. *International Journal of Electrochemistry*, 2011(2):1–22, 2011.

[68] May Quan, Daniel Sanchez, Mark F. Wasylkiw, and Diane K. Smith. Voltammetry of quinones in unbuffered aqueous solution: reassessing the roles of proton transfer and hydrogen bonding in the aqueous electrochemistry of quinones. *Journal of the American Chemical Society*, 129(42):12847–12856, 2007.